ACS POLYMERS Au
AN OPEN ACCESS JOURNAL OF THE AMERICAN CHEMICAL SOCIETY

pubs.acs.org/polymerau
Review

Advancements in Novel Mechano-Rheological Probes for Studying Glassy Dynamics in Nanoconfined Thin Polymer Films

Published as part of ACS Polymers Au virtual special issue "Polymer Science and Engineering in India".

Mithun Madhusudanan and Mithun Chowdhury*

Cite This: *ACS Polym. Au* 2024, 4, 342−391
Read Online
ACCESS | Metrics & More | Article Recommendations

ABSTRACT: The nanoconfinement effects of glassy polymer thin films on their thermal and mechanical properties have been investigated thoroughly, especially with an emphasis on its altered glass transition behavior compared to bulk polymer, which has been known for almost three decades. While research in this direction is still evolving, reaching new heights to unravel the underlying physics of phenomena observed in confined thin polymer films, we have a much clearer picture now. This, in turn, has promoted their application in miniaturized and functional applications. To extract the full potential of such confined films, starting from their fabrication, function, and various applications, we must realize the necessity to have an understanding and availability of robust characterization protocols that specifically target thin film thermo-mechanical stability. Being nanometer-sized in thickness, often atop a solid substrate, direct mechanical testing on such films becomes extremely challenging and often encounters serious complexity from the dominating effect of the substrate. In this review, we have compiled together a few important novel and promising techniques for mechano-rheological characterization of glassy polymer thin films. The conceptual background involved in each technique, constitutive equations, methodology, and current status of research are touched upon following a pedagogical tutorial approach. Further, we discussed each technique's success and limitations, carefully covering the puzzling or contradicting observations reported within the broad nexus of glass transition temperature−viscosity−modulus−molecular mobility (including diffusion and relaxation).

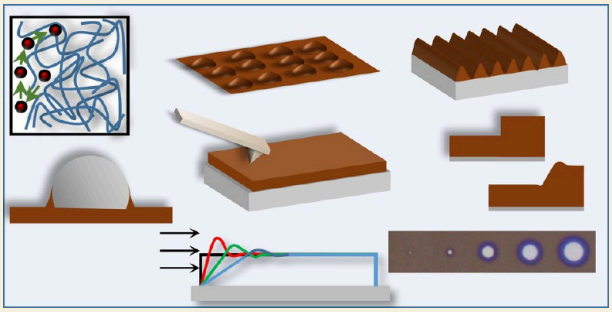

KEYWORDS: *confinement, glass transition, thin films, conformation, nanomechanics, rheology, nonequilibrium, interfaces*

INTRODUCTORY OVERVIEW

Primarily miniaturization has directed polymer research into nanoscale dimensions. Being part of miniaturized devices, exploring the thermomechanical stability of such polymers is of pertinent interest. In such applications, polymer thin films, especially atop a solid nonpolymeric substrate, have many uses, such as photoresists and coating layers in microelectronics,[1] active layers in organic solar cells and transistors,[2−4] coating layers in pharmaceuticals,[5] drug delivery,[6] and gas permeation membranes.[7] Conventional mechanical and rheological characterization techniques used for bulk polymer samples[8] (e.g., rheometer, universal tensile testing machine, dynamic mechanical analysis) are not suitable to characterize polymer thin films as their thickness is too small in the scale of nanometers and mostly beyond the scope of such instruments with their usual protocols for bulk samples. Additionally, in the case of supported soft films, it may accompany stiff substrate signatures.[9−11] Thus, the scientific community has developed a range of novel characterization techniques,[9] that often apply conventional testing protocols in a suitably modified context. Several nonconventional robust techniques for characterization are introduced to the community. Understanding the working principles of these diverse measurement methods is essential to fully understand their potential capabilities to explore a technologically relevant sample geometry to stimulate deep fundamental discussions on the niche of glass transition temperature−viscosity−modulus nexus. The most basic question could be whether smaller is stronger or weaker for these glassy polymer thin films. When the dimensions of interest become comparable to the radius of gyration (R_g) of polymers, those find themselves in a geometrically confined state. In such a state, the interfaces start playing a much more prominent role in deciding the properties of polymers,[12,13] such as the glass transition temperature (T_g), viscosity, modulus (stiffness), and

Received: March 15, 2024
Revised: June 17, 2024
Accepted: June 18, 2024
Published: July 18, 2024

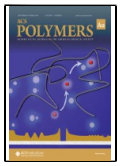

https://doi.org/10.1021/acspolymersau.4c00022
ACS Polym. Au 2024, 4, 342−391

relaxation. Among those, T_g in thin supported glassy polymer films gained considerable attention since its first observation by Keddie et al.[14] The idea behind such an observation has been propagated primarily from a liquid-like enhanced mobility film surface to a sluggish mobility substrate interface, depending on the interaction between the polymer−substrate pair, further extended toward gradient mobility along film thickness.[15,16] Advancement in this field of research further enlightens exotic nonequilibrium phenomena,[17,18] such as irreversible adsorption[19] and molecular recoiling stress or residual stress[17,18,20] related to polymer chain conformations. Since glass transition is a phenomenon accompanied by several orders of magnitude changes in viscosity and is expected to be related to the viscoelasticity of the glass,[21] the above scenarios certainly impose paramount importance in exploring and accounting for capabilities of mechano-rheological characterization of thin nanoconfined glassy polymer films.

Most of the review articles on confined glassy polymers[12,16,22−26] have been focused particularly on the glass transition phenomenon in great detail.[12,24,26,27] Those works certainly considered aspects of pseudo-thermodynamic thermal transitions and viscoelastic dynamic relaxation processes. Still, descriptions of "mechanical and rheological testing" approaches were largely missing. While compelling detailed descriptions of individual techniques like dewetting,[28] particle embedding,[29] and nanobubble inflation are available,[29] there is certainly scope for a comprehensive review article that can be represented as a critical account of all the major nonconventional mechano-rheological testing approaches applied in thin glassy polymer films to explore fundamental questions in this domain of research. Such comprehensive attempts are nearly nonexistent, except for a nearly close review by Vogt[9] on a few mechanical and viscoelastic properties, a few years ago. In a completely different context of mechanical characterization of thin, flexible electronics, few relevant approaches have been successfully explored periodically.[3,30] This review article focuses on addressing this gap in the literature to focus on different novel mechano-rheological characterization methodologies applied to thin glassy polymer films throughout in a pedagogical tutorial approach. Each technique and methodology has been explained using relevant underlying constitutive equations and important experimental observations, further pointing out its success, challenges, and limitations at the end. Before this section, relevant background aspects of confined glassy polymer films have been introduced in terms of defining pseudo-thermodynamic and dynamic properties, including glass transition, viscosity, modulus, viscoelasticity, relaxation, and diffusion. Additionally, focus on the various decoupling phenomena observed among these (mechano-rheological properties and glass transition) properties have been briefly mentioned. We have also included a brief scenario of relevant processing-induced (spin-coating method of film preparation) nonequilibrium phenomena in thin glassy polymer films, namely molecular recoiling stress or residual stress.[31−33] Those stem from polymer chain conformations and are known to impact the mechano-rheological properties of polymer thin films. Further, we conclude with a future perspective by highlighting the contrast in the behavior of polymer thin film investigated through different techniques. Throughout the article, we have only focused on thin, confined glass-forming amorphous polymer films with a central emphasis on polystyrene (PS) as a model system used in several studies. While we understand polymer nanocomposites also lead to comparable polymer nanoconfinement phenomena involving glassy dynamics and mechano-rheology,[34,35] we restricted ourselves to not covering that vast area, where relatively well-documented review articles exist.[36,37] Nonetheless, it is already established that most of the mechano-rheological characterization techniques discussed in this article can probe polymer-nanocomposite films and functional optoelectronic polymer films efficiently. Also, we did not cover atomic force microscopy (AFM) based direct nanomechanical (stiffness and viscosity) probing of the thin polymer film surface, as this area has been explored with great detail separately and nicely summarized.[38−42] In this review, we only narrowed our discussion on nonconventional novel mechano-rheological testing protocols applied to thin nanoconfined glassy polymer films.

RELEVANT ASPECTS IN CONFINED GLASSY POLYMER FILMS

Glass Transition

The glass transition temperature (T_g) delineates the transition between the glassy and rubbery phases of polymers, where the former exhibits high stiffness and brittleness, while the latter is soft and less brittle. When cooling down the liquid from temperatures well above the melting point, if sufficient time is not provided to arrange its structure into a crystalline order, the material falls into a supercooled liquid regime bypassing the crystalline phase. T_g marks the transition point from this supercooled liquid state to the out-of-equilibrium glassy state. Due to their inability to readily arrange long chains into crystalline order, polymers are typically classified as good glass formers.

The thermodynamic description of glass transition involves understanding the potential energy landscape. The polymer initially cools in state (a) (see Figure 1). If it could, it would go to state (c) and crystallize, but it ends up in state (b), where it

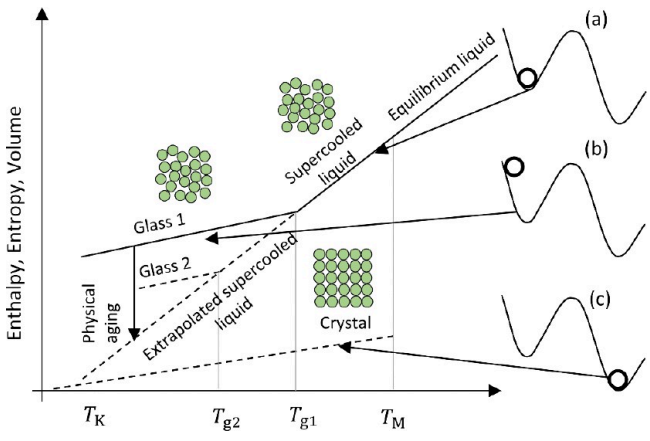

Figure 1. Representative figure shows the property (enthalpy, entropy, volume) changes with temperature for an amorphous material in comparison to a crystalline material. Instead of attaining the crystalline structure having a lower energy configuration, an amorphous material falls into the glassy regime, post the glass transition temperature (T_g) where the slope of the equilibrium liquid line changes instead of a discontinuity observed for a crystalline material at the melting point (T_M). The glass transition is a pseudo-thermodynamic phenomenon resulting in different glass transition temperatures (T_{g1}, T_{g2}) or fictive temperatures (T_{f1}, T_{f2}) for different cooling rates showing additional control by kinetics. [Used with permission from ref 43. Copyright 2014 IOP.]

https://doi.org/10.1021/acspolymersau.4c00022
ACS Polym. Au 2024, 4, 342−391

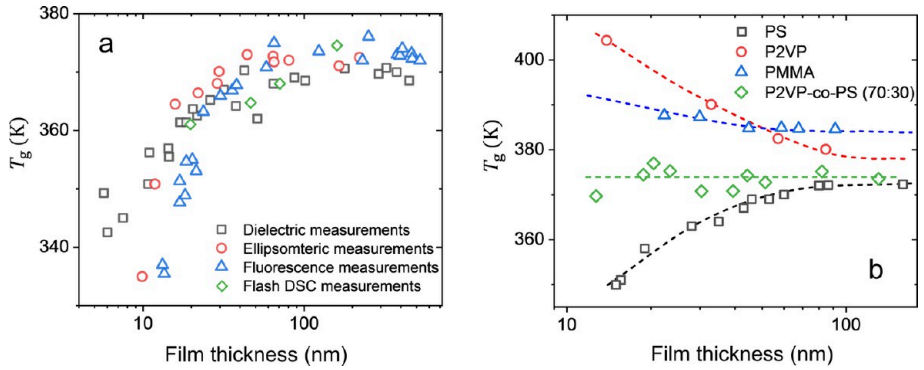

Figure 2. (a) Confinement effect showing the film thickness-dependent variation in glass transition temperature using different characterization techniques for polystyrene (PS) films, replotted from literature. The dielectric measurements data are from Fukao and Miyamoto,[49] the ellipsometric measurements data are from Keddie et al.,[14] fluorescence measurements data are from Ellison et al.,[50] and flash DSC measurements data are from Koh and Simon.[51] (b) Variation in glass transition temperature with film thickness for polystyrene (PS), poly(2-vinylpyridine) (P2VP), and poly(methyl methacrylate) (PMMA) showing that the chemistry of the polymer affects the variation in glass transition temperature (The dashed lines are a guide to the eye). In all the cases, polymer films were typically adhered atop a Si/SiO_x substrate. [Data replotted from refs 14,49−52.]

slowly traverses back toward state (a) upon physical aging.[12,26] T_g exhibits a dependence on cooling rate, with faster cooling rates resulting in the formation of glasses characterized by higher T_g values (e.g., $T_{g1} > T_{g2}$) in Figure 1. The time available for thermodynamic establishment of faster fluctuations is reduced at high cooling rates, resulting in higher T_g at experimental time scales. Consequently, it can be categorized as a pseudo-thermodynamic property since true thermodynamic properties should not rely on the cooling rate. Furthermore, unlike first-order phase transitions such as crystallization or melting, where there is a discontinuity in the first derivative of free energy, T_g does not exhibit such discontinuity. Instead, it is marked by a discontinuity in the second derivative of free energy, aligning it closer to a second-order thermodynamic phase transition according to Ehrenfest's classifications,[21] but not purely, as in addition to the kinetic aspect, it does not fulfill the criterion of the Prigogine−Defay ratio.[21,44]

In glass formers, below the melting point, as temperature decreases, the relaxation time linked with spontaneous molecular level thermal fluctuations exhibits strong temperature dependence, diverging from the behavior observed above the melting point, where it adheres to the Arrhenius law.[21] This discrepancy can be attributed to the higher length scales associated with these fluctuations, better described by the Vogel−Fulcher−Tammann (VFT) law and the Williams−Landel−Ferry (WLF) law.[8] Termed as the α-relaxation, these fluctuations are predominant above the glass transition temperature. Conversely, at least one faster relaxation time is associated with spontaneous thermal fluctuations occurring at much smaller length scales following an Arrhenius dependency. These are typically known as β-relaxations and can occur below the glass transition temperature. However, the glass transition is primarily associated with the α-relaxations. The α-relaxation is intricately tied to the Cooperatively Rearranging Regions (CRR) concept.[45] This notion underscores the collective movement of polymer segments over considerable length scales. The CRR measures the spatial extent of this concerted motion, indicating the number of polymer segmental units needing simultaneous rearrangement for the transition. As temperature decreases below the glass transition temperature, the polymer's free volume diminishes, reducing molecular mobility. Consequently, the CRR size increases inversely with temperature. More segmental units must rearrange at lower temperatures simultaneously, facilitating the rubbery-to-glassy transition. As the temperature nears the glass transition point, the CRR becomes substantial enough to halt polymer motion entirely, forming a glassy state. This concept of CRR offers a dynamic view of the glass transition where the relaxation times change to high values that the equilibrium structure cannot be attained in the experimental time scales.[21] Adam and Gibbs[45] introduced the dynamic relevance of configurational entropy, S_c = S(liquid) − S(crystal), by utilizing the fluctuations to overcome the local barriers in CRR.

$$\tau = \tau_B \exp\left(\frac{C}{TS_c}\right), \quad TS_c \propto (T - T_0) \tag{1}$$

T_0 is the Vogel temperature, and C is a constant calibrated at a reference time τ_B. The calculation of CRR using the S_c accurately required further development of molecular models. According to the defect diffusion model,[46] the size of the CRR corresponds to the diffusion length of the defects associated with the fluctuation time at the glass transition. The nonequilibrium glass characterized by the higher free energy in the system will tend to undergo structural rearrangement to achieve a minimum in the free energy landscape by decreasing its enthalpy, entropy, and specific volume. A phenomenon depicted in Figure 1 and known as physical aging. The structural relaxation time of physical aging depends on the temperature and time associated with the aging of the polymer. As the relaxation time increases tremendously on reducing the temperature below the T_g, it is evident physical aging and glass transition are related, and the interplay is complex.[26] For a given glass with a thermomechanical history (e.g., cooling rate), the transition point of it into a glass is rather described by fictive temperature (T_f), the temperature in which a glass at a certain thermodynamic state would be at metastable equilibrium corresponding to the supercooled liquid (see Figure 1). So, the evolution of T_g with physical aging certainly signifies thermodynamic driving (recovery) force toward reaching the most stable state of the metastable equilibrium and entropy of the polymer leading to densification. The recovery rate of equilibrium and decay rate of spontaneous fluctuations (responsible for glass transition) are identical behaviors leading to the nonexponential nature of glassy dynamics.[21,47] This is visible by the stretching exponent needed to describe recovery during physical aging, which is also the time decay function

https://doi.org/10.1021/acspolymersau.4c00022
ACS Polym. Au 2024, 4, 342−391

($\phi(t)$) associated with spontaneous fluctuations described by Kohlrausch–Williams–Watts (KWW) equation:[48]

$$\phi(t) = \exp\left(-\frac{t}{\tau}\right)^{\beta} \quad (2)$$

where τ is the characteristic relaxation time and $0 < \beta \leq 1$ is the stretching exponent associated with the breadth of the relaxation time.[48]

On confining the polymers to thicknesses in the length scales of the order of R_g of the polymer chain, the behavior can be found to differ from the bulk polymers.[12,13,53] Confining the polymers, so that their dimensions are in 2-D (1-D confinement), reduces the conformational space available for the polymer chains and hence traps them in a lower entropic state than the bulk polymers.[54] In addition, such confinement also results in the perturbation of the polymer properties by the interfaces due to the higher surface area to volume ratio, allowing the opportunity to investigate the interfacial effects in greater depth. The seminal report by Keddie et al.[14] showed that the T_g of PS films having thickness h < 30–40 nm have drastically reduced values compared with the $T_{g,bulk}$ of PS. The T_g variation with film thickness has been compiled from ellipsometric,[14] fluorescence,[50] and dielectric measurements[49] for PS thin films on the Si/SiO_x substrate in Figure 2(a). Independent of the measurement techniques, the glass transition temperature of PS film is found to decrease as the film thickness reduces. However, the decrease in T_g of PS is not a universal phenomenon. It has also been found to be decoupled from the segmental relaxation time.[55] The T_g of polymer thin films is dependent not only on the geometric factors,[56] but also on the nature of the interface,[14,57] and the heating/cooling rate.[58−60] The decoupling observed in the segmental dynamics and the T_g will be discussed in a later section.

The analogy of reduced T_g in polymer thin films near dissimilar stiffer interfaces has been explored with serious attention, generating several important observations.[12,13,53] Similarities can be drawn in the glass transition behavior of lightly loaded silica nanoparticles in PS, where the interparticle distance acts in the context of film thickness.[34,35] The role of the relative separation distance between softer polymer film from a relatively stiffer polymer has also been explored in polymer bilayers[61] and even in sequence-engineered block copolymers.[62] In all the cases, stiffer polymer acted almost analogous to substrate perturbing T_g, generating a broad gradient in it.[13,61,63] From Figure 2(a), we can say while the main outcome of entire studies is clear enough to show a decrease in T_g of PS film atop a Si/SiO_x substrate, stronger film thickness and molecular weight dependence of T_g for free-standing PS films[64−66] hint that factors beyond the film thickness might be responsible for it. One main factor is the interaction of the polymer with the nonpolymeric interface (e.g., Si/SiO_x substrate). Figure 2(b) shows the effect of a nonpolymeric interface in modifying the glass transition temperature of the polymer film as the film thickness is reduced. When the film's chemical composition changes, the interactions at the substrate (here Si/SiO_x) change, resulting in either an increase or decrease of the glass transition temperature. The greater attractive nature of poly(2-vinylpyridine) (P2VP) with the substrate results in an increase in T_g, and the relatively less attractive nature of poly(methyl methacrylate) (PMMA) increased T_g but to a lower extent. The noninteracting nature of PS results in a decrease in T_g. A random copolymer made of PS and P2VP showed an averaged-out effect, showing no film thickness dependence of T_g. This variation in the behavior of different polymers was explained based on the higher cohesive energy density of attractive polymers (with the Si/SiO_x substrate) compared to PS.[52,67] Thus, when polymer films are coated on a noninteracting or repulsive substrate, a decrease in T_g can be expected, and the same can be attributed to the perturbation of properties due to the presence of a higher mobility layer at the polymer–air interface.

Kawana and Jones[68] first proposed the existence of a liquid-like mobile surface layer (of thickness ca. 10 nm) in PS films, which does not depend on the temperature or total thickness of the film. However, the free surface effect would be felt according to them even in films ten times thicker than this length scale. On the contrary, Paeng et al.[69] measured the thickness of the liquid-like surface layer and found its thickness increases upon heating, reaching 7 nm at the $T_{g,bulk}$ of the polymer. Yang et al.[70] by introducing a mobility factor fixed the thickness of the mobile layer for unentangled PS at 2.3 nm. Most convincingly, works by Ellison and Torkelson[15] showed a layer-by-layer analysis of T_g distribution using fluorescence labeling of PS, which was similarly extended for structural relaxation by Priestley and co-workers.[71] Later, Ediger and Forrest[16] strongly agreed on the existence of the mobile layers within 10 nm extending from the surface, largely utilizing their experiences on dye diffusion and surface nanohole relaxation experiments. T_g in thin supported polymer film depends on the relative interaction between air–polymer and polymer–substrate interfaces, which is a well-accepted idea now, supporting a gradient distribution in T_g across film thickness, rather than a single averaged T_g, which is lowest at the film surface and highest (close to the bulk polymer value) at the substrate interface. Analogous experiments showing comparable convincing gradient descriptions of mechano-rheological properties were largely absent until recently.[13,63,72,73] Priestley and co-workers introduced the noncontact capillary nanoshearing (NCNS)[73] technique, being able to probe layer-by-layer shear mobility and viscosity in polymer films. Viscosity was low at the free film surface, gradually reaching the bulk value close to the Si/SiO_x substrate interface for both polymer (PS and poly(*n*-butyl methacrylate) (PNBMA)) films in their studies.[72,73] Interestingly, for PNBMA, a decoupling on the film thickness dependence of T_g, glass transition dynamics, and viscosity was observed.[72] Roth and co-workers recently demonstrated a long-range ca. 200 nm gradient in the local modulus when the polymer–polymer immiscible interface arises by putting glassy and rubbery polymer domains in contact.[63] This is consistent with their previously reported gradients in local glass transition temperature.[61] Utilizing surface nanocreep experiments and adequate theoretical supports, Hao et al.[13] clearly showed the size of the polymer chain conformations, segmental dynamics, and interfacial mobility gradient are jointly responsible for the development of a transient entangled rubbery surface on top of glassy polymer films.

Figure 3 shows two interesting scenarios where postprocessing of styrenic polymer films led to the disappearance of film thickness dependence of T_g. Ellison et al.[50] found that upon adding small molecule diluents as plasticizers (see Figure 3(a)), the confinement effect was completely eliminated in the polymer film. This was attributed to the reduction in the average CRR size by the diluent, resulting in the reduction in length scale that encompasses the breadth of cooperative segmental dynamics.[50] Mechano-rheological complementary experiments on the PS-

https://doi.org/10.1021/acspolymersau.4c00022
ACS Polym. Au 2024, 4, 342−391

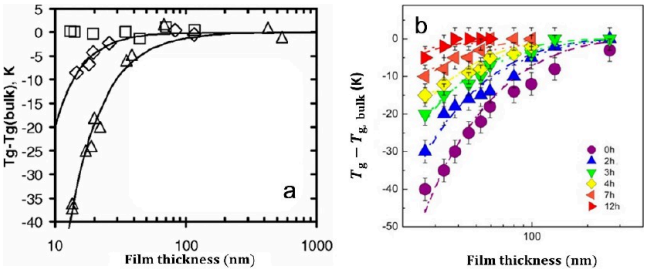

Figure 3. (a) Scenarios to reduce the polymer film thickness-T_g confinement effect by (a) the addition of small molecule diluent plasticizer showing a shift in T_g in pure PS (M_n = 263 kg mol^{-1}) (triangles), 2 wt % (diamonds) and 4 wt % (squares) dioctyl phthalate (DOP) diluents in pyrene labeled PS films. The solid curves are the least-squares fits using the empirical relation proposed by Keddie et al.[14] [Reprinted figure with permission from ref 50. Copyright 2004 APS.] (b) Thermal annealing showing shift in T_g in poly(4-*tert*-butylstyrene) (PTBS) film (M_n = 70 kg mol^{-1}) as a function of film thickness and the annealing time at 453 K. [Reproduced from ref 74. Copyright 2017 ACS.]

DOP plasticized thin confined films revealed that viscosity[75,76] and modulus[75] decrease as expected by the dilating softening effect by the plasticizer, it additionally leads to enhancement of molecular recoiling stress[75] in the polymer film stemming from preparation induced out-of-equilibrium polymer chain conformations. In a completely different scenario, Perez-de Eulate et al.[74] observed the confinement effect could be completely removed by annealing supported poly(4-*tert*-butylstyrene) (PTBS) films. On annealing, the polymer chains get irreversibly adsorbed to the Si/SiO$_x$ substrate surface. This pinning of chain segments to the substrate surface likely results in slowing down of the free volume diffusion from the surface of the polymer films to the substrate, which can affect the mobility of chains, resulting in the removal of the confinement effect in annealed films (see Figure 3(b)). This supports the vast studies by Napolitano and co-workers on the irreversible adsorption perturbing T_g of thin confined polymer films.[19] The segmental relaxation time of thin poly(4-chlorostyrene) (P4ClS) film reaches the bulk segmental relaxation time after annealing for time scale comparable to that of adsorption.[77] The irreversible adsorption has been identified as a mechanism of equilibration for spin-coated polymer thin films. The relaxation of spin-coated films does not depend on the segmental mobility of the entire film but on the relaxation modes promoting interfacial adsorption.[77] The kinetics of irreversible adsorption onto a substrate reveal two adsorption regimes. A linear regime with a constant rate of adsorption is followed by a logarithmic regime.[78] The transition is characterized by a crossover time (t_{cross}) and critical adsorption thickness (h_{cross}). The t_{cross} is M_w-independent and h_{cross} is T-independent. The crossover at t_{cross} occurs as the polymer−substrate pair achieves a critical surface coverage.[78] For adsorption time $t < t_{cross}$ the rate of adsorption is proportional to the monomer pinning rate. However, in the logarithmic regime, the rate of adsorption is additionally dependent on the interaction potential between the polymer and substrate.[79] This was confirmed by the difference in the behavior of the temperature-dependent adsorption rate and temperature-independent final adsorbed layer thickness when investigating PS, P4MS, and PTBS.[79] The equilibrium adsorbed amount is found to decrease with a decrease in the thickness of the polymer film. However, the value is dependent on the effective Hamaker's constant rather than the presence of a free surface.[80] Varying the thickness of the top layer of a bilayer polymer can result in an equilibrium adsorbed amount similar to that obtained by reducing the thickness of a single layer polymer film.[80] Rodríguez-Tinoco et al.[81] compared the presence of interfacial contacts at the substrate interface to obstacles that will affect the transport property at the interface. Increasing the amount of adsorption correlated with reduced translation diffusion coefficient for a tracer when investigated using dielectric spectroscopy. It was found that polymer films having the same thickness with varying annealing times can result in varying translation diffusion coefficients of the probes.[81] In addition to the Napolitano group, Koga and Tsui groups have contributed to the information available on the effects of adsorbed layers. While Koga and co-workers focused on the effect of the adsorbed layer on localized viscosity, Tsui and co-workers tuned the substrate−polymer interaction by chemical modifications and also investigated the effect of adsorbed layers on surface monolayer T_g. The local viscosity at the polymer−substrate interface was found to be higher than the bulk of the film.[82] The viscosity of the polymer film at the free surface was found to be 30% lower than the rest of the film.[83] As the magnitude of depression in T_g due to confinement could not be correlated to the reduction observed for viscosity, a decoupling between the T_g and viscosity under confinement could be inferred and hence the reduced viscosity at the free surface was attributed to the reduced entanglement at the free surface of the polymer film rather than the effect of a decreasing T_g due to confinement.[83] The presence of viscosity gradient in thin polymer film gave thrust to investigate the T_g at the substrate interface. This brought to light the presence of two T_gs for the adsorbed layer.[84] Such a result was observed irrespective of the nature of the interaction of the polymer with the substrate. Both PS and P2VP were found to show a bulk-like T_g and a higher $T_{g,high}$. The observed T_gs had a difference of 80−100 °C between them.[84] The local viscosity at the substrate interface was also higher for both PS and P2VP which was attributed to the presence of dead layers at the polymer−substrate interface. It was thus established that even weakly interacting polymer−substrate pairs have the ability to form irreversibly adsorbed layers.[84] Such an irreversibly adsorbed layer has the potential to even perturb the T_g of the surface monolayer in the polymer film. Yan et al.[85] showed that the confinement effect observed for surface monolayer T_g (T_g^{surf}) in PS thin films could be eliminated by performing thermal preannealing. The adsorption kinetics of polymer chains matched well with the time required for the saturation of T_g^{surf} value to the thick film T_g. By tuning the interaction of the polymer−substrate pair, the effective viscosity of a substrate-supported polymer thin film could be modified. UVO treatment of PS just for a second has been shown to increase the effective viscosity with a reduction in film thickness. The effect was observed for both Si−H substrates and Si−OH substrates. Without the UVO treatment, PS showed a decreasing trend of effective viscosity in reducing the film thickness.[86] The so-called dead layers near the substrate interface proved to be not so dead by showing a higher thermal expansion coefficient.[87] In addition it has been observed that the polymer chains at the free surface can get exchanged with the adsorbed layer chains.[88] The ability of the adsorbed chains to undergo desorption even from the flattened layer which is expected to be adsorbed at a maximum number of points with the substrate and get exchanged with the free polymer chains from above the adsorbed layer is against the conventional understanding of irreversible adsorption.

https://doi.org/10.1021/acspolymersau.4c00022
ACS Polym. Au 2024, 4, 342−391

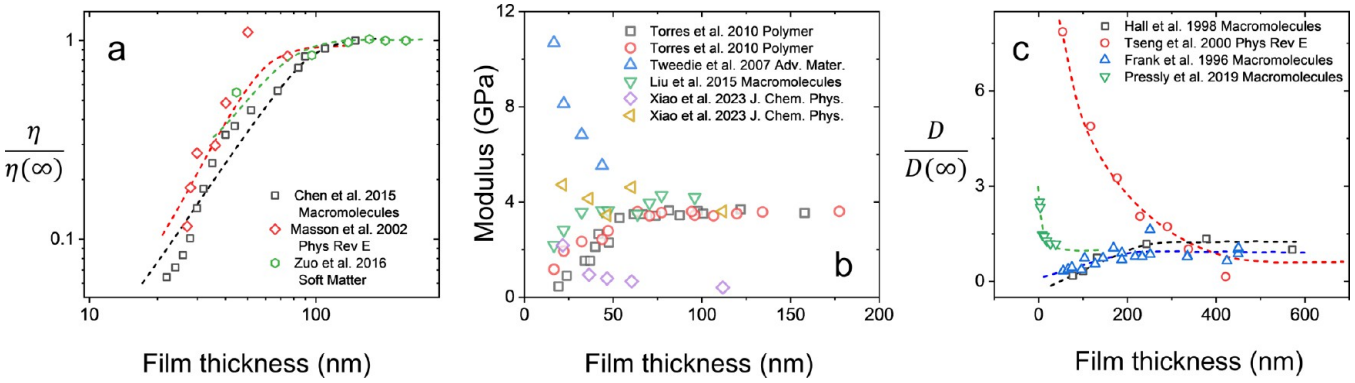

Figure 4. (a) Variation of polymer thin film viscosity (η) normalized by bulk polymer viscosity ($\eta(\infty)$) upon varying the thickness of the PS films using PSD[98] (PS, M_w = 940 kg/mol), dewetting[99] (PS, M_w = 130 kg/mol) and wetting ridge[100] (PS, M_w = 442 kg/mol) techniques. The dashed lines are guides to the eye. (b) Confinement effect on the modulus of thin PS films. The squares and circles are data using wrinkling[101] of PS, M_w = 990 kg/mol and 9.4 kg/mol, respectively. The triangles are data from the Indentation technique[10] (PS, M_w = 12 kg/mol). The inverted triangles are data from TUTTUT[102] (PS, M_w = 136.5 kg/mol). Diamonds and the left triangle are for data from the bubble inflation technique[103] (PS, M_w = 350 kg/mol); only diamonds show the rubbery modulus values, while all the other data sets in Figure (b) are glassy modulus values. (c) Variation in translational diffusion coefficient value normalized with the bulk diffusion coefficient for films of reducing thickness from probe diffusion in PS. Squares (M_w = 121 kg/mol),[104] circles (M_n = 347 kg/mol),[105] triangles (M_w = 31 kg/mol),[106] inverted triangles are simulation data by Pressly et al.[107] [Data from refs 10, 98−107.]

The above discussion clearly indicates processing protocols such as annealing and plasticization, which are known to impact the rheology of polymers, have a direct impact on the polymer film thickness−T_g related confinement scenario.

Viscosity, Modulus, Relaxation, and Diffusion

Discussion about the dynamic nature of glass transition in the previous section brings us to a common practice of defining T_g as the temperature where the polymer chain segmental relaxation dynamics (τ) is ∼100 s.[21,89] On approaching T_g from the liquid state, over a small range of temperature close to the glass transition, orders of magnitude increase in the relaxation time, i.e., slowing down of dynamics can be observed. Thus, a definition based on the segmental relaxation time signifies the typical time scale for a T_g to be defined in the laboratory time scale. This is a typical scenario in disordered materials exhibiting molecular motion beyond atomic vibrations, markedly different from crystalline solids. Thus, the time scale of relaxations should be intricately linked to the rigidity (representative of G, the shear modulus) and viscosity (η) of the glassy polymers.[21] It is quite instructive to define a glass with a rigidity that results from the freezing of a liquid of certain "viscosity" that connects the "time scale of thermal fluctuations" (τ) via the mechanical Maxwell model ($\eta = G{\cdot}\tau$) in their viscoelastic state.[21] In simple liquids, the time scale of thermal fluctuations shows an Arrhenius dependence. Such a behavior can be expected from liquids, including both simple liquids and polymers. Glassy polymers show such an Arrhenius dependence of fluctuations above the Arrhenius crossover temperature (T_A). Below T_A, the α-relaxation is dominant and the relaxation times associated with the thermal fluctuations and hence the viscosity of the glassy polymers become more temperature-dependent. They follow a super-Arrhenius behavior, expressed by VFT and WLF laws.[8,21] In addition to the primary α-relaxations which involve cooperative motion, there are secondary relaxations (β, γ), which involve the noncooperative motion of segmental units or side branches. While the α-process can be described by WLF or VFT behavior, β and γ processes follow an Arrhenius behavior. In the case of polymer chains, the β-process is considered the local mode of motion which occurs near "islands of mobility,"[90] whereas the α-process involves segmental or monomer level flow.[21] Below T_g, the α-relaxations are arrested but not the β- and γ-relaxations. At temperatures well above T_g, the β-relaxations merge with theα-relaxations and are not distinguishable. Recently another mechanism of relaxations has been observed via experiments for a large class of materials including small organic molecules in addition to polymers.[91] Named the slow Arrhenius process (SAP), it is found to be active above and below the T_g.[92] The SAP has temperature-independent activation energy spanning temperatures ranging from below T_g to well above it and has been found to follow the enthalpy−entropy compensation rule.[93] The SAP peak from the dielectric measurements has been found not to merge with the α-peak, distinguishing SAP from other Arrhenius relaxation mechanisms like β- and γ-relaxations. However, the preparation conditions of the polymer films have been found to affect the intensity of the SAP peak.[94] Comprehensive investigations on a large class of materials and processes are required to explore the SAP, which is likely the most probable sub-T_g relaxation mode in PS.

Understanding what kind of molecular motions are associated in the polymers above the glass transition temperature until the reptation time (τ_{rep}) requires a holistic view of varying length scales and time scales. Maintaining a polymer above the glass transition temperature activates the α-relaxation; the rate of relaxation is determined by the size of the CRR, which depends on the temperature at which the polymer is maintained.[21] The α-relaxation operates in the length scale associated with the CRR, and polymer chemistry plays an important role in this length scale. The time scales associated with the relaxations in this length scale are large due to the requirement of the coordinated motion between the segmental units.[21,54] Kuhn segments[54] can be considered the sequentially next larger length scale of interest. Considering the individual polymer segments that relax to have the size of Kuhn length, the chemistry of the polymer is not important in this length scale. Considering Kuhn length essentially makes the chain a freely jointed chain that does not correlate with the motion of corresponding segmental units (Kuhn segments). In this length scale, the Rouse modes[54] can be expected to be active. The absence of drag from the neighboring segments for relaxation results in faster time scales associated

https://doi.org/10.1021/acspolymersau.4c00022
ACS Polym. Au 2024, 4, 342−391

with the Rouse modes. Zooming out from the length scales further in entangled polymers helps us to view the collective Rouse action resulting in the reptation motion of the polymer chains.[54] The reptation of the polymer chains out of the confined entanglement tube results in a pure viscous polymer flow after reptation time.[54] This summarizes the simultaneous processes occurring in the polymer when held above the glass transition temperature until τ_{rep}. All the relaxation times in all Rouse modes having similar dependence on the temperature results in the expectation that the linear viscoelastic data taken at all temperatures can be superimposed on each other by applying a shift factor. This is known as the time−temperature superposition.[8,21,54]

In another way, the presence of a "characteristic time scale and length scale" along with a temperature (for glass transition) invokes the possibility of relating those simply by a stochastic process, which could be none other than molecular diffusion. Diffusion of a probe of size r is classically associated with the viscosity η of the medium via the Stokes−Einstein (SE) relation:

$$D_T = \frac{k_B T}{6\pi r \eta} \tag{3}$$

where D_T is the diffusion coefficient for translational motion. This relation is ideally valid for polymer melts at equilibrium and usually breaks down upon supercooling close to the glass transition. A critical temperature has been reported[95,96] as ≈1.2 T_g such that when the temperature is $T_g < T < 1.2\ T_g$ the SE and Debye−Stokes−Einstein (DSE) equations breakdown. It has been generally observed that there is an anomalous increase in the translational diffusion coefficient close to T_g.[97] There are two prevalent approaches to explain the observed phenomenon based on the framework of the coupling model, on how the different variables affect intermolecular cooperativity by having different coupling factors.

As we cross over to the confined polymer regime, it can be observed that in addition to the variation shown from the bulk value of glass transition temperature, as discussed before, the mechanical and rheological properties can also be observed to vary with film thickness. In the literature of confined thin polymer film glassy dynamics, "mobility" has been introduced as a term that "loosely" considers all types of relaxation processes that could affect the properties of the polymer. In all those cases, enhanced mobility is largely correlated with reduced T_g and vice versa. Figure 4 shows how the confinement of PS films to very low thickness affects the mechano-rheological properties (here viscosity, modulus, and diffusion) of the polymers. Independent of the technique used to probe, the viscosity and modulus can increase or decrease compared to the bulk polymer properties. The viscosity data in Figure 4(a) has been compiled from the dewetting technique,[99] wetting ridge technique[108] and PSD technique.[98] The increased mobility of the surface layer is thought to influence the entire film as the thickness of the film decreases, resulting in reduced viscosity. The modulus values in Figure 4(b) also get perturbed with a reduction in film thickness due to the mobile surface layer. However, the indentation studies by Tweedie et al.[10] reported increased modulus values. The bubble inflation technique has identified an increase in rubbery modulus value as the thickness of the film reduces. The perturbation of properties due to the confinement and film thickness extends even to the diffusion of the probe in a polymer matrix. Majorly explored using the fluorescence technique, the translational diffusion coefficient has been found to both increase and decrease with reducing thickness for PS films (see Figure 4(c)). Hall and Torkelson[104] utilizing fluorescence nonradiative energy transfer between donor and acceptor fluorescence dye molecules found a decreasing probe dye diffusion coefficient upon reducing the PS film thickness atop fused quartz substrate. In contrast, diffusivity did not change for PIBMA and P2VP films upon film thickness reduction. Similarly, Frank et al.[106] found a decrease in diffusion coefficient by following the periodic distribution of the fluorescent probes after having the sample photobleached at alternate sections in the film. However, Tseng et al.[105] found an increase in the translational dye diffusion coefficient upon decreasing PS melt film thickness compared to the bulk value. The effect started to appear as high as $20R_g$ of the polymer. A comparable decrease in calculated free volume and thermal expansion coefficient upon film thickness reduction explained this. A simulation study by Pressly et al.[107] also obtained similar film thickness dependence of diffusivity primarily attributed to the reduction in entropic barriers for relaxation in nanoconfined films.

Since the effective surface available for the diffusion of free volume holes in polymer thin films and polymer-nanocomposites has been correlated to the shift in T_g,[110] one can extrapolate the idea where reduction in tracer diffusion in polymers could be a result of a different distribution of free volume holes, not allowing their diffusion as efficiently as in bulk.[44] Such a condition could be, for example, achieved via a discontinuous packing density in polymers, such as in thin irreversibly adsorbed layers in the substrate, characterized by nonequilibrium polymer chain conformations rich in free volume, reducing upon further adsorption of chains.[44] With this idea in mind, recently, Napolitano and co-workers showed tracer diffusivity is not a mere function of the polymer film (matrix) thickness[109] but is dependent on the adsorbed amount of polymer. Adsorption of more chains, such as by thermal annealing, yields a reduction of the diffusion coefficient and consequently longer diffusion times through the dead adsorbed layer connected to the free volume hole diffusion. This is supported by them through a "density of obstacles" idea,[109] where the amount of surface free from obstacles (that is free from chain adsorption, Φ_N) promotes diffusion (see Figure 5). So, the degree of chain adsorption (adsorption of more chains) onto the substrate yields a reduction of the diffusion coefficient and, consequently, longer diffusion times through the dead adsorbed layer.

The elastic modulus of a solid is a measure of its stiffness and is related to the energy density of the bonds within the molecules. Beyond a popular customary definition of elastic modulus, as a quantity that relates tensile stress to tensile strain, it is also a measure of the density of strong or weak bonds defining the material as "stiff" or "floppy", respectively. Considering elastic modulus in terms of energy densities is advantageous as it makes it clear that even when material flows densely over a long time scale showing a macroscopic distortion, it still can have an instantaneous elastic response, sustaining a possible finite shear stress temporarily. This idea of response (relaxation) in time-dependent material behavior is viscoelasticity, an important property of polymers around the glass transition.[8] For geometrically confined thin polymer films, the realization of the material state is further complex due to their thickness and interfacial interaction dependent altered thermal stability and molecular level structures (e.g., polymer chain conformation and entanglement). In case T_g defines the thermal stability of a polymer film, the first thing that should come to our mind is

https://doi.org/10.1021/acspolymersau.4c00022
ACS Polym. Au 2024, 4, 342−391

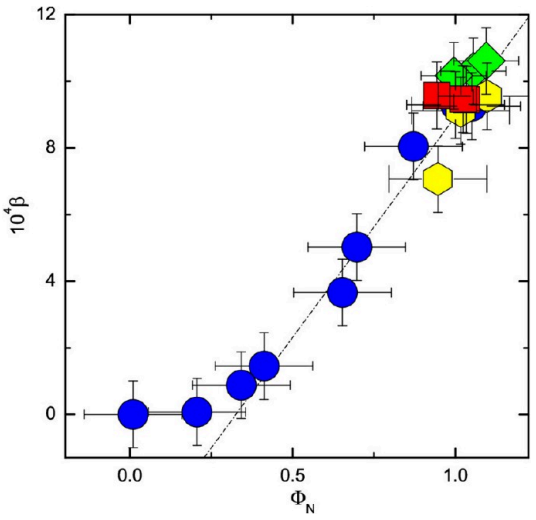

Figure 5. Reduction in tracer diffusion coefficient with respect to bulk value as a function of the effective surface not occupied by obstacles. Φ_N was obtained by normalizing the drop in dielectric strength measured after a sufficiently long time to the value measured in 3.8 nm thin samples of PS 97 kg/mol. Symbols are for varying PS molecular weights: 97 kg/mol (blue circles), 160 kg/mol (yellow hexagons), 640 kg/mol (green diamonds), and 932 kg/mol (red squares). Symbols are for varying PS molecular weights; 97 kg/mol (blue circles), 160 kg/mol (yellow hexagons), 640 kg/mol (green diamonds), and 932 kg/mol (red squares). [Reproduced from ref 109. Copyright 2020 ACS.]

whether the film thickness-dependent T_g-reduction scenario also applies to mechanical stability, signifying a comparable trend in terms of stiffness and deformation. But then, we should be interested enough to check why one should expect a correlation among those properties. The way polymer mechanics progressed well-defining few bulk rules paved the way for such correlations, namely time−temperature superposition of rheological data sets, where temperature-dependent shear modulus can be shifted to a master curve, as long as the viscoelastic response is in the linear regime, and broadly all of the viscoelastic material properties are interrelated.[8,21,54] However, there are instances in which changes in T_g upon confinement do not appear to be correlated with their mechanical properties.[72,111,112]

Decoupling of Glassy Dynamics in Polymer Thin Film Confinement

The anomalous T_g depression observed in thin polymer films led to a series of investigations to confirm the presence of faster segmental dynamics. This would mean that glass transition probed via dynamic and thermodynamic techniques remains the same. Fukao and Miyamoto[49] on investigating the dynamic T_g, observed that the peak of the dielectric loss curve happens at the same temperature for reduced PS film thicknesses until a M_w dependent critical thickness (ca. 10 nm for PS, M_w = 280 kg/mol) is reached. This critical thickness is much lower when compared to the thickness at which a confinement effect is shown in thermodynamic T_g. The result proved that the thermodynamic T_g is decoupled from the segmental dynamics. However, they observed a broadening of the peak at which maximum dielectric loss occurs.[49] The broader range of the α-relaxation times is the effect of reducing thermodynamic T_g. The absence of a peak shift compared to the bulk reveals the bulk-like segmental dynamics in the film. Several later investigations confirmed the presence of bulk-like segmental dynamics for polymer films under confinement.[110,113−115] The decoupling of thermodynamic T_g and the segmental dynamics in confined films foiled attempts to explain the well-documented anomalous variation in T_g with film thickness by way of segmental relaxation. This led Boucher et al.[115] to put forward an explanation for the variation in T_g of confined PS thin films via free volume hole diffusion theory (FVHDT). According to this theory, the glass transition happens at a temperature when the free volume holes present in the film cannot travel up to the free surface of the film to annihilate.[115] Confined films have a larger percentage of the free surface, which makes it easy for the free volume holes to travel to the surface and annihilate. This can effectively reduce the glass transition temperature of the thin film. Recently, Zha et al.[116] showed that the activation energy for free-volume hole diffusion is inversely proportional to the thickness of the film. Xu et al.[117] showed the decoupling between thermal expansivity and the T_g of PMMA films. While thermal expansivity and T_g were sensitive to the reduction in film thickness, only T_g was very sensitive to the substrate effect. This was attributed to the expansion of the free-volume holes near the free surface of the PMMA films.[117] At the free surface, the film is in contact with the air interface, which can be assumed as a reservoir of free volume. Hence, the free-volume holes near the air interface are swollen, increasing thermal expansivity.[118] The reduction in thickness will result in an increase in the fraction of the free-surface area in the polymer film and, hence, will result in an increase in thermal expansivity. The lack of free-volume addition at the substrate interface makes thermal expansivity insensitive to the substrate interaction.[117]

Another important decoupling observed in polymer films is the translational diffusion being decoupled from rotational diffusion. Cicerone and Ediger[119] used a holographic fluorescence technique to find out the translational diffusional coefficient for different probes in supercooled *o*-terphenyl, though it is not a polymer. They found a decoupling in the translational and rotational diffusion. An enhancement was observed in the translational diffusion coefficient near T_g. The translational diffusion was found to have a weak temperature dependence, while the rotational diffusion coefficient showed a strong temperature dependence. The same effect was observed by Deppe et al.[120] using a novel fluorescence nonradiative energy transfer technique in polymer films. The diffusion of small molecular probes in poly(isobutyl methacrylate) (PIBMA) and poly(ethyl methacrylate) (PEMA) was investigated. Both groups attributed the decoupling behavior to the spatial heterogeneities present in the film. Mandel et al.,[97] using a single-molecule fluorescence technique found a 400 times higher than expected increase in translational diffusion in PS thin films near the T_g which was decoupled from the behavior shown by the rotational diffusion coefficient. Other researchers also observed the decoupling between translational and rotational diffusion in thin polymer films.[95,121−123] Irreversibly adsorbed layers of PS showed differences in behavior comparing segmental relaxation and translational tracer diffusion.[109] Segmental relaxations remain the same as in bulk, but the translational diffusion is reduced tremendously.[109]

Probing the effect of geometrical confinement on viscosity in thin polymer films showed a decoupled behavior in the viscosity−film thickness−glass transition temperature nexus. According to Bodiguel and Fretigny,[124] PS film's viscosity is reduced as the ratio h/R_g decreases, where h is the film thickness. However, this reduction in viscosity cannot be coupled with the reduction in T_g shown by supported thin films.[124] The reduction

https://doi.org/10.1021/acspolymersau.4c00022
ACS Polym. Au 2024, 4, 342−391

in T_g in supported thin films is not M_w-dependent; however in free-standing films, it has shown a M_w-dependence.[125] However, the work by Ellison et al.[126] showed that even M_w's lower than the entanglement molecular weight showed a M_w-independent confinement effect. Thus, establishing that the genesis of the confinement effect is not related to the degree of chain end segregation or entanglement density but majorly due to the effect of interfaces.[126] Boucher et al.[55] and Keddie et al.[14] have showed the independence of confinement effect on M_w in high M_w polymers. In no experiment the reduction in T_g has been observed for film thicknesses higher than 100 nm for PS films. In the case of viscosity, a reduction has been observed in PS films even for $h/R_g \approx 7-8$.[124] Contrary to the above observations, investigations showed increased viscosity upon increasing the confinement.[82] Li et al.[127] obtained 3−4 times higher viscosity in thin PS films than in bulk through three different techniques. By measuring the capillary rise of styrene−butadiene-styrene block copolymer on a patterned cross-linked polydimethylsiloxane (PDMS) substrate, Suh et al.[128] showed an increase in viscosity as the copolymer film thickness reduced from 500 to 200 nm. This increase was temperature-dependent, as the reverse was observed at higher temperatures. Using the bead−spring model in molecular dynamics simulations Khare et al.[129] showed that as the thickness of the film decreased, there was an increase in the effective viscosity. Tsui and co-workers[111] used fluorescence recovery after photobleaching (FRAP) to compare the self-diffusion of PS and PIBMA as supported films to find a decreasing trend in effective viscosity upon confinement due to the reduction of film thickness, while their diffusion coefficient stayed invariant. Chowdhury et al.[72] using noncontact capillary nano shearing (NCNS) and Flash nanocalorimetry experiments in thin PNBMA films showed the T_g and intrinsic molecular mobility were coupled, leading to no film thickness-dependent variation, whereas, layer-resolved shear mobility was enhanced with a reduction in film thickness, leading to a decrease in the effective viscosity.[72]

Elastic modulus is also decoupled from the glass transition temperature trend in polymer thin films. Torres et al.[130] using the wrinkling technique showed that, for varying M_w's, thin PS films showed a decrease in elastic modulus lower than 30 nm film thickness. On increasing the quench depth ($T_g - T_{exp}$) of the experimental T_{exp} from T_g, the films showed commencement of confinement effects at higher film thicknesses.[130] Chang et al.[131] found no variation in elastic modulus upon the PS and PMMA film thickness variation. However, unlike in the case of Torres et al.,[130] Chang et al.[131] found an increase in elastic modulus on decreasing the film thickness for sub-R_g films. Askar and Torkelson[132] using the fluorescence technique showed increased stiffness for PS films when the film thickness was lower than 100 nm. The dominating effect of the substrate in controlling the stiffness compared to the free surface was hypothesized as the reason for such an effect. Xiao et al.[103] using the bubble inflation technique showed that the glassy compliance of PS films was invariant with the film thickness while the rubbery stiffness increased upon confinement. Kim et al.[133] using the Brillouin light scattering (BLS) technique observed that under 3-D confinement of PS into nanoparticles, the mobility of the surface segments of the nanoparticle was enhanced, resulting in the softness of the nanoparticles. However, there was no variation in T_g.

Spin-Coating Induced Molecular Recoiling Stress in Nonequilibrated Polymer Thin Films

Polymers, due to their long chains, are an entropy-dominated system that will always try to attain a state where it can minimize the free energy. However, while processing the polymers for specific needs, techniques like extrusion align chains, which trap the polymer in a nonequilibrium state.[17,33,134,135] Depending on the energy available, the polymer will gradually try to achieve its equilibrium state. In the context of thin polymer films, a similar effect is observed. Spin-coating is a technique commonly used to prepare thin polymer films. Hence, understanding the spin-coating process can better understand the nonequilibrium of thin polymer films.

The spin-coating technique comprises broadly four stages associated with the substrate rotation on top of which the polymer film is deposited from solution. The initial stage is the dispensing stage, which can be categorized as static or dynamic. In static dispense, a solution puddle is deposited onto the substrate surface, covering the entire area to enhance coating coverage. On the other hand, dynamic dispensing involves rotating the substrate at a low rpm before pouring the solution. It requires less solution as it results in uniform coverage with a minimum amount of the solution. Subsequently, the substrate enters the acceleration stage, where excess solution is expelled, and volatile solvents begin evaporating. This stage can lead to a significant solvent loss, up to 50% evaporating during substrate acceleration.[136] Controlling the acceleration of the substrate allows for tuning the film thickness. After reaching the desired spin-coating speed, the substrate enters a fluid thinning regime where viscous forces dominate, gradually reducing the film thickness. After this, solvent evaporation becomes dominant at a constant substrate rotation speed. During this stage, viscosity effects are limited, as the rapid loss of solvent prevents adequate flow. The film is considered prepared when solvent evaporation is complete.

By applying the principles of spin-coating to polymers being coated from a solution, a better understanding of the transformations happening to the polymer can be gained. In the acceleration stage, volatile solvents evaporate as the excess solution is expelled from the substrate. Subsequently, this swift solvent elimination leads to a decrease in the solvent concentration in the solution. Polymer chains, previously flexible in adopting various conformations in the solution state, now face constraints in achieving specific equilibrium conformations. This phenomenon can be elucidated by examining the manipulation of the polymer's glass transition temperature in solution.

When the polymer is in a solution, it is well above its glass transition temperature (for polymers having T_g above room temperature), quickly allowing the adoption of equilibrium conformations based on the prevailing conditions. However, as the solvent concentration decreases and approaches the critical solvent concentration (approximately 20%), the polymer's glass transition temperatures in the remaining solution become closer to room temperature. This leads to the freezing of polymer chain conformations. Further spinning will not result in substantial changes in polymer chain conformations; hence, the chains get locked in their nonequilibrium conformations. Reiter and de Gennes delved into the intricacies of the spin-coating process, uncovering the peculiar phenomenon of thickness augmentation in ultrathin films during and after spin-coating.[136] This unusual thickness increase in ultrathin films is explained by the shape memory effect displayed by the films. They systematically

https://doi.org/10.1021/acspolymersau.4c00022
ACS Polym. Au 2024, 4, 342−391

classified the thin film behavior into distinct stages,[136] commencing from when the polymer chains are immobilized.

As the solvent concentration drops as spin-coating proceeds, a compact structure starts forming. At critical solvent concentration, the chains get immobilized and create a rigid network. Such a condition where the film prevents further large-scale contraction is called the α-stage.[20] As the remaining solvent molecules are also removed and solvent concentration approaches zero value, the monomers replace the space previously occupied by the solvent, resulting in further compaction. This is the β-stage. Such squeezing of the network is also associated with a distortion energy with a rigidity constant for the network (K). On storing the polymer films, they will try to achieve its initial network structure when the solvent fraction is at a critical solvent fraction, i.e., the α-stage. This pumping-out stage is called the γ-stage. Thus, it has been shown that the polymer thin films have a memory of the initial frozen-in structure and would try to return to that structure over time.[20] Polymer films are generally expected to remain a compact structure and such a pumping out of the chains back to the α-stage resulting in increasing thickness is abnormal, yet found in PS films.[136−139] This anomaly is thus a manifestation of the nonequilibrium nature of the spin-coated films. Nonequilibrium in thin polymer films has also been seen to modify their rheological behavior.

As discussed previously, the nonequilibrium nature can be induced into the polymer thin films by spin-coating resulting in preparation-induced residual stress or molecular recoiling stress.[18,31,75] Such an effect can be considered analogous to the entropic spring effect in polymers, where stretching the polymer chains results in a restoring force that tries to achieve the coiled nature of the chains, leading to a possible recoiling upon appropriate relaxation. Major investigations regarding the nature and behavior of molecular recoiling stress were conducted using dewetting,[18,31,75] wrinkling,[140] and fluorescence techniques,[141] which will be explained in subsequent sections while introducing each technique separately. These techniques can be used to quantitatively and qualitatively determine the value of molecular recoiling stress in the polymer film. The magnitude of molecular recoiling stress is a function of polymer molecular weight, film thickness, and preparation conditions.[32,134,142] High molecular weight polymers lead to more significant molecular recoiling stress in films of similar thicknesses. Hence, contrary to the simple picture of viscosity and polymer molecular weight,[8,54] ultrahigh molecular weight polymer films can even flow (dewetting hole growth dynamics) at a higher velocity when heated over a nonwettable substrate.[142,143] Films having a lower thickness are found to have a higher magnitude of molecular recoiling stress.[135,142] The magnitude of the molecular recoiling stress can be modified by varying the spin-coating speed while preparing the films.[18,134] Much earlier than the polymer chain reptation time, relaxation of molecular recoiling stress can happen by physical aging[31,32] or by thermal annealing,[142] below and above the glass transition temperature of the polymer, respectively. This relaxation temperature dependence is Arrhenius in nature. The activation energy calculated was ≈100 kJ mol^{-1}. Since the activation energy was close enough to the activation energy of the β-process,[32] it was initially assumed that the relaxations happen via the β-relaxations. However, since the activation energy for the β-process cannot exceed $24RT_g$, which is ca. 75 kJ/mol for PS, the probability for a relaxation pathway dominated by other relaxation mechanisms cannot be neglected. Recently, the Napolitano group introduced the concept of a slow Arrhenius process (SAP),[92] which is active above and below glass transition and has an activation energy close to 100 kJ mol^{-1}. Thus, the relaxation of molecular recoiling stress could also be thought to relax through the SAP route. Although by annealing the molecular recoiling stress is found to relax, the Chowdhury group using an entropy generation approach showed that the relaxation of molecular recoiling stress may not happen in a single step and that the equilibrium might be achieved only through a series of metastable states.[18]

CHARACTERIZATION METHODOLOGIES

Power Spectral Density

Power spectral density (PSD) as a mechano-rheological probe is a technique that uses the morphological evolution of spin-coated thin polymer films on annealing to extract the rheological (viscosity, plateau modulus) properties of thin polymer films.[144,145] The spin-coating of films results in smooth surface morphology and uniform thickness, which, on annealing, evolves toward equilibrium via the formation of surface capillary waves and fluctuations due to thermal noise,[145] as shown in the schematic in Figure 6(a). The morphology is captured at

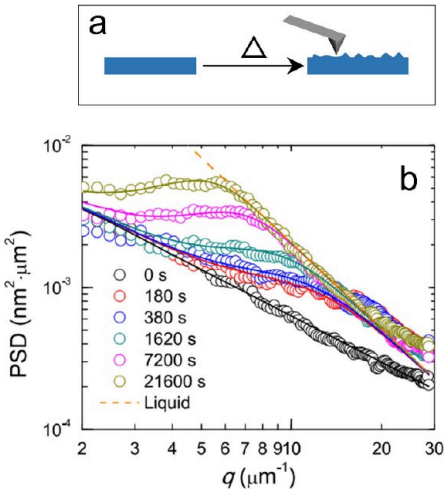

Figure 6. (a) Schematic showing the evolution of surface morphology from a spin-coated smooth surface to a surface populated with capillary waves. (b) Illustration of a representative set of PSDs[148] obtained from a PS film (M_w = 451 kDa, thickness = 23 nm) 1 s UVO-exposed and annealed at 172 °C for different times. [Reproduced from ref 148. Copyright 2019 ACS.]

different times using an Atomic Force Microscope (AFM) in tapping mode. Since the height data is not a pure sine wave, there would be leakage to adjacent frequencies when Fourier transformed. Hence a data windowing technique such as Welch windowing[146,147] should be used before performing the Fourier transform. After Fourier transformation, the data is radially averaged to get the PSD.[145] A representative set of PSDs has been shown in Figure 6(b) reproduced from Yu et al.[148] The figure shows the evolution of PSD as a function of annealing time for PS film. The peak in the PSD curve corresponds to the dominant wave vector in the sample.

According to the capillary wave theory, the surface of a liquid at equilibrium should be populated with thermally excited capillary waves with power spectral density determined by the equipartition law:[144,149]

https://doi.org/10.1021/acspolymersau.4c00022
ACS Polym. Au 2024, 4, 342−391

$$A_q^2(\infty) = \frac{k_B T}{\gamma q^2 - \frac{A_{eff}}{2\pi h_0^4}} \quad (4)$$

where T, h_0, γ, and A_{eff} are, respectively, the temperature, average thickness, surface tension, and effective Hamaker constant of the film; q is the wave vector, k_B is the Boltzmann constant and the $-A_{eff}/(2\pi h_0^4)$ term in the denominator arises from the van der Waals potential of the film.[144] When heated above the glass transition temperature, T_g, the film surface roughens as the film begins to evolve toward equilibrium. In the absence of any external force, equilibration takes place by thermally excited random motions, whereby the correlation function of the system order parameter evolves according to the solution to the Langevin equation:[150−152]

$$A_q^2(t) = A_q^2(0) + (A_q^2(\infty) - A_q^2(0))(1 - e^{2\Gamma_q t}) \quad (5)$$

In the lubrication approximation, Γ_q is given by[153,154]

$$\Gamma_q = \frac{h_0^3 q^2}{3\eta}\left(\gamma q^2 - \frac{A_{eff}}{2\pi h_0^4}\right) = \frac{h_0^3 q^2}{3\eta}\frac{K_B T}{A_q^2(\infty)} \quad (6)$$

where η is the viscosity of the film. Using the asymptotic limits of $A_q^2(t)$, an interpolation approximation of $A_q^2(t)$ can be derived as[144]

$$A_q^2(t) - A_q^2(0)\Theta(q^* - q) \cong \frac{k_B T}{\gamma q^2 - \frac{A_{eff}}{2\pi h_0^4} + \frac{3\mu_0}{h_0^3 q^2}} \quad (7)$$

where $\mu_0 \equiv \eta/2t$ and $\Theta(q^* - q)$ is the Heaviside step function, q^* is the wave vector, where $\Gamma_q t = 1$. Even if the polymers are entangled and viscoelastic, eq 7 can be used, but μ_0 vs t should remain as a plateau and $\mu_0 \equiv \eta/2t$ would recover only after the reptation time (τ_{rep}).[144]

Initial investigations using PSD were focused on unentangled polymers. The plateau modulus calculated for thin PS films was 100-fold lower than the bulk value, while the viscosity achieved bulk value on annealing.[144] This led to the inference that the metastable chain structures may not have a prominent effect on the relaxation behavior of the thin unentangled polymer films. This is because while probing the surface capillary waves, no deviations were found between the surface relaxation of the films and that expected from the thermal excitation of capillary waves.[144]

A shift in the cutoff wave vector in the PSD curve can be observed for polymers annealed at varying times. This was attributed to the thermal noise in the system.[145] In the absence of thermal noise, the maximum in the PSD curve at varying times should happen at the same cutoff wave vector. Later Lam et al.[155] using adiabatic approximation derived the expressions for PSD of homogeneous supported films incorporating the thermal noise. The derived expressions were based on the conditions that the amplitude of fluctuations was much smaller than the height of the film and that the wavelength of the fluctuations was much larger than the film thickness.

Yang et al.[70] found that for unentangled liquid-like polymer films, the Kauzmann temperature (T_K) followed a thickness dependence by fitting the effective viscosity data calculated from the PSD curves to the Vogel−Fulcher−Tammann (VFT) equation. The thickness-independent viscosity of the films having thicknesses below 9 nm, helped them introduce a two-layer model to explain the mobility in thin polymer films. According to them, the mobility of the polymer film had two components. One is due to the surface mobile layer, and the other is the bulk-like inner layer. Such a model could explain the film thickness independent viscosity observed for very low thicknesses. It was assumed that the top layer mobility is dominant in such a scenario and can alter the dynamics of the entire polymer film below this film thickness.

When studying the behavior of entangled PS thin films, it was found that annealing of the films increased effective viscosity until a saturation value was reached.[70] At thicknesses lower than 20 nm, it was found that the saturation viscosity decreased with a decrease in the thickness of the PS films.[70] PS films having thicknesses greater than 20 nm realized bulk-like viscosity,[70] but the plateau modulus remained 1 order of magnitude lower.[70,156] However, such realization of the bulk viscosity happens at 5−10 times the τ_{rep} of the polymer.[70,156] Clough et al.,[152] by investigating the glass transition temperature of the PS films on PS brushes of different molecular weights, found that the trend followed by the T_g of the films on the substrates did not show any correlation with the effective viscosity calculated for the same systems. The lowest T_g was shown by the PS-SiO_x system while the PS on 96k brushes showed T_g similar to the bulk. However, the effective viscosity of PS-SiO_x was the highest. Hence, it should mean that the decrease in glass transition temperature should not affect the dewetting parameters.[152] This appears opposite to the dewetting observed by Reiter and co-workers.[157]

The two-layer model could satisfactorily explain the behavior of entangled and unentangled polymer films. However, while studying the effect of strongly attractive substrate on polymer films, a three-layer model with an immobile layer at the substrate interface needed to be introduced.[148,158] There is competition between the higher mobile surface layer and the substrate layer of low mobility in determining the effective viscosity of the entire film. The dominance of each layer was found to be dependent on temperature.[158] There was an increase in the effective viscosity on decreasing the thickness of the PMMA film at temperatures above 110 °C. However, at lower temperatures, there was a decrease in effective viscosity.[158] Further studies were also performed in modifying the effective viscosity of the polymer films by plasticizing the polymer films[98] or by modifying the substrate using UV Ozone treatment[148] or chemical modifications.[159] Effective viscosity was also altered in copolymers by tuning the relative composition of the copolymers.[160]

Figure 7 shows an example of how the substrate (Si/SiO_x) can modify the effective viscosity of the polymer film. On exposing the substrate to UVO, the substrate became more attractive to PS and resulted in an increase in effective viscosity on reducing the film thickness (Figure 7(a)). However, the effect was noticeable in high molecular weight PS, which could be due to the greater extent of the chains from the polymer−substrate interface into the bulk of the film.[148] According to Figure 7(b), the increase in the effective viscosity of UVO-treated PS is much lower in Si (Si−H) substrates when compared to that in SiO_x substrates. Thus, it can be confirmed that the increase in effective viscosity is brought about by increasing the interaction between the UVO-treated PS and OH group in the substrate.[148]

PSD as a characterization tool has the ability to quantify the effective viscosity of thin polymer films, which takes into account the effects of the mobile surface layer and substrate layer having low mobility. Even though the technique probes the evolution of the surface morphology of the polymer films, PSD is sensitive enough to the phenomena transpiring in the bulk of the film.

https://doi.org/10.1021/acspolymersau.4c00022
ACS Polym. Au 2024, 4, 342−391

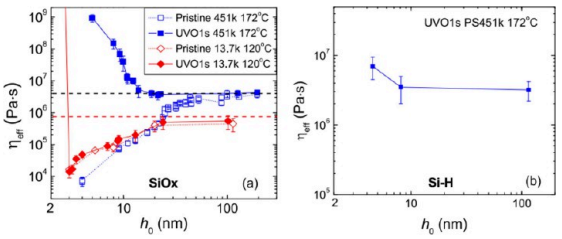

Figure 7. (a) Difference in thickness dependence of the Effective viscosity, η_{eff}, versus h_0 of two different M_w's of PS, both pristine and after 1 s UVO exposure, supported by SiO_x when measurements were done at two different temperatures. The upper and lower dashed lines indicate the bulk viscosity of PS451k and PS13.7k, i.e. PS of M_ws 451 kDa and 13.7 kDa, respectively. (b) η_{eff} versus h_0 of PS451k films treated by UVO as in (a) but supported by HF-etched Si (Si−H). [Reproduced from ref 148. Copyright 2019 ACS.]

The absence of capillary wave formation at temperatures below the T_g makes the technique unable to probe the glassy properties. In addition, the PSD technique majorly relies on model-dependent analysis, the raw data for the analysis is obtained from the AFM. Hence, the properties obtained using the PSD are dominantly dependent on the quality of the raw data provided by AFM. However, the possibility of such an error is not highly probable.

Bubble Inflation

The bubble inflation technique was developed to find the biaxial extensional flow in viscoelastic materials under constant stress. If the strain rate can be controlled, this method will give the biaxial extensional viscosity.[161] The technique was later modified to be used as a characterization technique for polymer thin films in investigating the viscoelastic properties of the film.[162] In contrast to the original method, where the sample is clamped before applying the pressure to inflate a bubble, the film adheres to a filter with regular arrays of channels through which a predetermined air pressure is applied.[162] Figure 8(a) shows the schematic of film in the bubble inflation technique.

In the domain for which the membrane remains hemispherical, the stress (σ) is related to the pressure, P; the film thickness, t_0; and the radius of curvature, R of the membrane as[162]

$$\sigma_{11} = \sigma_{22} = \frac{PR}{2t_0} \tag{8}$$

The biaxial deformation or strain, $\epsilon_{11} = \epsilon_{22}$, at the pole of the bubble is related to the bubble geometry by the following expression:[162]

$$\epsilon_{11} = \epsilon_{22} = \frac{s}{2R_0} - 1 \tag{9}$$

Here, $s = 2R\sin^{-1}\left(\frac{R_0}{R}\right)$ is the segment length of the bubble and R_0 is the radius of the membrane before inflation (the hole radius). This technique leverages the imaging capabilities of AFM for deformation measurements, mitigating challenges associated with contact mechanics inherent in scenarios where AFM serves as a nanoscale mechanical testing or indentation device.[162] The critical parameter for stress and strain calculations in the inflated bubble is the radius of curvature (R). Determining R involves analyzing the bubble profile and fitting it to the equation of a circle:

$$R^2 = (x - a)^2 + (y - b)^2 \tag{10}$$

where R is the radius of curvature, x and y are the x position and height data for the bubble profile, respectively, and a, b are offset constants for a circle not centered on the coordinate axes.

Stress and strain are determined based on the radius of curvature of the bubble, which is easily obtained by measuring the dimensions of the bubble and applying the circle equation. The evolution of the bubble profile at various times is illustrated in Figure 8(b).[163] However, a direct comparison of the results from the bubble inflation test with the bulk creep tests is challenging due to the unknown complete stress history of the film.[162,164,165] Therefore, the known stress is used, and the Boltzmann superposition is applied.[163,165] It is noted that the rubbery plateau region has been reached when the strain comes to a constant value (Figure 8(c)).[163]

O'Connell et al.[162] investigated poly(vinyl acetate) (PVAc) films using the nanobubble inflation technique. They found a decrease in rubbery compliance compared to the bulk value in thin ca. 30 nm PVAc films, while the glassy compliance was comparable to the bulk values. The well-known increased mobility in thin polymer films could thus be decoupled from the rubbery modulus.[162] However, it should be noted that since bubble inflation is a highly nonlinear technique[103] involving

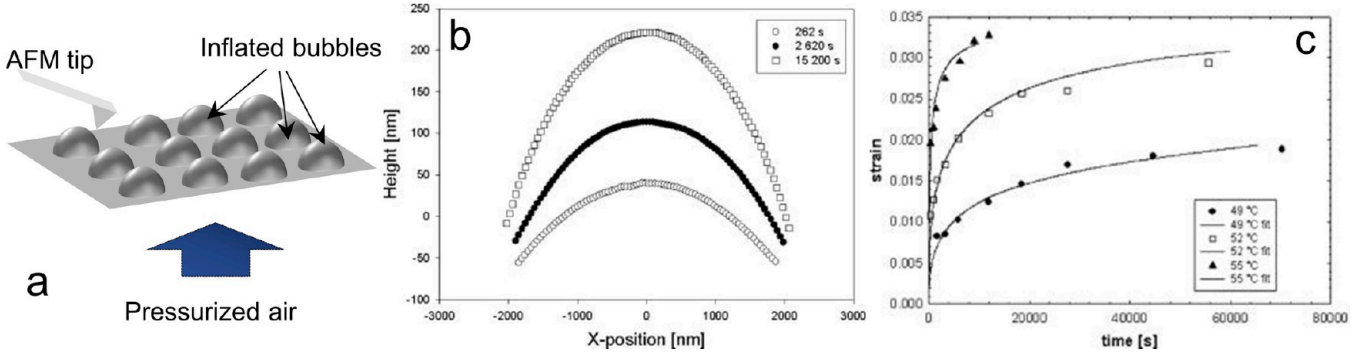

Figure 8. (a) Schematic of the nanobubble inflation technique. When air pressure is applied from below to the frame on which the film has adhered, bubbles are formed in the film. (b) Centerline profile plots of a bubble from a 70.1 nm thick PS (994 kg/mol) film at 80 °C removing extraneous points at three widely separated times. Open circle, filled circle, and open square at 262, 2620, and 15200 s, respectively. (c) Strain as a function of time for a 22.7 nm thick PS (994 kg/mol) film at a pressure of 124 kPa (18 psi) and at temperatures of 49 °C (filled circle), 52 °C (open square), and 55 °C (filled triangle). Solid lines are exponential fits of experimental data. [(b) and (c) were reproduced with permission from ref 163. Copyright 2007 AIP.]

https://doi.org/10.1021/acspolymersau.4c00022
ACS Polym. Au 2024, 4, 342−391

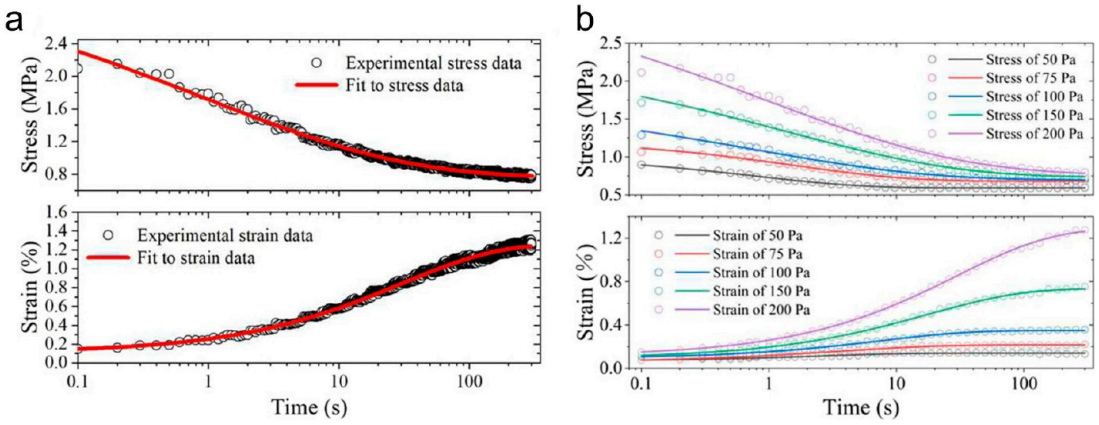

Figure 9. (a) Representative stress and strain data for a 113 nm PS film (M_w = 350 kg/mol) tested at 86 °C and 200 Pa. Solid lines are fitted experimental data by modified KWW function. (b) Fitted stress and strain curves vs time for a 113 nm PS film tested at 86 °C and various pressures. The hollow points represent raw data, with 50 selected data points well distributed on the logarithmic axis. [Reprinted with permission from ref 103. Copyright 2023 AIP.]

large polymer deformation, it does not deliver the intrinsic response of the glass both in terms of mechanical properties and, above all, molecular mobility. Moreover, the technique captures the linear viscoelastic and nonlinear viscoelastic-viscoplastic responses of the polymer film to such large deformations. Thus, rather than capturing the intrinsic mobility of the chains the stiffening observed in the technique could be due to the confinement effect on the viscoplastic response of the polymer films. Further investigations done on PS and PVAc films of varying thicknesses revealed a 2-order reduction in rubbery compliance values.[164] To account for the decrease in compliance at low thicknesses, the contribution from surface tension was investigated.[166] However, the surface tension could not account for the 2−3 orders of magnitude increase in the stiffness of the ultrathin polymer films.[166] The molecular or confinement-induced stiffening and the surface tension effects can be considered to be acting together in reducing the rubbery state compliance value. Poly(butyl methacrylate) (PBMA) showed a weaker thickness-dependent increase in rubbery stiffness.[167] The varied behavior shown by the PBMA films compared to the PVAc and PS films exhibits the influence of chemical structure on the stiffening of ultrathin polymer films.[166,167] To study the effect of the shape of the bubble being formed, the circular bubbles were compared to rectangular bubbles.[168] The rubbery plateau stiffening was observed in both the geometry of bubbles. In experiments conducted on polycarbonate (PC) thin films, even at thicknesses as low as 3 nm, where the glass transition temperature is known to decrease by 122 °C, the phenomenon of rubbery stiffening aligns with an extrapolation based on the behavior observed in PS and PVAc films.[169] Ngai et al.[170] asserted that the distinction between α-relaxation and the Rouse modes, along with the separation of the sub-Rouse modes from the Rouse modes in polymer thin films, explains the rubbery stiffening phenomenon observed in such films. They proposed that the segmental α-relaxation coupling parameter, denoted as n_α, indicates the degree of this separation. This is consistent with the rubbery stiffening dependence on thickness observed for PS, PVAc,[165] PC,[169] PBMA,[167] and PEMA.[171] The rubbery stiffness index was found to be linearly correlated to the coupling parameter n_α and the fragility of the polymers.[171] Fragile polymers showed a higher stiffening index and strong polymers showed a lower rubbery stiffness index.[171] On investigating the rubbery stiffness and rupture stress of polyisobutylene (PIB), the correlation between rubbery stiffness and n_α was found as expected.[172] However, the stiffness index did not fall in the linear correlation expected with fragility. It is hypothesized that the broad distribution of the relaxation times expected of the low-fragility materials in PIB could be the reason for this deviation in behavior. The thickness of the film influences the behavior of rupture stress and strain.[172] As the film thickness decreases, the rupture stress increases while the rupture strain decreases. Furthermore, the energy needed for the failure of the PIB film was found to increase initially with decreasing thickness until 30 nm and then begin to decrease.[172]

Chapuis et al.[173] introduced a new interferometric measurement technique to aid the measurement instead of AFM. The interferometric method is purely noncontact, with the added advantage of measuring multiple bubbles simultaneously. The precision of such a measurement depends on the film's deflection.[173] The greater the deflection, the better the accuracy of measurement. On measuring the evolution of PVAc films and PS films during the bubble inflation process to compare with the measurements made by AFM, the PVAc measurements were found to be consistent with the prior work, while PS showed a new nonlinear response regime that could be due to the plasticity of the film.[173] Further, to understand the plastic nature of deformation, Xiao et al.[103] varied the pressure of the gas that deforms the polymer film from 50 to 200 Pa in a bubble inflation experiment. The representative stress and strain curves are shown in Figure 9(a). They found that the increase in value of the strain at the end of the test (300 s) is ten times (Figure 9(b)) while the increase in stress at the same time for increased pressure of gas is only 1.4 times. Thus, a viscoelastic-viscoplastic regime should be considered. For this, the total strain observed should be viewed as a sum of both viscoelastic and viscoplastic effects.[173] The 1-D Schapery equation is used for the viscoelastic part[174−176] of the strain, and the 1-D Perzyna model is used for the viscoplastic part.[177]

The bubble inflation technique is one of the few techniques that can perform creep tests on thin polymer films. However, there are a few associated challenges with the bubble inflation technique. The technique requires specialized equipment which takes considerable effort to set up. The requirement of precise pressure control, stand alone AFM scanning, and customized substrates with precise apertures for conducting the test increases the complexity and duration of the technique. The

https://doi.org/10.1021/acspolymersau.4c00022
ACS Polym. Au 2024, 4, 342−391

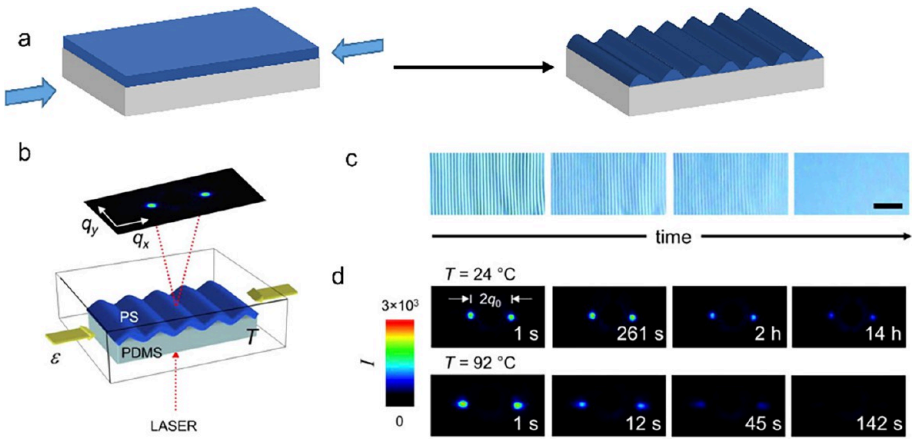

Figure 10. (a) Schematic showing the principle of surface wrinkling. Thin film on top of the compliant substrate on compression will result in the generation of wrinkles characteristic of the film's modulus. (b) Schematic illustration of the custom-built small angle light scattering (SALS) apparatus equipped with a temperature-controlled chamber and a strain stage for measuring the temporal evolution of a pre-wrinkled polymer film on a compliant substrate. A laser beam is passed through the wrinkled film, and the resulting scattering pattern is projected onto a screen and acquired by a CCD camera. Thick arrows indicate the direction of compressive strain. (c) Representative optical microscopy images for a 31 nm thick PS film wrinkled at T = 92 °C as a function of time, depicting the wrinkling amplitude decay (scale bar = 10 μm). (d) Time-sequential SALS images of a 31 nm thick PS film (M_w = 654.4 kg/mol) at a temperature of T = 24 °C (upper row) and T = 92 °C (lower row), clearly indicating the decay of scattering intensity as a function of the annealing time. [Figures (b), (c), and (d) are reprinted with permission from ref 188. Copyright 2017 AIP.]

analysis of the information from the technique requires considering mathematical models applicable for viscoelastic and viscoplastic regimes, which could make analyzing the data more tedious. However, the versatility of the technique in being able to accommodate supplementary apparatus helps in improving the data collection capability such as the incorporation of interferometric techniques in capturing data in a purely noncontact manner and augmented the ability by being able to study more than one bubble.

Wrinkling

The wrinkling technique for the characterization of thin polymer films is based on the principle that thin films, when subjected to compressive or tensile stress, undergo a surface instability to reduce the stress.[178] It deforms out-of-plain periodically, forming wrinkles. The dominant wavelength of the pattern will be such that the stress is reduced to a minimum value.[179] On solving the force balance equation and further minimizing the value of force to the wrinkle wavelength, a useful relation that relates the elastic modulus of the film (E_f), substrate (E_s) and the wavelength (λ) of the wrinkle instabilities formed in the sample can be obtained.[178] Considering a plane strain condition (films on semi-infinite compliant substrates), the classic equation of bending is[180]

$$\overline{E_f} I \frac{d^4 z}{dx^4} + F \frac{d^2 z}{dx^2} + kz = 0 \tag{11}$$

Here $\overline{E_f} = \frac{E}{(1-\nu^2)}$ is the plain strain modulus, ν is the Poisson ratio, E is the elastic modulus, I is the moment of inertia of the film, F is the applied force or load, k is the Winkler modulus of an elastic half space.[181] Applying a sinusoidal displacement in the z-direction and solving yields an expression of force[180]

$$F = 4\overline{E_f} I \left(\frac{\pi}{\lambda}\right)^2 + \frac{\overline{E_s} w}{4} \left(\frac{\pi}{\lambda}\right)^{-1} \tag{12}$$

where w is the width of the film having a thickness h. To find the wavelength that minimizes the stress in the system the expression is minimized for wrinkle wavelength, λ;[180]

$$\lambda = 2\pi h \left(\frac{\overline{E_f}}{3\overline{E_s}}\right)^{\frac{1}{3}} \tag{13}$$

The critical stress (σ_c) and strain (ϵ_c) required to induce the wrinkling in a film can be obtained by dividing the critical force (F_c) with a cross-sectional area[180]

$$\sigma_c = \frac{F_c}{hw} = \left(\frac{9}{64} \overline{E_f} \overline{E_s}^2\right)^{\frac{1}{3}} \tag{14}$$

$$\epsilon_c = \frac{\sigma_c}{\overline{E_f}} = \frac{1}{4} \left(\frac{3\overline{E_s}}{\overline{E_f}}\right)^{2/3} \tag{15}$$

Thus, the critical strain depends only on the modulus ratio.

Ever since the seminal paper by Bowden et al.,[182] the research into the wrinkling phenomenon gained momentum. It included various dimensions like patterning the films, orienting the patterns as required, and characterizing the mechanical properties of the films.[183−185] We focus our discussion on the characterization part. Bowden and co-workers[182] used a thermally expanded substrate and then cooled it down to apply compressive stress on the film. The process was modified further, and the stress source was diversified. Accordingly, we could classify the wrinkling process into mechanically induced wrinkling, thermally induced wrinkling, capillary wrinkling, etc. Mechanically induced wrinkling processes induce stress on the system by applying a tensile or compressive strain. The relatively thick and compliant substrate is initially pre-strained, by either compressive or tensile as required. The film is then coated onto the prestrained substrate.[180] Once the restraint is removed, the strain is applied onto the film by the restoring force, i.e., tensile pre-strain will produce a compressive strain on the film on the removal of restraint. This strain applied to the film will create a periodic wrinkling pattern.[180] The wavelength is dependent on the modulus of the film, and the amplitude is dependent on the strain (under the plain strain condition for small strains).[186,187] In addition, the strain can be applied on the films after transferring the as-cast films to the compliant substrate and then

https://doi.org/10.1021/acspolymersau.4c00022
ACS Polym. Au 2024, 4, 342−391

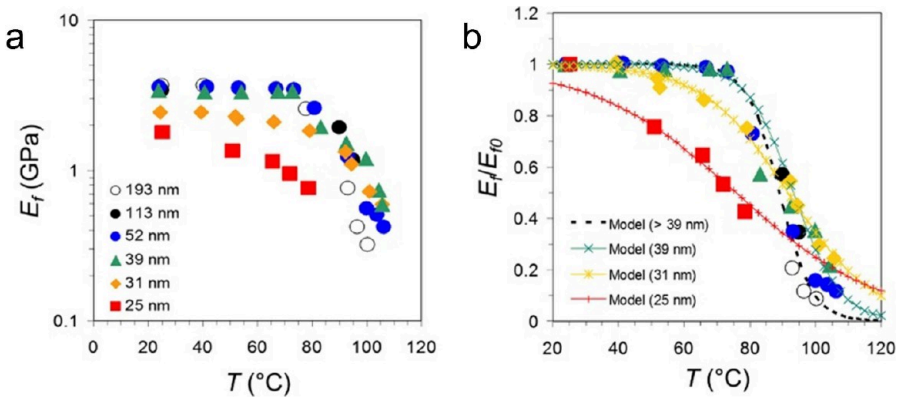

Figure 11. (a) Measured high-frequency Young's modulus (E_f) for PS films (M_w = 654.4 kg mol^{-1}) with different thicknesses (h_f) as a function of temperature (T). (b) Normalized Young's modulus (E_f/E_{f0}) as a function of T and h_f. The symbols are the same as in (a). The dotted curves represent model fits to the data using $E_f/E_{f0} = 1/\{1+\exp[\Delta H - T\Delta S)/RT]\}$ with the following fitting parameters: $h_f > 39$ nm ($\Delta H = -171$ kJ mol^{-1}, $\Delta S = -472$ J mol^{-1} K^{-1}); $h_f = 39$ nm ($\Delta H = -125$ kJ mol^{-1}, $\Delta S = -342$ J mol^{-1}K^{-1}); $h_f = 31$ nm ($\Delta H = -84$ kJ mol^{-1}, $\Delta S = -231$ J mol^{-1} K^{-1}); and $h_f = 25$ nm ($\Delta H = -52$ kJ mol^{-1}, $\Delta S = -150$ J mol^{-1} K^{-1}). [Reprinted with permission from ref 188. Copyright 2017 AIP.]

applying strain on the system in a controlled manner.[188] The schematic for the same can be seen in Figure 10. Figure 10(a) shows wrinkle formation on applying compressive stress. Figure 10(b) shows the schematic illustration of the custom-built small angle light scattering (SALS) technique used by Chung et al.[188] to measure the wavelength of the wrinkles and the scattering pattern obtained on the screen. Figures 10(c) and (d) show the optical images and time-sequentialized SALS images, respectively.

Thermally-induced wrinkling involves either heating a polymer layer sandwiched between a metal layer and substrate layer or cooling the bilayer (polymer film-compliant substrate) after the initially heated substrate on which the polymer film is coated.[189] The origin of wrinkles in this context lies in the difference in thermal expansion upon heating. This mechanism helps to avoid the additional stress that clamping could produce. However, it is important to note that the films are not entirely immune to the residual stress generated during the deposition process.[189] Certain researchers have utilized liquid crystal elastomers as a compliant substrate, which will show a difference in patterns formed on heating and cooling above and below the formation temperature.[190]

Capillary wrinkling utilizes the capillary forces arising at the interfaces between a nonwetting fluid and the polymer as a source of stress application.[191] The bilayer is immersed in distilled water after coating the PS film on top of a glass substrate. The polymer thin film, which is hydrophobic, separates and floats on water. On placing a drop of water in the center of the film or by poking at the center or placing a solid disc at the center, wrinkles develop. Quantities measured are number of wrinkles and length of wrinkles. The length of the wrinkle increases by increasing the amount of water added to the film's center.[191]

On applying axial stress, the difference in the Poisson ratio of the bilayer results in the generation of a biaxial stress state that leads to the formation of wrinkles. Stafford et al.[178] introduced the technique to deduce the film modulus by considering the dominant wavelength of the wrinkle. The consideration of dominant wavelength is valid in the limit of

- Low strain
- The elastic modulus of the film is much greater than the substrate
- The substrate has to be much thicker than films.
- Amplitude of buckles ≪ the wavelength

Stafford et al.[178] extensively investigated mechanical properties of polymer thin films using the wrinkling technique. The glassy modulus of PS of film thicknesses above 100 nm was comparable to the bulk values.[178] They also captured the reduction in elastic modulus value on adding plasticizer (DOP) and were found to follow a comparable behavior as observed in bulk polymers. Upon investigating the thickness dependence of modulus for different polymers (PS, PMMA), it was found that the modulus varied with the thickness of the films.[187] Wrinkling studies on a wide range of thicknesses of PS films show that as the film thickness reduces, there is a linear decrease in the value of amplitude and wavelength of the wrinkle patterns.[7] However, the modulus of the films remained the same until they reached a thickness of 30 nm. When the film thickness decreased further, the modulus started decreasing. When extrapolated, the amplitude and wavelength plots intersect the thickness axis close to 2 nm.[7] On developing a bilayer model considering a soft surface layer of 2 nm thickness having a modulus of 0.1 GPa while considering the rest of the film has a modulus of bulk value, the thickness dependence of the modulus could be fit to the experimental data points with appreciable accuracy.[7] The wavelength of the pattern formed on the thin films was not a function of applied strain. Still, the pattern amplitude was modified by varying the strain (assuming the strain value is within the limits where the equations expressed earlier are valid).[178] At constant strain, the amplitude of the wrinkles decreased with decreasing thickness; for large strains, the wavelength was strain-dependent which was validated using a perturbation method for an analytical solution and then using a finite element method.[192,193]

Figure 11(a) shows the elastic modulus of the PS films being measured for varying temperatures and thicknesses. As the temperature increased, there was a reduction in the glassy modulus, as expected in any glassy polymers. Figure 11(b) shows the reduced modulus of the thin PS films on increasing the temperature, which is normalized with respect to the apparent modulus at room temperature. The data is fitted using a model for the shear modulus of amorphous polymers by Lin et al.[194]

Chan et al.[189] could deduce the rubbery plateau modulus using the thermal wrinkling process using a sample structure where metal is deposited on top of PS thin film. The bilayer is

https://doi.org/10.1021/acspolymersau.4c00022
ACS Polym. Au 2024, 4, 342−391

heated above the glass transition of the polymer film. As the time exposure to temperature increased, the dominant wavelength (d) and amplitude (A) of the wrinkles increased.[189] Finally, reaching an equilibrium value (d_r, A_r) beyond which there was not much increase in wavelength. This was reported as the rubbery plateau region, and the corresponding modulus agreed with the previously reported rubbery plateau modulus. On heating the sample above the glass transition temperature, the elastic modulus at the rubbery limit is given by[189]

$$E_{i,r} = \frac{(1-2\nu_i)(1+\nu_i)}{12(1-\nu_i)}\left(\frac{h_i}{h_f}\right)\left(\frac{2\pi h_f}{d_r}\right)^4\left(\frac{E_f}{1-\nu_f^2}\right) \quad (16)$$

Subscripts i and f stand for polymer layer and metal film, respectively. With an increase in the annealing temperature, there is enhanced softening. Similarly, the shear viscosity could also be obtained from the growth rate of the amplitude during annealing. Thus, temperature-dependent viscoelastic behavior could be obtained from the wrinkling experiments.[189] By studying the time-dependent stress relaxation behavior at different temperatures and using time−temperature superposition, Chan and co-workers created a modulus master curve for PS thin films.[195] Chung et al.[140] observed that the theoretical strain observed was 3-fold lesser than the experimentally found value which was attributed to the presence of residual stress in the system. This tensile residual stress leads to an increase in the compressive stress required for wrinkle formation.[140] The residual stress started decreasing with the addition of a plasticizer or by thermal annealing. Torres et al.[130] showed that the glassy modulus of different polymers showed a thickness-dependent modulus after a critical film thickness, which is a function of the quench depth (the difference in temperature at which the experiments are performed from the T_g) of the polymer. This was explained by the presence of a liquid-like surface layer, the thickness of which could be determined by extrapolating the wavelength-film thickness curve to meet the film thickness axis. The point where the curve intersects the thickness axis is the point below which the wrinkles are no longer stable, characteristic of a liquid-like layer.[130] The nearer the film is to its glass transition temperature, the thicker its mobile surface layer, which results in the perturbation of modulus at a higher critical film thickness. Interestingly, this film thickness dependence of modulus could be circumvented by ultraviolet and ozone treatment or by the addition of DOP to the system. It is intriguing that although DOP would act as a plasticizer in bulk polymers, which would suggest increasing the compliance of the polymer, its presence here is found to result in avoiding the thickness-dependent reduction in modulus.[196] The thickness-dependent compliance of the films was also dependent on the polymer's chain architecture and molecular weight.[101,197]

A perfect wrinkling-based investigation will require a perfect interface between the substrate and the thin film. The substrate needs to be compliant and relatively thicker.[178] But when these conditions are not met, surface delamination is possible. Mei et al.[198] introduced a concomitant wrinkling delamination scenario. Here, the authors tried to bring in the sequential development of both processes for a compliant substrate. The buckling without delamination theory considers the interface to be perfectly bonded and that there is no tangential displacement. Once the tangential displacement is considered, it can account for the delamination following the wrinkling process.[198] As the strain increases beyond the critical strain, the amplitude of wrinkles increases proportionately. This will increase the normal and shear traction along the interface, hence tangential displacement followed by delamination.[198] In the case of very compliant substrates having inherent delamination, the delamination occurs first by localized buckling delamination followed by periodic wrinkle formation. These wrinkles, once formed, will also have the same dependence of elastic modulus on the wavelength.[7,198] Increased strain is accommodated by the amplitude of the delamination and successive relaxation of nearby wrinkles. Nolte et al.[199] tried to bridge the divergence in the investigation based on buckling delamination and wrinkling instability.

Beyond the modulus measurement, the wrinkling phenomenon can be used to find out the fracture strength of the polymer film and the strain at the onset of fracture.[200] When the thin polymer film on top of a compliant substrate is applied with tensile stress and the strain increases, wrinkles and cracks start appearing. The fracture strength can be obtained using the following relation from the average space between the cracks ($\langle d \rangle$).[200]

$$\langle d \rangle = \frac{2h\sigma^*}{E_s \bar{\epsilon}} \quad (17)$$

Here, σ^* is the fracture strength, h is the film thickness, and $\bar{\epsilon}$ is the applied strain after the onset of cracking. d is a measurable quantity; all other values are available. By extrapolating the $(1/\langle d \rangle)$ vs ϵ curve to zero crack density, the onset fracture strain can be extracted.[200] These values are very important in the manufacturing of sensors and miniaturized electronic devices.[201,202] This wrinkling-cracking method assumes that the interface is perfectly bonded so that no delamination occurs and that maximum stress occurs at the midpoint of the film. Thus, there should be no defects present.[200] A tensile strain applied to the films creates wrinkles and cracks, as shown in Figure 12(a).

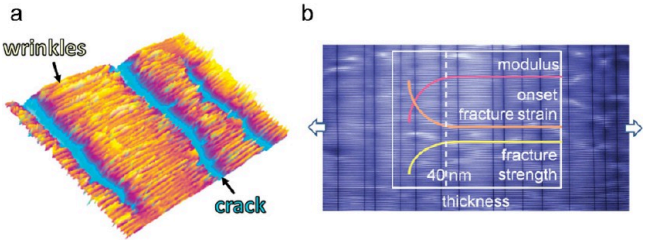

Figure 12. (a) Representative 3-D image of the crack and wrinkles formed on polyamide membrane on a compliant PDMS substrate. [Reproduced from ref 200. Copyright 2011 ACS.] (b) A representative image showing the variation of fracture strength, modulus, and the onset of fracture strain with the thickness of the film. [Reproduced from ref 203. Copyright 2012 ACS.]

Cracking tends to occur first in brittle films, while wrinkling occurs first in ductile or relatively tougher films.[200] The tests are conducted within the linear elastic strain behavior regime. The cracks and the applied strain were also found to have no significant effect on the wavelength of the wrinkles formed. Therefore, it can be confirmed that the wavelength of wrinkles is predominantly dependent on the elastic modulus of the film. Figure 12(b) shows a representative image of polymer film properties that varies with thickness. The elastic modulus and fracture strength decreased below a film thickness of 40 nm while the onset fracture strain increased in value. The increased

https://doi.org/10.1021/acspolymersau.4c00022
ACS Polym. Au 2024, 4, 342−391

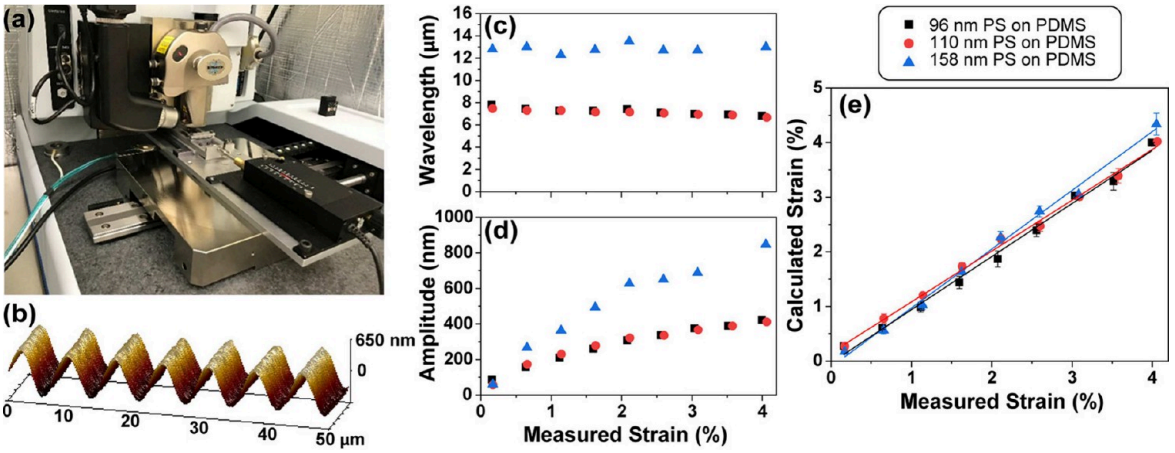

Figure 13. (a) Photograph of the strain stage mounted on a Bruker Dimension Icon AFM for conducting in situ AFM measurements while maintaining the applied strain. (b) AFM image of PS (h_1 = 96 nm) on PDMS wrinkled at 2.1% compressional strain. (c) Wavelength and (d) amplitude as a function of applied strain for h_1 = 96, 110, and 158 nm on PDMS. (e) Calculated strain versus applied strain for h_1 = 96, 110, and 158 nm. Here h_1 is the polymer brush layer modified by cystamine so that it forms a cross-linked skin layer. [Reproduced from ref 206. Copyright 2020 ACS.]

mobility of the films due to the increased dominance of the surface layer has been attributed as the reason.[200,203,204]

Analytical solutions were derived by Cao et al.[204] for determining the onset of critical strain for wrinkling and the wrinkling wavelength. The solutions are based on a model where the elastic substrate has a variable elastic modulus. The two models considered are the variation of substrate modulus as a power function and another as an exponential function.[204] They conducted theoretical and finite element analysis and correlated the critical characteristics with the pattern formation. Gurmessa and Croll[205] reported the onset of plastic deformation in thin films using wrinkling. Even after removing the applied strain, the presence of wrinkles proves that the material has undergone plastic deformation. They defined a critical strain for plastic failure. The onset of plastic deformation occurs at lower strains compared to the bulk polymers. In addition, the critical strain was found to increase as the thickness of the film was reduced below 100 nm. They concluded that the effect being shown is not related to the entanglement in the structure, instead, the same phenomenon responsible for the lowering of glass transition caused this effect.

Surface wrinkling has also been used to find Young's modulus of ultrathin polymer brushes. The value of the modulus of poly(2-hydroxyethyl methacrylate) (PHEMA) brushes grafted on PDMS was determined and was found to closely match the values obtained for a film of 50 nm thickness.[207] However, the strain applied during the wrinkling could not be easily obtained in such systems as the compression is applied through solvent-induced swelling or thermal strain. Recently Reese et al.[206] have introduced a methodology to quantify such strains that are applied on the polymer brushes by using the modification of the brushes to create a cross-linked skin layer (h_1) and unmodified substrate layer (h_2). Using an in situ AFM measurement system, when the strain is maintained as constant, the wavelength is obtained by 2-D fast Fourier transform power spectrum, and the amplitude is obtained from the cross-section of the AFM image using an analyzing software. The AFM attached to the strain gauge can be observed in Figure 13(a). After measuring the strain values experimentally, they found that the values were comparable to the calculated strain values (Figure 13(e)).

The main advantage of the wrinkling experiment is the relative simplicity of the experimental setup required which makes it a cost-effective relatively robust technique. In addition, the technique is sensitive to very fine changes in the properties of polymer films. The ability of the technique to modify the source for wrinkling and the possibility to add additional measurement units, e.g. the SALS as mentioned in Figure 10(b) makes it versatile and enhances the range of application. However, the wrinkling technique is limited by the domain in which the basic equations for wrinkling are valid.[178] Also, the wrinkling measurements do not have the ability to probe spatially resolved properties in the polymer film. It rather provides information on the film as a whole. The technique has a wide application range as it can in addition to the glassy and rubbery modulus of thin polymer films, can capture the fracture strain and strength by slight modifications which is an added advantage.

Capillary Leveling

An undisturbed liquid thin film maintains stability, exhibiting no vertical or lateral motion due to a consistent and uniform Laplace pressure across the film. However, upon introducing a perturbation, the Laplace pressure increases in specific regions relative to others in the film,[208] leading to lateral and vertical fluid movement until the surface regains a flat configuration. This phenomenon is known as capillary leveling and is governed by the Laplace pressure gradient along the film, with viscosity playing a crucial role in damping.[209] Capillary leveling provides a means to investigate the rheological properties of the material, and perturbations like cylindrical holes, rectangular trenches, and stepped bilayers can be introduced to study film evolution.[210−213] The step-edged bilayer is commonly used and is illustrated in the schematic shown in Figure 14(a). The evolution of the step profile over time when captured using AFM scans[208] can be seen in Figure 14(b).

The polymer thin film is prepared by spin-coating onto a mica substrate. The film is then floated on deionized water and picked up using a previously scratched silicon wafer. Once placed on the wafer, the film cleaves, creating a step edge along the prescratched plane. Subsequently, the film is floated on the water again and picked up by a silicon wafer that has been spin-coated with polymer. This process results in a step-edge bilayer film approximating a Heaviside step function. A preannealing step is performed to eliminate residual stress immediately after spin-coating. Following bilayer preparation, the film is annealed well above the glass transition temperature for varying

https://doi.org/10.1021/acspolymersau.4c00022
ACS Polym. Au 2024, 4, 342−391

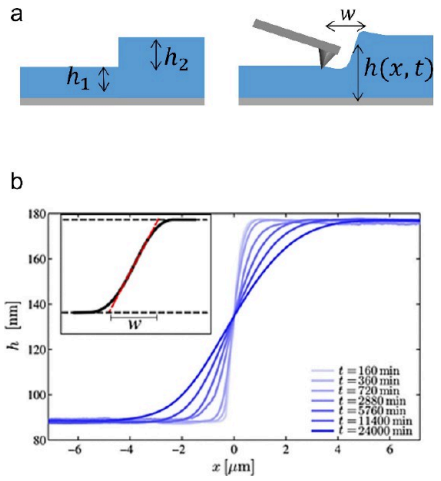

Figure 14. (a) Schematic showing a stepped bilayer, in time, will try to flatten out to minimize the Laplace pressure in the system when the temperature is above T_g. The width of the stepped edge broadens with time. (b) AFM profiles of a freestanding PS (M_w = 55 kg/mol) stepped film with $h_1 = h_2$ = 176 nm, for different times t spent above T_g at T = 110 °C. As sketched in the inset (arbitrary units), the profile width w is defined from the tangent (tilted dashed) line in the middle of the step and the film thickness. [Figure (b) reprinted with permission from ref 208. Copyright 2016 APS.]

durations.[208,209] After each annealing period, the sample is quenched to room temperature to measure the evolving profile of the step edge. At room temperature, the motion of the step edge profile ceases, and measuring the profile yields consistent values.[209]

Over time, the step height profile of the bilayer film undergoes a reduction in height and a simultaneous transformation in its profile, accompanied by an expansion in width.[209,214] The widening of the profile is directly correlated with the viscosity of the polymer. Consequently, the width of the profile (w) serves as the experimental parameter to monitor. This relationship offers valuable insights into extracting the viscosity of the polymer film.[211]

Due to the very small height of the sample, the gravitational effects can be neglected. Capillary pressure becomes dominant:[209,215,216]

$$p(x, t) \approx -\gamma \partial_x^2 t \tag{18}$$

where γ is the surface tension. No-slip boundary conditions at the bottom layer and no shear layer at the free interface allow the application of lubrication approximation. Thus, it can be assumed that vertical velocity is negligible compared to horizontal velocity.[214−216]

$$\partial_x p = \eta \partial_z^2 v; \quad v_{z=0} = 0; \quad \partial_z v_{z=h} = 0 \tag{19}$$

where $v(x,z,t)$ is the horizontal velocity. This indicates that pressure is invariant in the vertical direction and corresponds to the Poiseuille flow. The time scale of the experiment is much larger than the longest relaxation time, which will ensure that the behavior as a Newtonian liquid having high viscosity. Thus, the capillary-driven thin film equation is arrived at, by applying the boundary conditions and careful considerations as:[214−219]

$$\partial_t h + \frac{\gamma}{3\eta} \partial_x (h^3 \partial_x^3 h) = 0 \tag{20}$$

The solution to the above-mentioned thin film equation (TFE) is not easily obtained analytically. However, on linearizing and nondimensionalizing the equation, a numerical self-similar solution of the first kind exists for the equation. This self-similarity of the height profile evolution in time has been seen in experiments too.[209] An intermediate asymptotic theory was developed using Green's function to solve the nondimensionalized linearized thin film equation.[214,219−221] As a stepped geometry cannot be brought under the lubrication approximation, the self-similar solution cannot be used to explain the short term evolution of the height profile.[211] But after a long time, the solution holds.[211] Zheng et al.[213] also derived a self-similar solution that holds from the beginning of the leveling process as opposed to that by Backholm et al.,[211] which is applicable only when the air−liquid interface almost flattens.

Within the lubrication approximation, the width of the stepped profile is found to grow as a power in time as[209]

$$w^4 \sim \frac{\gamma h_0^3 t}{\eta} \tag{21}$$

where γ is the surface tension of the liquid, η is the viscosity, h_0 is the height of the film halfway between the thick and thin portion of the stepped profile, and t is the time of annealing the sample. To study surface energy dissipation of the stepped film, the excess contour length due to the height profile of the film compared to the final flat profile at infinite time can be followed.

Theoretically, it was proved that any initial height profile would eventually approach a self-similar attractor shape, as shown in Figure 15.[212] The process will include an asymmetric

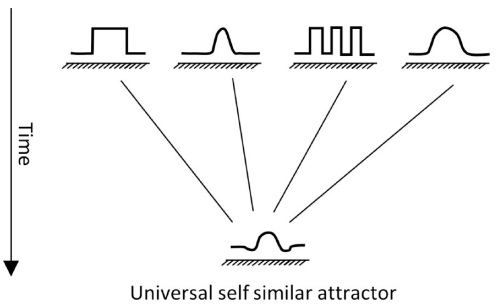

Figure 15. Schematics of the intermediate asymptotics of the capillary-driven thin-film equation. No matter the initial condition, any summable profile converges in time toward a universal self-similar attractor. [Redrawn from ref 212.]

regime where the edges of the perturbation do not interact and a symmetric regime where the edges start interacting. Crossover to the symmetric portion will show a change in the scaling relation of reduction in surface energy with respect to the time.

Increase in width of the profile scales with viscosity, as mentioned before. On increasing the molecular weight of the polymer, the rate of change in the width shows variation, as expected from theory.[209] An increase in the molecular weight of the polymer increases viscosity. The viscosity of the film obtained through the capillary leveling technique is also found to follow a similar scaling as found through other techniques. Below the critical molecular mass, it follows $\eta \sim M$ due to the rouse modes of relaxation, and when $M \gg M_c$, it leads to reptation-related scaling of $\eta \sim M^{3.4}$.[209] Hence, capillary leveling can be considered an effective characterization technique to obtain viscosity for thin polymer films. On following the reduction in excess contour length of the film, a scaling relation

https://doi.org/10.1021/acspolymersau.4c00022
ACS Polym. Au 2024, 4, 342−391

of surface energy reduction is obtained which scales $\sim t^{-1/4}$.[219] Polymers of different molecular weights for the stepped and thinner portion did not show a bidispersion effect in the result.[222] The observations were similar to that of a monodispersed sample having a molecular weight which is a weighted average molecular weight of the two molecular weights used. However, on experimenting with immiscible bilayers, a unique mechanism cannot be pinpointed for the dissipation. The viscosity ratio is assumed to play an important role in that case.[223]

At $T < T_g$, assuming the presence of a mobile layer of constant thickness h_m and viscosity η_m, Chai et al.[224] introduced a glassy thin film equation (GTFE) which is similar to the linearized TFE

$$\partial_t h + \frac{\gamma h_m^3}{3\eta_m}\partial_x^4 h = 0 \tag{22}$$

The solution of the GTFE is also self-similar[224] in $xt^{-1/4}$ Experimentally, glassy films below T_g obey this self-similar solution. A parameter χ was introduced which captures the transition from the glassy thin film equation below T_g to the thin film equation above T_g.[224]

$$\chi = \frac{\int dx(h_{exp} - h_{TFE})^2}{\int dx(h_{GTFE} - h_{TFE})^2} \tag{23}$$

where h_{exp} is the self-similar experimental profile, h_{TFE} is the numerical solution of the TFE,[220] and h_{GTFE} is the analytical solution of the GTFE.[214] The χ value will be 1 when the experimental data is explained by the GTFE equation and 0 when the experimental values are described by the TFE equation, this results in a sharp transition that is observed near the glass transition region, as shown in Figure 16. The effective viscosity of the films can be extracted by following the scaling analysis by Stillwagon and Larson.[215] Using the analysis on stepped films, Chai et al.[224] could provide evidence for the existence of a mobile surface layer on glassy thin films. Rivetti et al.[225] showed that even a monolayer polymer strip on smooth Si/SiO_x substrate showed stationary contact line leveling following self-similar evolution until receding dewetting starts.

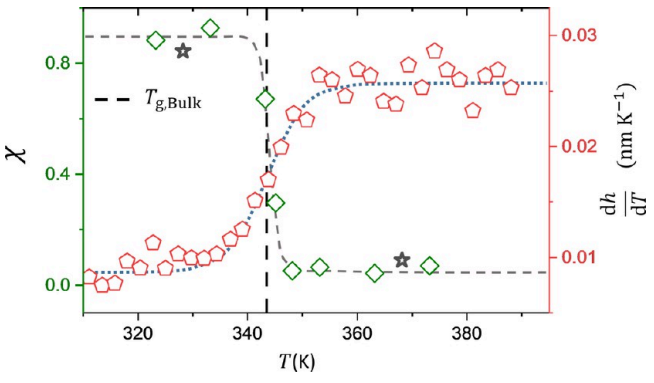

Figure 16. Temperature dependence of the correlation function and thermal expansivity. The correlation function χ(T) defined in eq 23 is given by the diamond symbols (left axis) for samples with $h_1 = h_2 = 90$ nm. Here h_1 is the thickness of the film at the lower portion of the step, and h_2 is the step height. The thermal expansivity for an independent flat 87 nm sample is given by the pentagons (right axis). The black star symbols are $\chi(T)$ for a single sample that was held first for 90 h at $T < T_g$, then measured and heated to $T > T_g$ until the self-similar profile was reached. [Data replotted from ref 224.]

Instead of a stepped film, when a perturbation on the surface of the film is applied, the capillary leveling phenomenon shows similar behavior. This was utilized in investigating the leveling of a rectangular trench and cylindrical hole.[210,211] In both systems, as time passed, the two noninteracting asymmetric steps crossed over to an interacting symmetric regime. This crossing over also resulted in the variation in time dependence of the excess contour length. On crossing over to an interacting regime, the excess contour length showed an increased dissipation, which scaled $\sim t^{-3/4}$ in the case of a rectangular trench,[210] while the cylindrical hole showed $\sim t^{-1}$ dependence.[213] The initial defect size profoundly influenced the time required for leveling the hole which according to Zheng et al.[213] scaled as (r_0^4/h_0^3), where r_0 is the defect size and h_0 is the initial hole height.

Capillary leveling experiments on free-standing thin polymer films showed increased flow dynamics. The growth of width scales as $\sim t^{1/2}$ which emphasizes the effect of the substrate in slowing down the dynamics in thin films.[208,226] At the same time, both supported and free-standing films showed the same capillary velocity. This further confirms the ability of the technique to extract the useful flow properties of the film. Molecular dynamics simulations of the capillary leveling technique were utilized by Tanis et al.[227] to claim the increased surface mobility of the thin polymer films below the glass transition.

When employing a soft, compliant substrate instead of a rigid one for the study of capillary leveling, an elastocapillary phenomenon is evident, as noted by Rivetti et al.[228] in their work. This process induces substrate deformation, leading to qualitatively and quantitatively distinct behaviors compared to capillary leveling on a rigid substrate. Notably, the liquid−air interface, i.e., the contour of the stepped edge, exhibits a scaling behavior of $\sim t^{1/6}$, contrasting with the $\sim t^{1/4}$behavior observed on a rigid substrate.[228] Pedersen et al.[229] investigated the elastohydrodynamic and stochastic leveling of an elastic plate on a viscous film, revealing canonical regimes through numerical solutions, scaling analysis, and experiments. Key factors include the driving mechanism (elastic bending or thermal fluctuations) and the aspect ratio (bump height to film height), with a notable crossover between asymptotic regimes controlled by the aspect ratio.

The capillary leveling technique is theoretically well-founded. The results of the technique are synchronous with the results obtained from other techniques. The strong mathematical framework behind the technique allows for simulating a wide range of experimental conditions. A disadvantage of the technique could be that all of the major research in capillary leveling considers Stoke's flow-based thin film equation. This considers the flow at regions well above the glass transition temperature, and hence, probing the purely viscoelastic nature of the film is not possible. Benzaquen et al.[230] derived a Maxwell-based viscoelastic thin film equation. This thus plugs the gap in the capability of the technique to probe the properties of polymer thin films from viscoelastic to viscous regime. Although the capillary leveling probes the viscosity of the polymer thin film as a single unit without providing the localized viscosity at various layers, the application of the GTFE equation below the T_g allows probing the viscosity of the mobile free surface layer.

https://doi.org/10.1021/acspolymersau.4c00022
ACS Polym. Au 2024, 4, 342−391

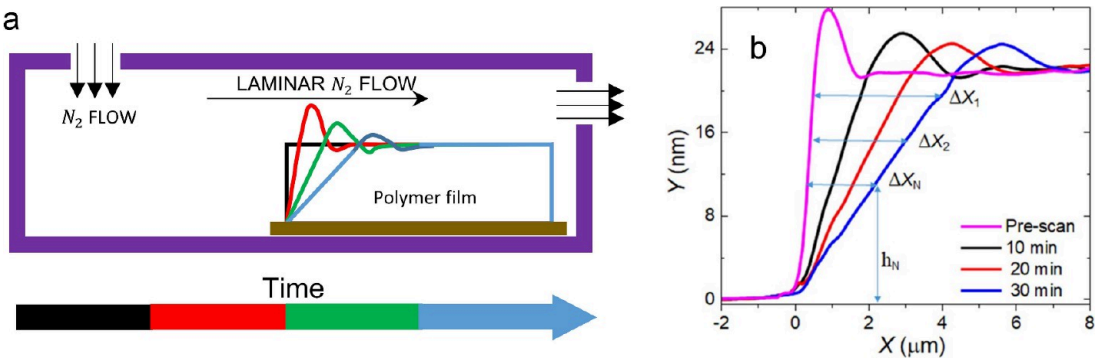

Figure 17. (a) The laminar flow of N_2 gas applies a constant shear on the polymer film, which eventually deforms according to the height-resolved mobility within the polymer film. The representative shapes over time have been shown using black, red, green, and blue in sequence. (b) The time-resolved growth of the edge profile was scanned using an AFM in tapping mode at regular intervals during an NCNS experiment in PNBMA. [Reproduced from ref 72. Copyright 2022 ACS.]

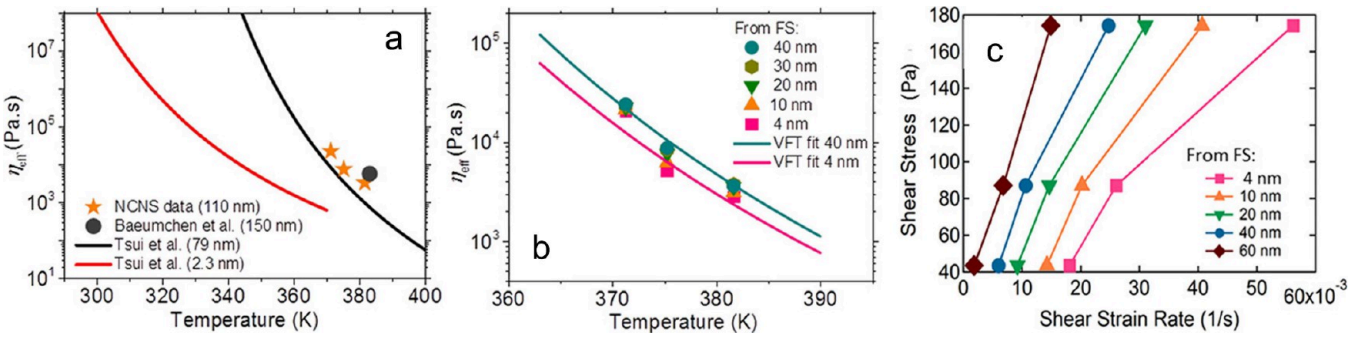

Figure 18. (a) Effective viscosity data comparison of PS films (M_w = 2.5 kDa) using the NCNS technique (stars) with values from the literature for comparable molecular weight. The solid lines are the VFT fit of values from experiments from Yang et al.[70] (b) Variation in viscosity at various distances from the surface layer. The solid lines are the VFT fit for two locations inside the film, 4 and 40 nm from the free surface. (c) Stress−strain rate relationship shows shear thinning in the vicinity of the free surface. The data points are obtained from short-time (5 min) blow-off measurements applying different stress levels on ∼110 nm PS films at 108.5 °C. [Reproduced from ref 73. Copyright 2017 ACS.]

Noncontact Capillary Nanoshearing (NCNS)

The noncontact capillary nanoshearing (NCNS) method is a direct rheological measurement technique. This technique was introduced by Priestley and co-workers[73] inspired by the blow-off method, first introduced by Derjaguin and other researchers.[231−233] The technique involves applying constant shear stress on the nanofilm and observing the deformation of the film over time. A schematic of the experimental setup can be seen in Figure 17(a). A thin film of liquid is supported on top of a solid substrate and placed inside a microchannel. The microchannel dimensions and the nitrogen gas velocities are maintained such that the flow inside is laminar.[73,232] The shear stress is applied by the flow of nitrogen gas. The step edge of the sample is gradually, with time, seen to change as can be observed in Figure 17(b) on the application of shear. The different layers of the polymer thin film undergo change to varying extents over time.[73]

The shear stress (τ) is calculated from the Hagen−Poiseuille relationship.[232,233]

$$\tau = \frac{\Delta P d}{2L} \tag{24}$$

where L and d are the geometric parameters of the chamber. The cell is designed to produce a pressure drop ΔP for a shear stress range of 40−175 Pa. The shear mobility $\chi(h)$ is defined for each layer parallel to the free surface for a height h from the substrate and having a lateral deformation $\Delta X(h)$ as

$$\chi(h) = \frac{\Delta X(h)}{\tau t} \tag{25}$$

where t is the time elapsed since the start of the shear. The effective viscosity is calculated from the shear mobility as[73]

$$\eta_{\text{eff}}(h) = \left(\frac{d\chi(h)}{dh}\right)^{-1} \tag{26}$$

The technique helps us to resolve the effective viscosity at different depths inside the film. The effective viscosity values obtained via this technique are comparable to those obtained by other techniques for polymer films having the same thickness and similar molecular weight as observed in Figure 18(a), where the effective viscosity obtained by NCNS compared well with the viscosity values observed by Tsui group[76] using PSD technique and Bäumchen et al.[210] using capillary leveling.

NCNS couples the lower viscosity and hence higher shear mobility observed for surface layers of polymer thin films. The layer resolved effective viscosity obtained at various distances from the surface of the PS films follows the VFT behavior as shown in Figure 18(b). The technique also allows us to plot the layer resolved stress−strain. From Figure 18(c), it can be understood that the shear thinning in the layers close to the surface is much greater compared to the layers further away from the free surface.

Chowdhury et al.[72] used the layer-by-layer shear mobility obtained for low molecular weight PNBMA films to calculate the

https://doi.org/10.1021/acspolymersau.4c00022
ACS Polym. Au 2024, 4, 342−391

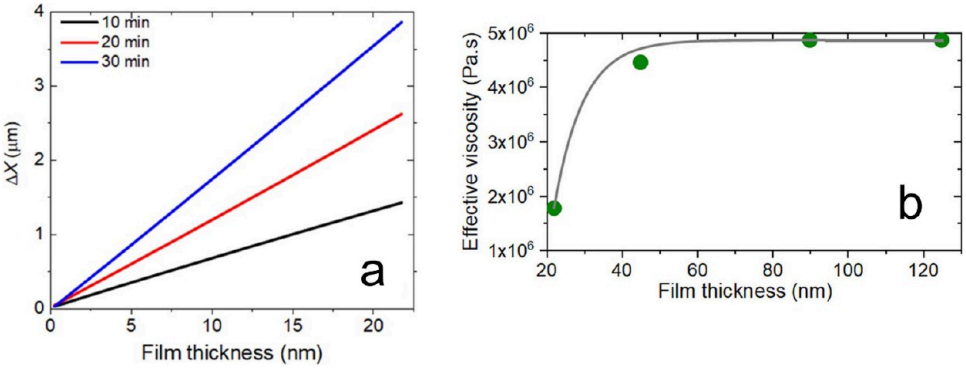

Figure 19. (a) Amount of lateral deformation (tilt) in the step-edge (ΔX) upon conducting NCNS of PNBMA 2.8 kDa, 22 nm film at 45 °C (ca. $T_{g,\,bulk}$ + 24 °C) with applied shear stress during NCNS τ = 174 Pa. (b) Thickness-dependent variation of effective viscosity of PNBMA (M_w = 2.6 kDa) films using the NCNS technique. [Reproduced from ref 72. Copyright 2022 ACS.]

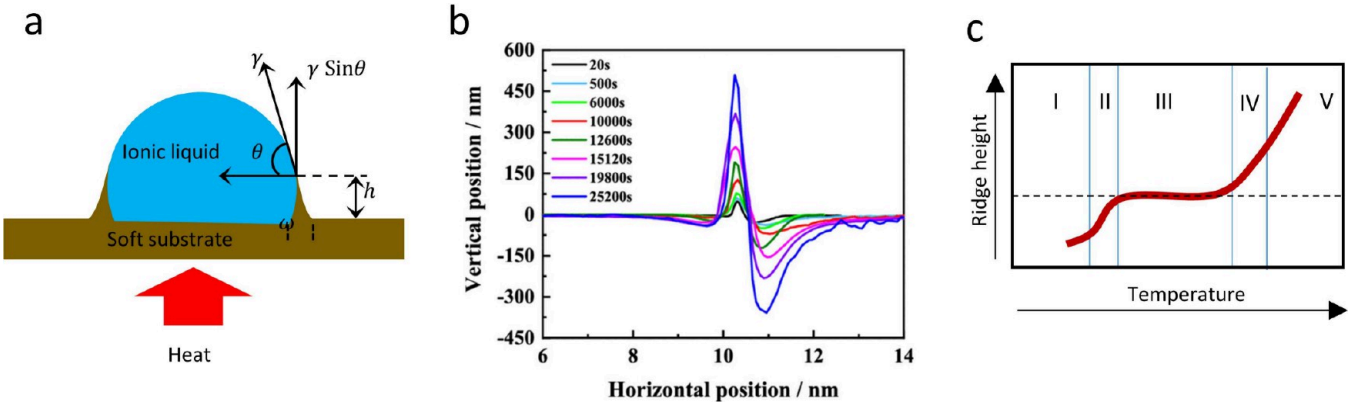

Figure 20. (a) Schematic of how the wetting ridge forms on a soft substrate due to the vertical component of Young's unbalanced force. (b) Height profile of a wetting ridge on the PS film with time. Film thickness: 400 nm; T = 403 K. [Reproduced from ref 238. Copyright 2021 ACS.] (c) Representative diagram illustrating the progression of ridge height growth at different temperatures, akin to the changes observed in the modulus value of a polymer with temperature variation.

effective viscosity in these films and found that the effective viscosity is thickness-dependent. Figure 19(a) shows the variation in the tilt produced at a particular point in the step edge by varying the film thickness. The increase in shear mobility of the film toward the surface is evident, resulting in the reduced effective viscosity of the film as shown in Figure 19(b). However, from the fast scanning calorimetry results, a thickness-independent T_g was observed for the same film, which resulted from the thickness-independent intrinsic molecular mobility, thereby decoupling the glassy dynamics from the viscosity in these thin supported films.

NCNS, although an innovative technique for directly observing the layer-by-layer resolved effective viscosity, has more room for further exploration. not been explored enough. More investigations using the technique spanning a variety of polymers can open up new directions in nanorheology research. The technique appeared to be applied to low molecular weight polymers with relatively appreciable viscous flow; largely due to the system's limited range of temperature control, especially for the flowing hot air or nitrogen. It is easy to confuse tilting in a step-edge by capillary leveling-induced self-similar flow with shear-induced tilting in a step-edge during NCNS. However, the notion of a nonstationary contact line in NCNS (akin to shearing during dewetting) identifies tilting during NCNS is indeed unique and different from capillary leveling.[73]

Wetting Ridge Technique

A liquid droplet on a hard substrate will undergo spreading or dewetting based on the interaction at the three-phase contact line.[234] According to Young's equation, the normal components cancel out, and only the horizontal components decide the spreading or dewetting behavior of the combination. When a liquid droplet is placed on a soft substrate like a viscoelastic material or a liquid, the capillary force's vertical component comes into play. It will locally deform the substrate by forming microscopic protrusions. This deformed region is known as the wetting ridge.[235−237] Figure 20(a) shows the schematic of the principle of wetting ridge formation.

The wetting ridge technique evolved as a tool for the characterization of the properties of soft materials as an extension of the dynamic wetting of a fluid on a soft substrate.[239,240] This phenomenon of dynamic wetting was a result of the stick−slip behavior shown by the wetting fluid. It was observed that the droplet spreads abruptly for a certain time and then remains static before the next jump. This was attributed to the deformation of the soft substrate by the formation of wetting ridges that affected the spreading of the droplet.[239,240] The spreading of the drop thus becomes influenced by the properties of the substrate. The motion of the wetting front results in viscoelastic dissipation. The asymmetric nature of the tip of the ridge and constant included angle at the tip throughout the developmental stage as observed by Park et al.[241] proves that

https://doi.org/10.1021/acspolymersau.4c00022
ACS Polym. Au 2024, 4, 342−391

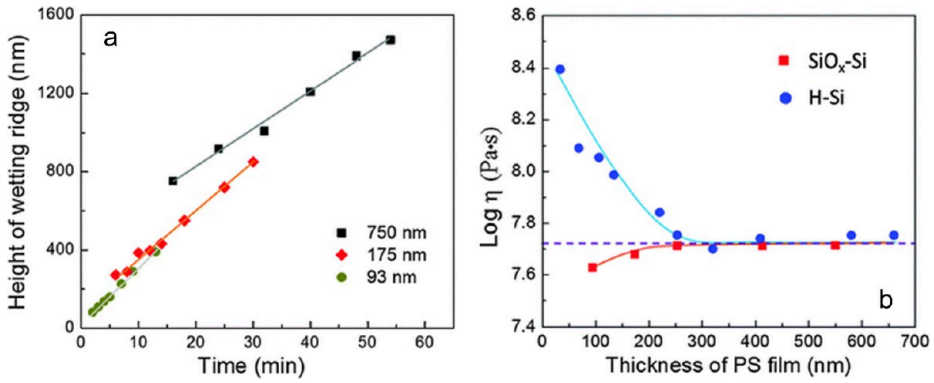

Figure 21. (a) Plots of the height of the wetting ridge (h) against the droplet deposition time (t) for 750, 175, and 93 nm PS films supported on the SiO_x−Si substrate; (b) viscosity as a function of the thickness of PS films on SiO_x−Si (square) and H−Si (circle) substrates, as measured by the proposed method. The errors in the data are within 5%. (T = 433 K; M_w = 442 kg mol^{-1}). [Reproduced with permission from ref 100. Copyright 2016 RSC.]

the deformation is only due to the viscous behavior of the film and the forces acting are invariant. It is also found that the ridge profile is independent of the modulus of the substrate.[240]

Shanahan and Carré[235−237,242] conducted a comprehensive analysis of the surface deformation characteristics of elastic solids, offering valuable insights into the wetting ridge phenomenon. They proposed an estimation for the height of the wetting ridge, approximating it to be on the order of $\gamma \sin \theta/G$, where G represents the modulus of the solid material. This insight into the geometric features of the wetting ridge provides a foundation for understanding its structural dimensions and the material's elastic properties. Subsequent studies by Severtson[243] and Park[241] delved deeper into the dynamics of wetting ridge growth, particularly on soft polymer surfaces. Their findings revealed the time-dependent nature of the growth process, intricately linked to the relaxation behavior of the polymer substrate. This temporal aspect adds a dynamic dimension to the wetting ridge phenomenon, emphasizing the role of polymer relaxation kinetics in shaping surface morphology. In alignment with these observations, Zuo and co-workers[244,245] contributed to understanding wetting ridge formation on ultrathin polymer films. A crucial aspect that emerged from these studies is the pronounced influence of viscoelastic properties and segmental relaxation dynamics within the polymer film. The interplay between these material characteristics and the temporal evolution of the wetting ridge highlights the intricate relationship between surface morphology and the internal dynamics of the polymer substrate.[244−246] As a result, it was postulated that the increase in height of the wetting ridge should be related to the viscoelastic properties like glass transition, segmental relaxation time, and effective viscosity of the soft substrate being used.[100]

The wetting ridge helps us to understand the viscoelastic information on the polymer substrate in two ways. (i) Understanding the behavior of polymer with respect to variation in the temperature and (ii) Understanding the time-dependent properties at a fixed temperature. Figure 20(b) and (c) show the AFM scans of the wetting ridge evolution over time and a representative image of the temperature dependence of the wetting ridge evolution, respectively.[100,108,244] The experiment involves placing an ionic fluid droplet on the polymer after preheating the polymer film. To study the temperature-dependent behavior of the polymer film, a wetting ridge height vs temperature plot is obtained, which can be divided into five regions (see Figure 20(c)).[100] There is not much rim formation in the glassy region; however, as the system's temperature increases, the ridge starts increasing in height. There is a steep increase in the height of the ridge as the polymer transitions from a glassy to a rubbery regime. In the rubbery region, the ridge height remains constant, similar to the behavior shown by the modulus of a polymer in the rubbery region. Beyond this regime, there is an increase in the height of the rim at higher temperatures where the polymer falls in the viscous regime.[13,100]

The viscosity of the polymer films can be obtained by analyzing the time-dependent behavior of the wetting ridge height. The height of the wetting ridge at a particular temperature where the growth is possible will show an initial nonlinear regime with respect to time. After a certain time the wetting ridge shows a linear regime. This linear regime should be related to the viscous flow of the polymer film.[100] Considering the response of the viscous flow, the strain rate is $\dot{\epsilon} = \frac{\sigma}{\eta}$, where, according to the consideration of the perturbation of the soft substrate by Shanahan,[235,242] $\sigma = \frac{\gamma \sin \theta}{\omega}$ is the stress acting over a distance ω. For a wetting ridge of height h, the strain is of the order h/ω. The strain rate $\dot{\epsilon} = \frac{h}{\omega t}$. Thus, the stress−strain relationship leads to $h(t)/t = k \approx \gamma \sin \theta/\eta$.[108] Hence, from the slope of the linear regime (k) in the wetting ridge height vs time plot, we can obtain the viscosity of the soft substrate. The generalized equation including a parameter α that takes into consideration of the polymer and ionic liquid being used, we get:[108]

$$\eta = \alpha \frac{\gamma \sin \theta}{k} \tag{27}$$

Investigation into the relaxation of polymer films floating on different ionic liquids led to the conclusion that the ionic liquids do not interfere with the relaxation of the polymer.[247] Hence, ionic liquids can be utilized for characterization applications.[245] The only characteristics to look out for are

- Negligible evaporation at measurement temperature.
- Immiscible with the substrate.
- Relatively large surface tension to guarantee a drop with a contact angle greater than 30°.

On exploring the time-dependent behavior of ridge height, Zuo et al.[100] constructed a master curve illustrating the polymer flow with increasing temperature. Remarkably, this curve was similar to the temperature-dependent modulus variations

https://doi.org/10.1021/acspolymersau.4c00022
ACS Polym. Au 2024, 4, 342−391

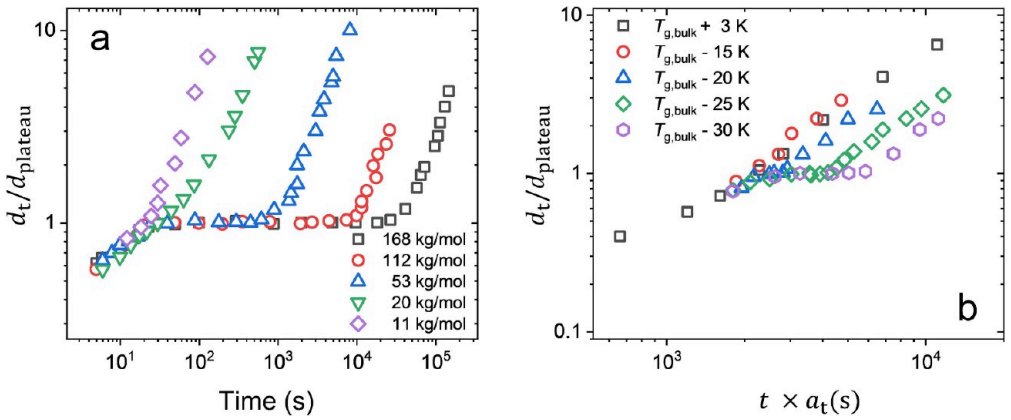

Figure 22. (a) Height of wetting ridge (d) as functions of creep time for PS film with various molecular weights (T = 378 K). The plateau disappears upon reducing the PS molecular weight to below 20 kg/mol, which is close to the entanglement molecular weight of PS (ca. 13 kg/mol). (b) Master curves of $d_t/d_{plateau}$ versus t for an unentangled PS (M_w = 11 kg/mol). [Data replotted from ref 13.]

observed in glassy polymers. This insightful correlation suggests an intriguing connection between the flow dynamics of the polymer and its modulus response to temperature changes, providing valuable insights into the material's behavior under varying thermal conditions. Additionally, the wetting ridge height was also dependent on the film thickness of the polymer. Thicker films showed a greater magnitude of ridge height in comparison to the film having a lower thickness. Observing Figure 21(a), it can be understood that although the magnitude of ridge height is lower for the thinner films, the rate of increase in ridge height is greater for thinner films in comparison to the thicker films. This could be due to the increased mobility expected for thinner films.[100]

Further investigations[100,108] into the influence of substrates on thin polymer films yielded noteworthy findings. Notably, the viscosity decreased with decreasing film thickness, a trend explicitly observed for the bare Si/SiO_x substrate. In contrast, substrates with hydrogen passivation and those featuring an increased phenyl group percentage exhibited an opposite behavior, showcasing an increase in viscosity as film thickness decreased.[100] The effect of hydrogen passivation on the effective viscosity calculated for PS films can be seen in Figure 21(b). This substrate-dependent viscosity modulation underscores the intricate interplay between the polymer and substrate, revealing how the substrate composition can influence the polymer flow characteristics. A similar result has also been observed and discussed in the section on PSD (Figure 7).

Additionally, the research shed light on the impact of interfacial layers on chain mobility, uncovering that this effect is contingent on molecular weight. The height to which the interfacial layer influences chain mobility was found to vary based on the molecular weight of the polymer. This nuanced understanding of the interplay between substrate, film thickness, and molecular weight contributes to the broader comprehension of polymer dynamics in thin films.[108]

Recently Wang et al.[238] showed that on confining the polymer thin films to geometries lower than ≈3.3R_g, the chain entanglement density decreased and the entanglement molecular weight increased. They correlated the time at which there is a transition in the ridge height from a constant value in the elasticity-dominated regime to linearly increasing values where the viscosity is more dominant to the disentanglement time when the chains are no longer entangled and can slide over one another.

Hao et al.[13] have investigated the surface mobility gradient in unentangled PS thin films and observed the breakdown of time−temperature superposition at the surface mobile layer. The wetting ridge technique was used to investigate the creep behavior of the films and separately study the effect on the bulk of the films and the surface layer by experimenting above and slightly below the glass transition temperature. Increasing the temperature above T_g results in increased mobility in the bulk of the polymer; hence, the wetting ridge growth captures the information on the entire film. However, on experimenting just below the bulk glass transition temperature, it was observed that although the wetting ridge forms, the increase in the height of the ridge is much less compared to the case where $T > T_g$. Thus, the ridge formation could be due to the surface layer alone, which is mobile even below the T_g. The plateau region in the ridge height vs time plot, which is supposed to be temperature-independent and only M_w-dependent (Figure 22(a)), showed an increasing value as the experimental temperature was reduced below T_g. In Figure 22(b), the plateau region, which usually signifies the entangled nature of the polymer chains, becomes prominent upon decreasing the temperature of the creep experiment below T_g. The presence of an entanglement-related feature in an unentangled polymer film was attributed to the presence of a mobility gradient in the film.[13] However, the presence of multiple intrinsic time scales in polymers could also have impacted such behavior of the wetting ridge in this case, as the time scales of relaxations are temperature-dependent.

The wetting ridge technique utilizes a very simple experimental setup making it a very cost-effective method to characterize polymer thin films. Identification of the probe fluid is of prime importance as care should be taken to avoid any interaction with the polymer film being tested. The technique is nondestructive and provides quantitative information on thin polymer film properties. Other than the bubble inflation technique and the thin film creep testing, the wetting ridge is the prominent technique that provides the opportunity for studying the creep behavior of polymer thin films. Although the wetting ridge majorly probes the surface of the polymer film, it is not immune to the substrate effects. Thus, the properties extracted are an effective value as is the case with PSD.

Dewetting

When a fluid is dropped on a substrate, the interaction between the fluid and the interface results in either spreading or dewetting, depending entirely on the interfacial forces at play. At

https://doi.org/10.1021/acspolymersau.4c00022
ACS Polym. Au 2024, 4, 342−391

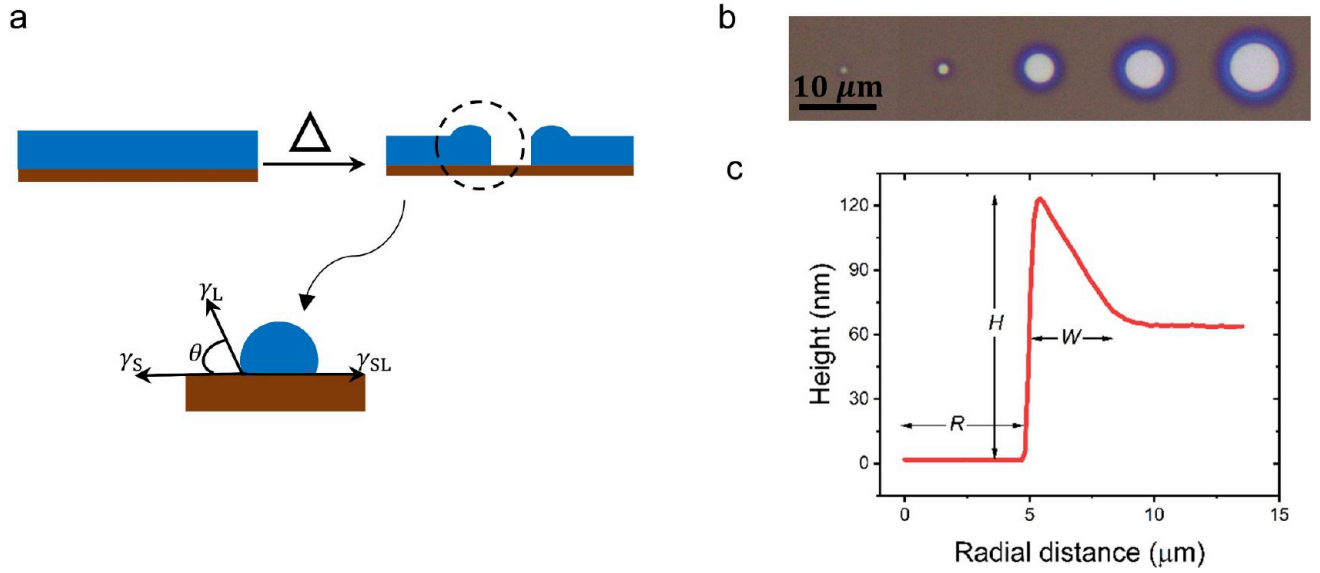

Figure 23. (a) Schematic showing the principle of dewetting. The films start dewetting when heating the polymer films above the glass transition temperature. The net capillary stress acting on the dewetting films will depend on the interfacial forces at play. (b) Optical images depicting the sequential growth of a hole in a PTBS film (M_n = 1100 kDa, h_0 = 60 nm) during dewetting at a temperature of 180 °C illustrate the temporal progression of the process. (c) AFM profile of half of the hole showing the radius of hole R, rim width W, and rim height H.

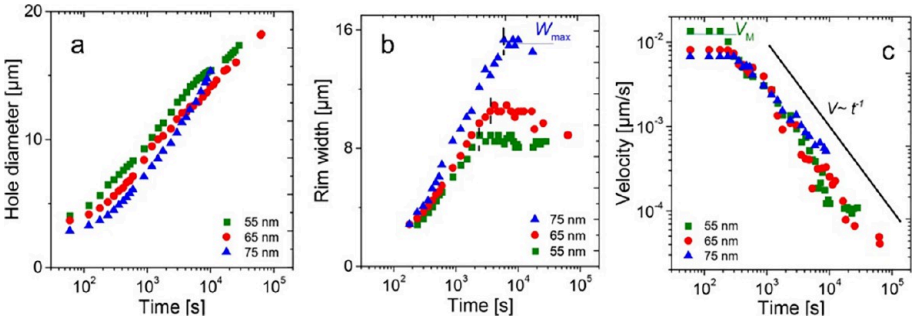

Figure 24. Temporal evolution of (a) dewetting hole diameter ($2R$) and (b) width (W) of the rim of holes growing in thin PS films of M_w = 1000 kDa at 125 °C for indicated film thicknesses. The times τ_w when W reached a maximum value are indicated by short dashed lines in (b). (c) Corresponding decrease in dewetting (hole growth) velocities with time, for the holes shown in (a and b). [Reproduced with permission from ref 142. Copyright 2017 John Wiley and Sons.]

the three-phase contact line, where the fluid meets the substrate, three interfacial interactions govern this behavior.[234] The substrate−liquid interfacial tension (γ_{SL}), the substrate−air interfacial tension (γ_S) and the liquid−air interfacial tension (γ_L).[234,248,249] The resultant of the three interfacial tension decides the spreading or dewetting tendency of the fluid on the substrate (Figure 23(a)). The dewetting technique leverages the tendency of a fluid to retract from a nonwettable substrate to attain its equilibrium contact angle, thereby providing insights into the properties of the polymer film. The presence of a slippery layer is ensured by preparing an adsorbed layer of PDMS on top of a silicon substrate. Polymer films, when well below the glass transition temperature, exhibit no dewetting from the slippery substrate due to the restricted mobility of the polymer chains. However, upon heating the film−substrate system above the glass transition temperature, the polymer film undergoes dewetting, above a critical film thickness marked by the nucleation and growth of holes.[31,234,248]

These holes represent regions where the material is removed and subsequently redistributed. When the hole radius (R) is small in the initial stages, the material redistributes into the film around the hole. At this early phase, viscous dissipation within the polymer film dominates as the primary dissipation mechanism.[142] When the holes reach a critical size, the interfacial friction becomes prominent, impeding the redistribution of the material into the film. This results in the accumulation of polymer around the hole, forming a discernible rim.[142,250] The rim can be seen in Figure 23(b) as the blue boundary between the holes and the polymer film. The same can also be observed in the AFM scan of the hole shown in Figure 23(c). The width of this rim (W) grows as the dewetting process progresses (Figure 24(b)).

The dynamics of dewetting are characterized by the radius of hole growth (R), the velocity of hole growth (V), and the growth of the rim width (W). The optical images of the increase in hole radius during the dewetting experiment can be seen in Figure 23(b). The parameters characterizing hole growth for variable thickness have been shown in Figure 24. As the thickness of the dewetting film reduces, the hole radius increases for the same dewetting time (Figure 24(a)). The increased rate of hole growth in thinner polymer films results in a higher V_{max}, as can be observed in Figure 24 (c); however, after the initial period of dewetting, the V vs t plot for all films following a similar scaling. The rim width attains the maximum value at an earlier dewetting

https://doi.org/10.1021/acspolymersau.4c00022
ACS Polym. Au 2024, 4, 342−391

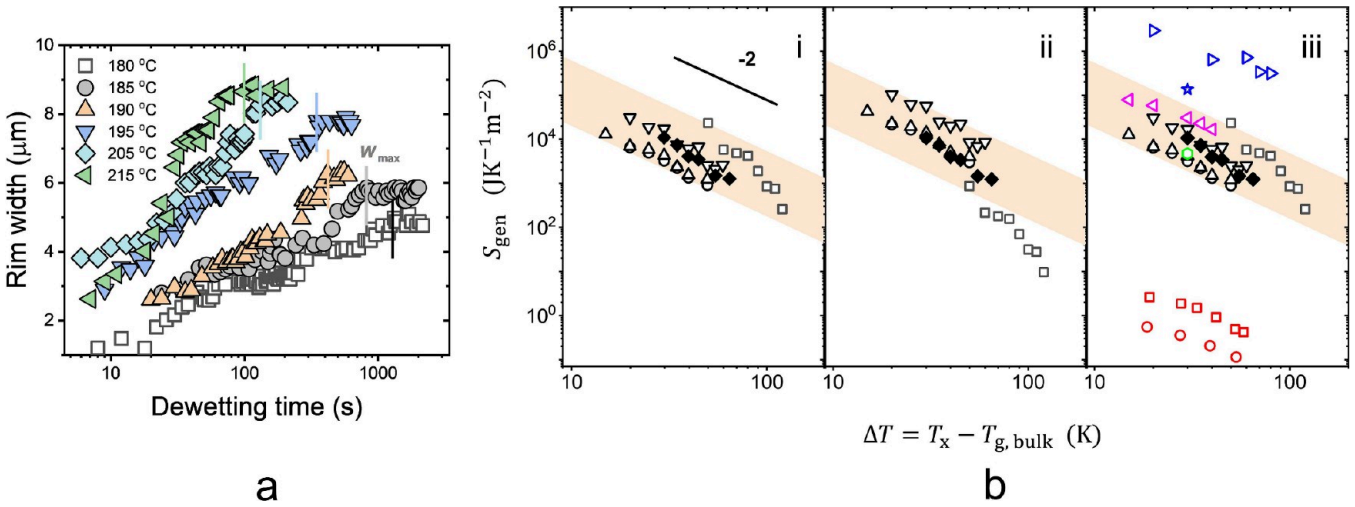

Figure 25. (a) Rim width vs dewetting time plot of PTBS thin film (M_n = 1100 kDa, h_0 = 60 nm). The increase in dewetting temperature results in an increase in W_{max}, and τ_w is achieved at an earlier time. (b) (i): Entropy generation values upon varying dewetting temperatures [plotted as ($T_x - T_{g,bulk}$), where $T_x = T_{dew}$] for PTBS (M_w = 1100 kDa, h_0 = 60 nm, black solid diamonds) plotted along with those calculated for other dewetting experiments reported in the PS (PS) film dewetting literature. Open black circles (PS, M_w = 2500 kDa, h_0 = 40 nm),[142] open black triangles (PS, M_w = 4840 kDa, h_0 = 40 nm),[142] open black inverted triangles (PS, M_w = 16800 kDa, h_0 = 40 nm),[142] open black squares (PS, M_w = 540 kDa, h_0 = 180 nm).[135] (b)-(ii): Same plots as in (b)-(i) but film thicknesses have been scaled to 60 nm by using $\tau_w \sim h_0^3$.[142] (b)-(iii): plots including the entropy generation until the reported characteristic relaxation times (τ) in other experiments from published literature. All the black symbols represent dewetting data on slippery solid substrates, as used in our experiments, and carry the same meanings in (i-iii). Except the green open hexagon is obtained from dewetting of PS (M_w = 286 kDa, h_0 = 135 nm) over a liquid substrate.[259] Magenta open tilted inverted triangles are the residual stress relaxation time as $\tau = \tau_{res}$ from fluorescence spectroscopy experiments on PS (M_w = 200 kDa, h_0 = 680 nm).[141] Blue symbols denote S_{gen} calculated from irreversible adsorption experiments considering the crossover time as $\tau = \tau_{crossover}$:[74,78] blue open tilted triangles represent PS (M_w = 325 kDa, h_0 = 300 nm),[78] blue open stars represent PTBS (M_w = 70 kDa, h_0 = 200 nm).[74] Red symbols denote S_{gen} calculated from dielectric spectroscopy measurements for SAP studies considering molecular relaxation time as $\tau = \tau_{mol} = \tau_{SAP}$:[92,260] red open squares are PS (M_w = 955 kDa) and red open circles are PTBS (M_w = 156 kDa). Film thickness in both cases is ca. 200 nm. For experiments beyond dewetting T_x could be considered as T_{ann}, annealing temperature above the respective $T_{g,bulk}$. [Reprinted with permission from ref 18. Copyright 2024 AIP.]

time for thinner films (Figure 24(b)). The scaling relations of the dewetting liquids are well explored in the literature.[234,248,249,251−254] The velocity of hole growth for a Newtonian fluid dewetting on a substrate is supposed to scale with dewetting time as $V \sim t^{-1/3}$.[234,251] However, in general, a scaling of $V \sim t^{-1/2}$ can be characterized as the scaling for the dewetting of viscoelastic films until the reptation time is reached.[31,250,255] After attaining the reptation time, viscoelastic nature of the polymer changes to pure viscous fluid and the scaling becomes $V \sim t^{-1/3}$.[234,251] Reiter et al.[31] have observed scaling of $V \sim t^{-1}$ when dewetting the polymer films having a molecular weight much higher than the entanglement molecular weight of the polymer. The observed scaling presented an intriguing aspect, leading to the postulation of an additional driving force that is quickly diminishing during dewetting. This resulted in a more pronounced reduction in dewetting hole velocity than what is typically observed for normal viscoelastic polymer films. An interesting shift was noticed in the scaling behavior from $V \sim t^{-1}$ to $V \sim t^{-1/2}$ as the dewetting progressed.[31,250,256,257] This shift indicated a relaxation time for the additional driving force, molecular recoiling stress (σ_{rec}). Notably, the relaxation time of σ_{rec} was considerably lower than the actual reptation time of the polymer at the dewetting temperature.[17,32,142,257] This suggests that the relaxation of σ_{rec} requires motion of only extremely small units within the polymer chain segments, and not entire segments as in α-process. Chowdhury et al.[32] investigated the relaxation of recoiling stress below the glass transition temperature and identified that the activation energy associated with such relaxation is comparable to the β-relaxations, which do not involve main chain segmental relaxations. Later they discussed this with a similarity to SAP relaxation.[18,92,94]

In the context of σ_{rec}, the height of the rim is a crucial parameter that provides valuable insights from dewetting experiments on polymer films. As the dewetting progresses, the height of the rim (H) increases over time. Unlike the symmetrical rims typically observed in normal liquid dewetting, polymer films undergoing dewetting exhibit asymmetrical rim shapes, with the steeper side facing the hole.[250,255] This asymmetry results from the elastic nature of the viscoelastic polymer thin films, resisting the formation of a symmetrical (promoted by Laplace pressure) rim and responding to the driving force by increasing the height of the rim.[250] Consequently, the increase in rim height relative to the original film thickness can be considered as the strain (ϵ) in the film.[89,256] The stress acting on the film can then be determined using the bulk value of plateau modulus (G) of the polymer film.

$$\sigma_{tot} = G \cdot \epsilon = G \cdot \left(\frac{H - h_0}{h_0} \right) \tag{28}$$

where H is the height of the rim, h_0 is the original film thickness, and σ_{tot} is the total stress acting as the driving force. This includes both σ_{rec} and capillary stress (σ_{cap}). The capillary stress can be obtained from the surface tension of the dewetting film ($\sigma_{cap} = \frac{\gamma\theta^2}{2}$).[234,258] The nonequilibrium polymer chain conformation-induced molecular recoiling stress can be calculated by subtracting the capillary stress from the total stress in the film, assuming capillary stress would remain the same during the entire dewetting experiment.

https://doi.org/10.1021/acspolymersau.4c00022
ACS Polym. Au 2024, 4, 342−391

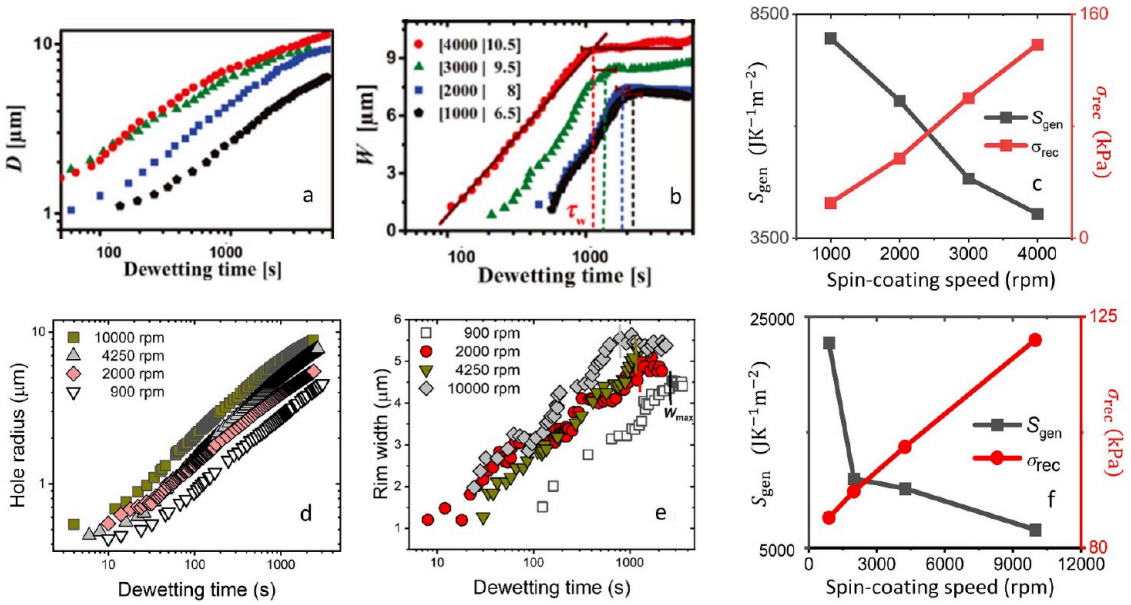

Figure 26. Increase in dewetting dynamics, and entropy generation associated with the decrease in τ_w for increased spin-coating speed for PS (M_w = 1260 kDa, h_0 = 50 nm) from the work of Kchaou et al.[262] and for PTBS (M_n = 1100 kDa, h_0 = 60 nm) from the work of Madhusudanan and Chowdhury.[18] (a) and (d) show the increase in dewetting hole diameter for PS and hole radius for PTBS films, respectively. (b) and (e) show the increase in rim width as the dewetting proceeds and attains a maximum value of W_{max} at τ_w for PS and PTBS, respectively. The entropy generation values per unit area (S_{gen}) are calculated for (c) PS and (f) PTBS films. [Figures (a) and (b) reprinted with permission from ref 262. Copyright 2018 APS. Figures (c)−(f) reprinted with permission from ref 18. Copyright 2024 AIP.]

$$\sigma_{rec} = \sigma_{tot} - \sigma_{cap} \tag{29}$$

In addition to the change in scaling of the dewetting velocity with dewetting time due to σ_{rec}, the evolution of rim width while dewetting also indicates decay in σ_{rec} as a dominant driving force. On following the growth of rim width over time while dewetting, it is observed that the rim width attains a maximum value at dewetting time τ_w and remains constant on further dewetting (Figure 25(a)). This is also the point of time (τ_w) when the scaling of the velocity of dewetting changes from the $V \sim t^{-1}$ scaling to $V \sim t^{-1/2}$. From the early works,[31,250,255−257] it is clear that the rim width attains a W_{max} when the hole growth reaches the stage where σ_{rec} is no longer a dominant driving force. The τ_w, which marks this point of transition from the σ_{rec}-dominated regime to the σ_{cap}-dominated regime, shifts with variation in dewetting temperature. However, one might anticipate that the entropy gained until τ_w for films of the same polymer dewetting at different conditions would be identical, given that the relaxations in polymers far from equilibrium are entropy-driven, Madhusudanan and Chowdhury[18] demonstrated through an entropy generation (S_{gen}) approach that the entropic states achieved by polymer films until τ_w under different dewetting conditions are not similar.

Madhusudanan and Chowdhury[18] considered the dewetting of polymer thin film on a heating stage analogous to a thermodynamic system that receives heat from a high-temperature reservoir and transfers it to a low-temperature reservoir. As per the second law of thermodynamics, there is entropy generation in the polymer system due to the heat transfer.[261] This entropy generated until τ_w was calculated considering the Claussius' inequality. The entropy change during an irreversible process is always greater than zero.[261] It was found that as the dewetting temperature is increased, there is a reduction in entropy generated until τ_w. This means that the state of entropy reached at τ_w for higher dewetting temperatures is not the same as that achieved at lower dewetting temperatures.[18] On calculating the entropy generation values for various experiments from literature, considering the relaxation times (Figure 25(b)) obtained for that particular experiment, all the entropy generation values can be found to approximately follow a similar scaling with respect to ΔT which is $T_x - T_{g,bulk}$. Here T_x is the experimental temperature, where the film is getting annealed (dewetted). Figure 25(b)(i) shows the S_{gen} values calculated from dewetting experiments conducted at varying dewetting temperatures (T_{dew}) for PS and PTBS.[18,135,142] The increase in T_{dew} results in a decrease in S_{gen} until τ_w and is found to follow an approximate scaling of $S_{gen} \sim \Delta T^{-2}$. Figure 25(b)(ii) shows the same plots as in (i) however, the thicknesses of the dewetting polymer films have been rescaled to a common thickness of h = 60 nm. This rescaling was performed following the relation established by Chowdhury et al.,[32] $\tau_w \sim h_0^3$ where h_0 is the polymer film thickness. Figure 25(b)(iii) shows in addition to the data in (i), the S_{gen} calculated from fluorescence, irreversible adsorption, and dielectric spectroscopy measurements. The S_{gen} values were obtained by considering the characteristic relaxation time as residual stress relaxation time for fluorescence experiments,[141] crossover time from the linear to logarithmic growth of adsorption layer in the irreversible adsorption experiments[74,78] and the molecular relaxation time from SAP experiments using dielectric spectroscopy.[92,260] All the data can be found to follow a similar scaling with respect to ΔT, which could be due to a common mechanism associated with the entropy generation.

The observed reduction in entropy generation values until τ_w for polymer films undergoing dewetting at higher temperatures or until the corresponding relaxation times in other experiments raises the possibility that the entropic states achieved by the polymers in the course of experiments are not identical. This suggests that, despite similar initial conditions in film preparation, i.e., equal initial entropic states, the corresponding

https://doi.org/10.1021/acspolymersau.4c00022
ACS Polym. Au 2024, 4, 342−391

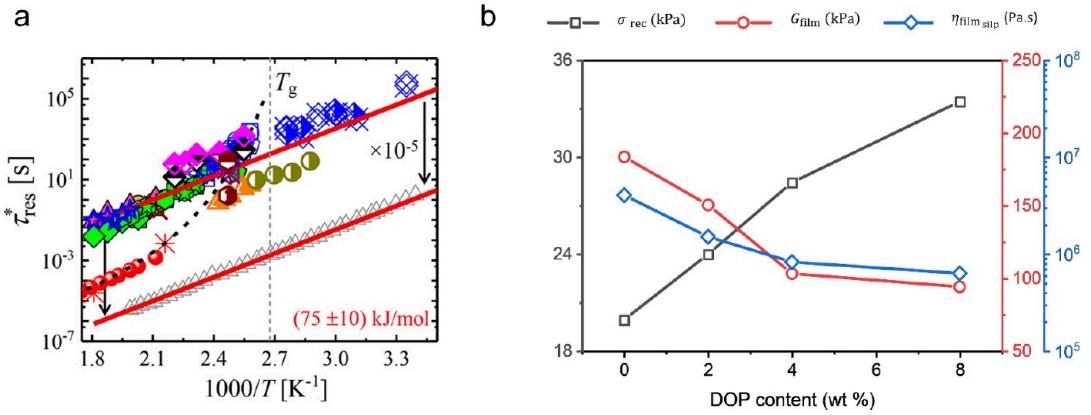

Figure 27. (a) Normalized relaxation time following an Arrhenius dependence with temperature showing an activation energy close to 75 kJ mol^{-1}. The data points include the relaxation time calculated from dewetting experiments, fluorescence studies, and irreversible adsorption studies. [Reproduced from ref 135. Copyright 2019 ACS.] (b) Increase in DOP mass fraction with respect to PS (M_w = 963 kDa, h_0 = 90 nm) resulting in increased σ_{rec} while reducing the modulus and viscosity of dewetting films. [Reproduced from ref 75. Copyright 2023 ACS.]

relaxation times at varying temperatures would only guarantee that the polymers have attained an initial metastable state beyond which the relaxation of stress in the system would happen through sequential attainment of different metastable states.[18] The shift of τ_w, where a relaxation of σ_{rec} is expected, to earlier times during dewetting at higher temperature was explained based on the frustrated relaxation of a higher number of polymer chain segments resulting in an initial metastable state at τ_w where the σ_{rec} has partially relaxed.

Chowdhury et al.[142] extensively investigated the dewetting of polymer thin films focused on the relaxation of σ_{rec}, which manifests the nonequilibrium in the spin-coated polymer films. The dewetting parameters like the initial dewetting velocity (V_{max}), the hole radius (R), and the rim width maxima (W_{max}) are sensitive to the magnitude of σ_{rec} present in the polymer film. Reducing the thickness of the polymer films resulted in an increase in R for similar times of dewetting. When compared to thicker films,[142] V_{max} was also found to have a greater value for thinner films.[142] Since the σ_{cap} is the same as the polymer being used is same, the only variable in the driving force is σ_{rec}. Thus, the increase in σ_{rec} can be correlated to the reduced thickness.

Based on the ratio of time required for full relaxation of the polymer chain (τ_{eq}) and the time available for relaxation of the polymer chains (t_{prep}), Chandran et al.[134] defined a preparation parameter ($\mathcal{P} = \frac{\tau_{eq}}{t_{prep}}$). This preparation parameter helped quantify how far the polymer film is, from its equilibrium. The $\mathcal{P}$ value was varied by varying the speed at which the polymer films were prepared by spin-coating. As the preparation parameter was increased, the σ_{rec} increased.[134,262] This was attributed to the polymer chains being trapped in conformations further away from equilibrium as the evaporation rates are higher at higher spin-coating speeds. The number of holes forming in the dewetting experiments was also directly proportional to the preparation parameter. Chandran and co-workers[134] established a scaling law that relates the σ_{rec} to the preparation parameter as $\sigma_{rec} \sim \mathcal{P}^{2\pm0.2}$. The increase in σ_{rec} by an increase in $\mathcal{P}$ was coupled with a decrease in the τ_w value. Figure 26 shows the effect of increasing spin-coating speed resulting in a higher rate of hole growth for PS (Figure 26(a)) and PTBS (Figure 26(d)) thin films. Figure 26(b) and (e) show the reduced τ_w associated with an increase in σ_{rec} for PS and PTBS films, respectively. This decrease in the value of τ_w for varying spin-coating speeds was correlated to a reduced S_{gen} in the polymer films until τ_w while dewetting them at the same T_{dew}.[18] The reduced S_{gen} associated with an increase in σ_{rec} is shown in Figure 26(c) and (f) for PS and PTBS, respectively.[18] The simultaneous relaxation of a greater number of polymer chain segments in a film having higher σ_{rec} results in a greater probability of frustrating the relaxation of adjacent chain segments and trapping them in a metastable state where the relaxation of the σ_{rec} is only partially attained. This result indicates the qualitative difference in the entropic states achieved by polymer films having varying σ_{rec} dewetting at the same dewetting temperature.[18] Chandran and Reiter[135] investigated PS films of varying molecular weights using dewetting experiments and obtained relaxation times that follow an Arrhenius dependence with temperature. On comparing the relaxation times obtained for PS films which were already published in the literature using complementary experiments, they found a similar Arrhenius dependence with temperature with a common activation energy of ≈75 kJ/mol (Figure 27(a)). They suggested that the wide range of relaxation times that cross the reptation time and the activation energy being unaffected by the glass transition would mean the relaxation of σ_{rec} could be different from the glassy dynamics of segments and reptation-like motion of chain diffusion. The relaxation happens via the rearrangement of correlated segments having relaxation times longer than the segmental relaxation time.[135]

Tuning the σ_{rec} can also be achieved by adding a plasticizer to the polymer film. Madhusudanan et al.[75] observed a decoupling in the effect of plasticizer on the σ_{rec} in comparison to its impact on the modulus and viscosity of dewetting polymer thin films (see Figure 27(b)). The addition of plasticizer (DOP) resulted in enhanced V_{max} and W_{max} in addition to a reduction in the value of τ_w by an order of magnitude. From Figure 27(b), we can observe that as the mass fraction of the plasticizer increased, the strain in the films increased driving dewetting. The increase in strain could be either due to the increase in σ_{rec} or a decrease in the modulus of the film due to plasticization. Although all dewetting dynamics-related parameters indicated an increase in σ_{rec} due to the presence of DOP, to remove any contribution to the total strain from reduction in modulus due to plasticization, the actual modulus was also calculated experimentally utilizing the analysis introduced by Mulama et al.[263] that involves the relation between viscosity and modulus which derives from

https://doi.org/10.1021/acspolymersau.4c00022
ACS Polym. Au 2024, 4, 342−391

Maxwell's model ($\eta = G{\cdot}\tau$).[264−266] Here, τ is the characteristic relaxation time obtained by fitting an exponential decay function to the V_{max} of successive generation of holes during dewetting.[263] There is a progressive decrease in V_{max} of the hole formed in successive generations due to the relaxation of σ_{rec} during dewetting. η is the viscosity obtained by analyzing the AFM profile of the rim using the method initially introduced by Fetzer et al.[267] The experimentally obtained modulus could not accommodate the entire strain observed, and hence, it could be inferred that the enhanced dynamics of hole growth were due to the increased σ_{rec}. Thus, the addition of plasticizer resulted in a reduction in modulus and viscosity but enhanced σ_{rec}. Later, Sarkar et al.[268] showed that incubation of the polymer film in nonsolvents can also affect the stability of the film.

Dewetting as a characterization technique has been explored very well in literature to establish it as a nanorheology tool. The ability of the method to be sensitive to the segmental level polymer chain dynamics and experimentation largely using a series of optical microscopic images, making it a simple and robust technique. The dewetting technique is highly sensitive to surface contamination as the heterogeneities can nucleate holes, which may not reflect the true properties of the polymer films. A reproducible nonwettable substrate is very important to have reliable dewetting dynamics. The requirement of AFM is essential to analyze the morphology of dewetting holes, but it is minimal. The size of dewetting holes is typically in microns, which is larger than the molecular level length scale of dynamic heterogeneity responsible for glass transition, which makes the dewetting technique limited to be sensitive to probing possible heterogeneity in polymer chain associated properties.

Brillouin Light Scattering

Brillouin light scattering (BLS) is a nondestructive technique that can be employed to determine the mechanical properties of a material. Every material possesses thermally activated phonons that modulate the dielectric properties of the material, even at room temperature.[269] When a monochromatic light source is focused onto the material's surface, it interacts with these phonon-induced modulations, resulting in light scattering.[270,271] The inelastic scattering of incoming photons by the thermally activated phonons in the material is utilized to extract information about the material.[272−274] Various acoustic guide modes are present in the material, and these can be identified by carefully analyzing the scattering data in terms of polarization studies of incoming and scattered radiation at different incident angles.[275] Figure 28 illustrates a backscattered configuration used in conventional BLS experiments.

The shift in the frequency (f) of the scattered radiation can be correlated to the velocity (v) of the acoustic wave. From the conservation of momentum in the plane of the film, the phonon wave vector:[276]

$$Q_{II} = \left(\frac{2\pi}{\lambda}\right)(\sin\theta_i + \sin\theta_s) \tag{30}$$

where θ_i is the angle of incidence and θ_s is the angle of scattering. The phonon velocity is obtained from[276]

$$v = \frac{2\pi f}{Q_{II}} \tag{31}$$

The elastic constants (C) of a material can be derived from the velocity of the acoustic wave. The acoustic velocity is the square root of the material's mechanical stiffness ratio to its mass density (ρ), which gives[276,277]

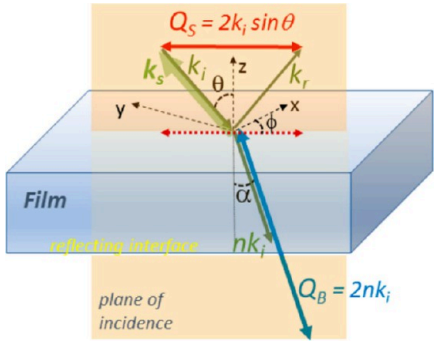

Figure 28. Backscattering geometry for conventional surface Brillouin light scattering (surf-BLS) experiments. The wave vectors of the incident, reflected, transmitted, and scattered light are indicated in green, while acoustic waves are in red (surface waves) or blue (bulk waves). All are contained in the plane of incidence. [Reproduced from ref 275 available under CC BY license. Copyright 2018 MDPI.]

$$C = \rho v^2 \tag{32}$$

Different acoustic modes provide information about the various components of the elastic constant. The number of elastic constant components required depends on the type of sample used.[277,278] In the case of thin films, it is often considered that they are isotropic to an excellent approximation. The longitudinal and transverse elastic constants adequately describe the properties of such films. Forrest et al.[278] utilized the Brillouin scattering technique as a probe to determine the glass transition temperature of thin, freely standing polymer films. By observing the movement of the symmetric Lamb mode (S_0) while increasing the temperature, they identified a distinct rate of shift in the peak at temperatures both above and below the T_g.[278] This method allowed them to ascertain the glass transition temperature of the film. Furthermore, Forrest et al.[57] demonstrated the thickness dependence of the glass transition temperature, attributing it to the free surface effect in thin films. Interestingly, this variation in glass transition temperature with thickness did not translate to a significant variation in elastic constants. Using multilayered films, Forrest et al.[277] showed that the variation in elastic constants was minimal. In freely standing films, the thermal expansion, mass density, and mechanical stiffness were found to align with bulk values despite significant variations in T_g values being observed.[65,276] Hartschuh et al.[272] investigated the elastic modulus of the polymer film under both 1-D and 2-D confinement. They observed no variation in the elastic modulus down to 80 nm film thickness. However, as the thickness of the ridge in the grating reduced, the peak broadness increased. This could be due to the increased damping from the sides of the ridge. Transmission scattering[279] probed the mechanical properties of films on a transparent substrate. This was the first time the experiment was conducted on a transparent substrate. This prevented the heating issue in opaque substrates.

Gomopoulos et al.[274] used the reflective mode BLS to prove the in-plane and out-of-plane isotropy of the PS and PMMA thin films from 40 nm to 3 μm. The first report of the thickness dependence of elastic modulus of thin films using BLS was brought to notice by Johnson et al.[273] The decrease in modulus, as obtained through BLS, was found to align with values obtained via buckling, providing consistency in the results. Further advancements involved coupling BLS with Raman spectroscopy to gain additional structural information.[280]

https://doi.org/10.1021/acspolymersau.4c00022
ACS Polym. Au 2024, 4, 342−391

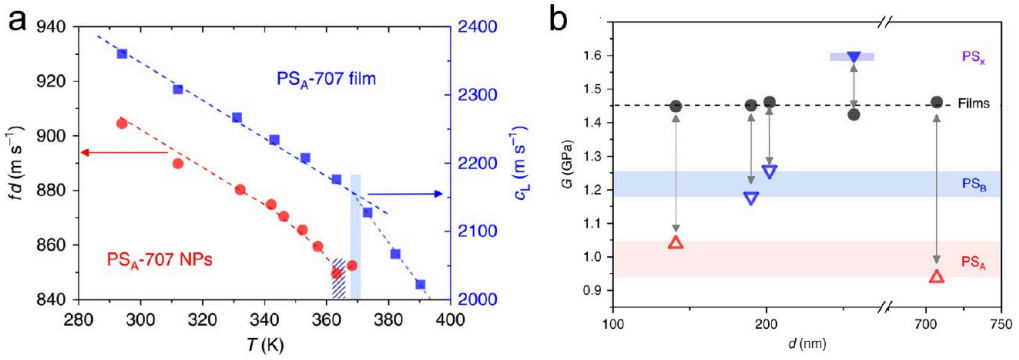

Figure 29. (a) Temperature-dependent $f(s,1,2)$ (which is the lowest frequency BLS active mode). Polystyrene nanoparticles (PSNPs) with diameter d = 707 nm, referred as PS$_A$-707 and cortresponding annealed bulk film. The subscripts A and B indicate different emulsion polymerization conditions while preparing those polymer nanoparticles. Red and blue circles represent the scaled frequency $f(s,1,2)\cdot d$ for NPs (left y-axis) and the longitudinal sound velocity (c_L) of the annealed bulk film (right y-axis), respectively. The hatched and filled areas in (a) indicate the softening (T_s) and glass-transition (T_g) temperatures, respectively. (b) Shear modulus (G) of nanoparticles and the corresponding annealed films. The black dotted line indicates the average value of G in the annealed bulk films. Arrows indicate the nanoconfinement effect of NPs compared to their corresponding films. Blue and red areas refer to the softening of PS$_A$ and PS$_B$ type NPs, respectively. The purple area above indicates the hardening of cross-linked PS$_X$ NPs. [Reproduced from ref 133 available under CC BY license. Copyright 2018 Nature.]

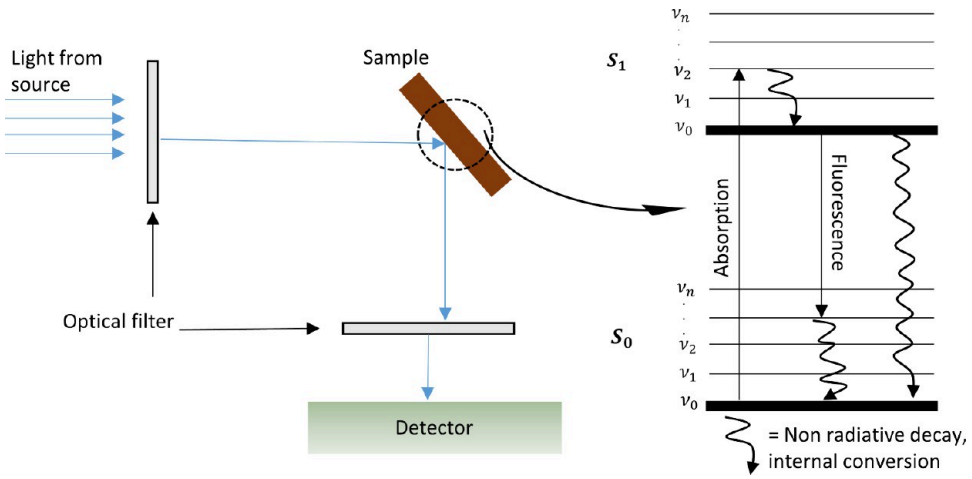

Figure 30. Schematic showing the principle of fluorescence technique. The electrons in the samples get excited by the incident photons to a higher energy state S_1 from S_0. The excited electrons can either return to their ground state by nonradiative decay or fluorescence, as represented in the figure.

The change in elastic properties of polymers in 3-D confinement was investigated by Kim et al.[133] using polystyrene nanoparticles (PSNPs). The confinement effect was observed due to a softening observed at a temperature lower than the glass transition temperature of annealed films (Figure 29(a)). The frequency $f(s,1,2)$ in the figure is the lowest frequency mode that is BLS active. The shear modulus can also be found to decrease for the nanoparticles; however, the cross-linked PS nanoparticle showed an increase in shear modulus (Figure 29(b)). An interesting finding was the absence of confinement effect on the glass transition in the nanoparticles. However, the nanoparticles showed softening and interactive behavior among each other owing to the higher mobility of the surface chains. Thus, it was hypothesized that there was a requirement of a critical thickness of the surface mobile layer that would be required to influence the glass transition temperature.[133] Graczykowski et al.[281] explored 1-D confined films using BLS, demonstrating the manipulation of destructive interference of different modes through variations in incident light polarization and phonon wavenumber. They also presented a measurement of shear horizontal waves in thin membranes. In a study by Oh et al.[282] the mechanical properties of poly(ether imide) (PEI) and poly(ether sulfone) (PES) were investigated under varying pressure conditions. PEI and PES exhibited a significant increase in bulk and elastic modulus, while the Poisson's ratio remained constant. The acoustic velocity and mass density showed a rapid increase on increasing pressure to 2 GPa, followed by a relatively slower increase up to 11 GPa.[282]

BLS requires the user to be very specific about the sample configurations as the data obtained can be affected by the isotropy of the sample and the effect of substrate on scattered data, etc. The acoustic mode selection to determine the phonon's velocity is also important.

Fluorescence

Fluorescence-based methodologies have proven highly effective in studying glassy polymer thin films, primarily due to their capability as precise and location-specific labeling markers and tracers with high resolution. A comprehensive and engaging overview of recent advancements in fluorescence techniques for characterizing nanoconfined glassy polymers can be accessed.[283] In our brief discussion we have divided our discussion into two parts: steady-state fluorescence-based methods and fluorescence-based tracer tracking methods. The latter part involving tracer particles can be broadly subdivided further into single

https://doi.org/10.1021/acspolymersau.4c00022
ACS Polym. Au 2024, 4, 342−391

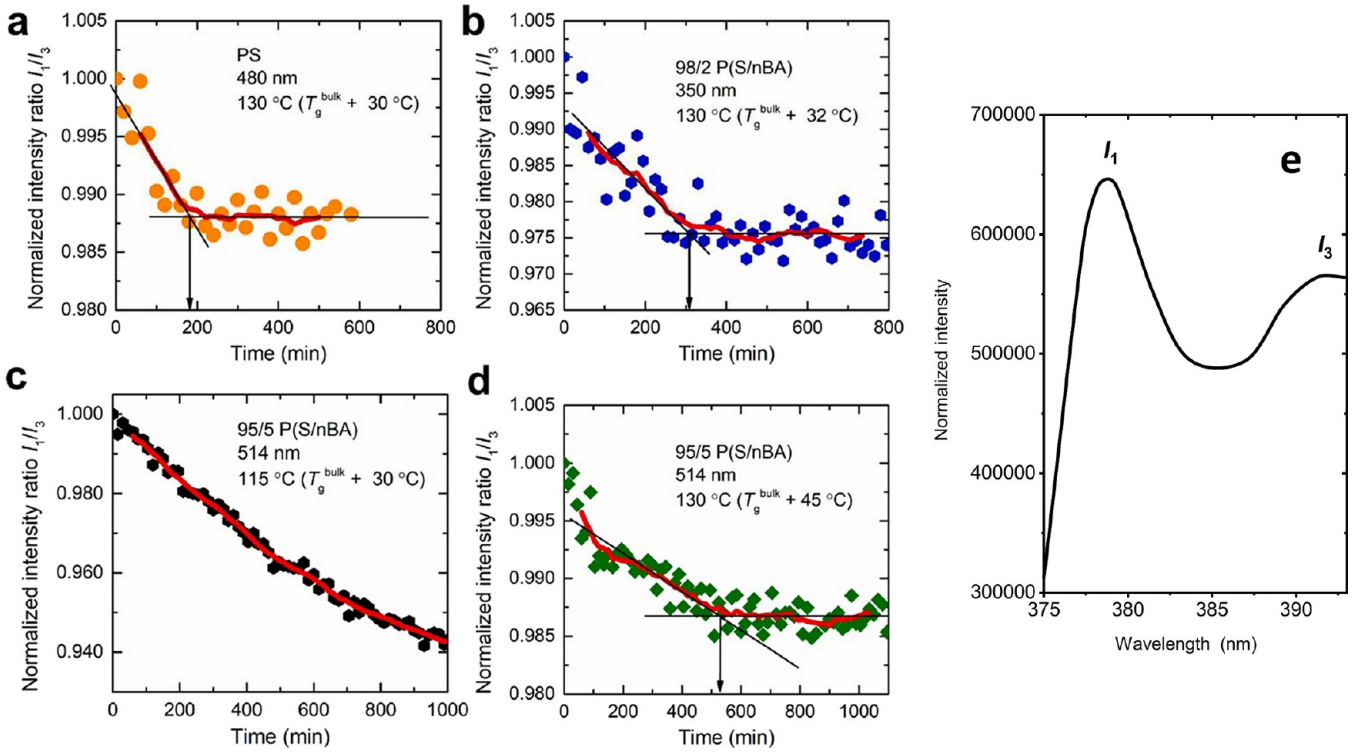

Figure 31. Fluorescence characterization of I_1/I_3 values as a function of annealing time for pyrene-labeled bulk (a) PS, (b) 98/2 P(S/nBA), and (c) 95/5 P(S/nBA) films at $T_{g,bulk}$ + ∼30 °C and for (d) 95/5 P(S/nBA) at $T_{g,bulk}$ + ∼45 °C. (Red curves represent smoothed data obtained via an adjacent averaging method over a window of 120 min.) (e) Fluorescence emission spectra of a 514-nm-thick, pyrene-labeled, single-layer 95/5 P(S/nBA) film. [Reprinted with permission from ref 291. Copyright 2022 Elsevier.]

molecule (particle) based tracking, rotational fluorescence correlation microscopy-based tracking, and photobleaching techniques (to identify rotational anisotropy of fluorescent tracers and translational diffusion or self-diffusion of polymer chains).

Steady-State Fluorescence-Based Methods. Steady-state fluorescence has been a well-established method to find the T_g of thin polymer films. The volume of work that has been carried out using this technique on the subject of glass transition and related molecular mobility is tremendous.[120,284−289] To find the glass transition temperature, the principle used in such experiments is the variation in dependence of fluorescence intensity with temperature. The intersection of the two linearly dependent regions in the fluorescence intensity vs temperature curve gives the T_g, due to a drop in intensity past the glass transition of the polymer. Typically, a low mol% of fluorophores is labeled as a part of polymer chains via polymerization of the monomer functionalized by the fluorophore. In this section, we will mostly limit our scope of discussion to the results relating to stress relaxation utilizing the intensity ratio-based principle. Although the technique has been popular for a long, the sensitivity of the technique to stress relaxation in thin films has been explored only recently.[141]

When a molecule absorbs a photon, it transitions to an excited state as the electron jumps to a higher energy vibrational state. The molecule will return to the ground state when the excited electron returns to its low-energy vibrational state. The molecule can do this either by nonradiative decay (rotational and vibrational motion), radiative decay (fluorescence), or both. According to the pathway chosen by the electron, the wavelength of the fluorescence observed varies. The schematic can be observed in Figure 30. The intensity of fluorescence at different wavelengths depends on the energy transitions from different energy levels to the ground state. Unimolecular fluorescence can be expressed by the following rate equation,[283]

$$\frac{d[M^*]}{dt} = I_0 - (K_f + K_i)[M^*] \tag{33}$$

$[M^*]$ is the concentration of the excited molecules, I_0 is the constant dependent on the properties of the spectrofluorometer, and K_f and K_i are the rates of the radiative and nonradiative mode of energy transfer. Under steady-state conditions, the LHS can be considered as 0. This gives the dependence of fluorescence intensity on the nonradiative decay rate as follows.[283]

$$I_F = I_0 \frac{K_f}{K_f + K_i} = I_0 \phi_f \tag{34}$$

Here, ϕ_f is the quantum efficiency, and I_F represents steady state fluorescence intensity at aparticular wavelength.[283] Nonradiative decay of fluorescence depends on the density and local environment. Polymer thin films labeled with fluorescence probes will behave differently according to the environment around them. As the stiffness of the sample increases, the fluorophores get caged between the chains, reducing the chances of nonradiative energy transfer from the excited state.[283] This increase the fluorescence intensity at a lower wavelength than a higher one. The I_1/I_3 ratio is the parameter that gives us the qualitative image of the mechanical response of the thin polymer film. The higher the ratio of I_1/I_3, the greater the caging of the dye, meaning the higher the stiffness of the film.[283] Figure 30 shows the effect on fluorescence intensity.

https://doi.org/10.1021/acspolymersau.4c00022
ACS Polym. Au 2024, 4, 342−391

Askar et al.[141] utilized this ratio of intensities to probe the stress relaxation in thin polymer films. Annealing for higher time and at higher temperatures was found to reduce the residual stress accumulation due to the processing pathway imposed. This relaxation in stress was not found to vary the glass transition of the sample. The activation energy from the fluorescence experiment closely matched the activation energy for the β-relaxation. Hence, the stress relaxation mechanism was assumed to be through β-relaxations, which also aligned with the dewetting studies by Chowdhury et al.[32] Interestingly, an associated increase in the intensity ratio was observed in reducing the thickness of the films. This was attributed to the increase in caging effect when the film thickness reduced and hence should be related to the increased stiffness of thinner films. The films also had a stiffness gradient, which reduced from the substrate surface to the free surface. This increase in stiffness is attributed to the substrate effect.[132,290] Unlike the free surface effect dominating the glass transition of the thin supported films, the substrate effect dominates in the case of stiffness and was observed for films at temperatures above and below the glass transition. However, the critical thickness below which the effect becomes dominant was different above and below the glass transition.

Hu et al.[291] investigated the residual stress relaxation behavior of styrene acrylic random copolymer films and compared it to neat PS films. Figure 31 shows how the increase in mol % of the *n*-butyl acrylate (nBA) units results in increasing residual stress relaxation time. The hypothesis suggests the capability of small quantities of nBA to influence the molecular or segmental dynamics. The modification of the relaxation behavior of P(S/nBA) films may be attributed to dipole−dipole interactions between the ester groups in nBA units which slows down the subsegmental relaxation process of the film.

The steady state fluorescence technique to determine polymer film stiffness and residual stress can be applied to a wide range of polymers, and there are no major limitations regarding the material that can be probed except the labeling of polymers by fluorescent probe requires extensive controlled synthesis protocol. The major drawback of fluorescence technique as a probe based on intensity ratio is that the technique is mostly qualitative. It needs to be coupled with an AFM measurement or Nanoindentation to determine the film's exact value of modulus. The use of fluorescence as a particle-tracking technique will be discussed in the next section.

Fluorescence-Based Tracer Tracking Methods. The particle (tracer) tracking method encompasses a wide variety of techniques. Fluorescence-based techniques can be loosely divided based on the probe being used as fluorescence-based single-molecule or single particle tracking techniques. Other than classifying based on the probe used, based on the number of particles being tracked, the technique can be classified as single particle tracking or multiple particle tracking. The basic governing principles are the same for all the classifications. The probe particle moving through a medium can be used to find out the viscosity or viscoelastic properties of the medium. The technique, generally involves capturing the motion of the probe particle or particles, which has a contrast concerning the medium in which it moves as the first step. Figure 32 shows a schematic of the probe particle motion through the medium. From the video or image series that captures the motion of the probe particle, the mean square displacement (MSD) can be calculated as MSD = $2nD\tau$.[292] Here, n is the dimensionality of the diffusion process. For 2-D diffusion $n = 2$.

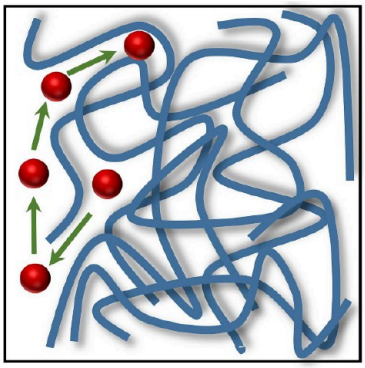

Figure 32. Schematic showing the diffusion of a particle through a medium.

However, in most cases, the MSD follows a power law as MSD = $2AD\tau^{\alpha}$ where A is a prefactor and the power $\alpha = 1$ means that the MSD follows a linear relationship with τ as predicted by the Stokes−Einstein relation. $\alpha < 1$ implies a subdiffusive motion and $\alpha > 1$ implies a condition of super diffusive motion. The diffusion coefficient can be obtained from this relation as $A = nD$. According to the diffusive conditions followed by the probe, the relevant equation can be utilized to determine the medium's viscosity. For the simple case when the Stokes−Einstein condition is followed, the viscosity can be obtained from the relation[293] $D = \frac{k_B T}{6\pi\eta r_h}$. Here k_B and T are the Boltzmann constant and temperature, respectively. η is the viscosity of the medium, and r_h is the hydrodynamic radius of the probe. However, the properties of complex fluids cannot be determined from the simple Stokes−Einstein relationship. This requires a generalized Stokes−Einstein relation (GSER), which considers the hydrodynamic drag felt by the particle as it moves through the medium (Stokes component) and how a particle moves through the medium with a defined hydrodynamic drag (Einstein component).[294−296] The frequency-dependent shear modulus (G) can be obtained using the GSER:

$$G(s) = \frac{k_B T}{\pi a s \widetilde{\mathrm{MSD}}(s)} \tag{35}$$

where $\widetilde{\mathrm{MSD}}(s)$ represents the Laplace transformed mean square displacement, and s is the Laplace frequency.

Although the errors are reduced by using the GSER equation, the approach has associated limitations. The generalized equation becomes invalidated if the experimental conditions defy the conditions required for the Stokes or the Einsteins approach. Thus, this can be used for only probe motions due to thermal fluctuations and where the material through which the probe is moving can be considered as a continuum (which requires the probe size to be much larger than the characteristic length of the medium). Although the Stokes−Einstein (SE) and Debye−Stokes−Einsteins (DSE) relations were developed for large tracer particles, they hold in specific contexts, including liquids with small molecule tracer particles or when self-diffusion is measured. This is used in the fluorescence-based tracking techniques to quantify the translational and rotational diffusion coefficient. $D_T = \frac{k_B T}{6\pi\eta r_s}$ and $D_R = \frac{k_B T}{8\pi\eta r_s^3}$ are the SE and DSE equations, respectively. Here, D_T and D_R are the translational and rotational diffusion coefficients, respectively, T is the temperature, η is the host viscosity, and r_s is the hydrodynamic

https://doi.org/10.1021/acspolymersau.4c00022
ACS Polym. Au 2024, 4, 342−391

radius of the tracer particle. The D_T is obtained by fitting a slope to the *MSD* values when plotted against the lag time (t) using the equation MSD = 4 $D_T t$ + ϵ where $\epsilon \approx 4\sigma^2$ and σ is the localization error. The rotational relaxation time is most commonly used for quantifying the rotational dynamics, $\tau_c = \frac{4\pi\eta r_s^3}{3k_B T}$. By fitting the linear dichroism autocorrelation function to the stretched exponential function, $C(\tau) = C(0)\cdot \exp(\tau/\tau_{fit})^{\beta}$, the stretching exponent (β) and τ_{fit} can be obtained, from which $\tau_c = (\tau_{fit}/\beta)\cdot\Gamma(1/\beta)$ can be calculated further. Here, the fractional exponent (β) of the KWW function is quite useful in explaining the breakdown of DSE and the SE relations between diffusion and viscosity or relaxation time.[47,97] It assumes regions of differing dynamics leading to the KWW relaxation function in ensemble averaging measurements. The decoupling between self-diffusion and rotation occurs because D and τ_c are averaged over different moments of the distribution of relaxation times, with $D \propto \langle 1/\tau \rangle$ emphasizing fast dynamics, while $\tau_c \propto \langle \tau \rangle$ is determined predominantly by the slowest fraction of molecules.

Deviation of β value from 1 is typically considered the degree of heterogeneity in a polymer. Wöll and co-workers tracked the translational diffusion of free perylene dyes in supported PS thin films, at high temperatures well above the glass transition using single-molecule fluorescence.[297] They found a greater extent of dynamic heterogeneity in thinner PS films. Heterogeneous motion displayed a portion of immobile molecules progressively vanishing as temperature rises. The quantity of immobile molecules is likewise highly dependent on the thickness of the coating. Molecules become mobile sooner and more gradually in thinner films (see Figure 33).[297] Probe size is important to properly sense the dynamic heterogeneity (including its spatial and temporal variation) of a glass-former in single-molecule fluorescence measurements. Paeng et al. demonstrated that an appropriate probe is similar in size and mobility to the host glass-former.[298] They further showed that in the supercooled regime of PS, a compact perylene dicarboximide probe replicates both the segmental dynamics and heterogeneity of those dynamics, whereas a larger perylene dicarboximide probe does not.[299] Chowdhury and co-workers investigated spatiotemporal heterogeneity during moisture-induced plasticization of poly(vinylpyrrolidone) (PVP) films supported by the non-Gaussian nature of angular jump distributions for dipolar reorientation of single molecule dye.[300] In fact, their earlier work clearly showed tracer dye molecules display a wide variety of translational motion even at a fixed ambient humidity, clearly pointing out the extremely inhomogeneous environment of plasticized PVP network.[301] A recent study by Joung and co-workers[302] reveals that the configuration of polymer chains within a polymer network significantly influences the nanoscale structural heterogeneity and flexibility. A polymer network formed by self-entangled chains, achieved through controlling polymer−solvent interactions thermodynamically, exhibits greater structural heterogeneity compared to a standard network with interchain entanglement. Single-molecule (particle) fluorescence tracking in polymers is a useful technique and detailing it is beyond the scope of this discussion, while few dedicated review articles have looked into it, quite insightfully.[303,304]

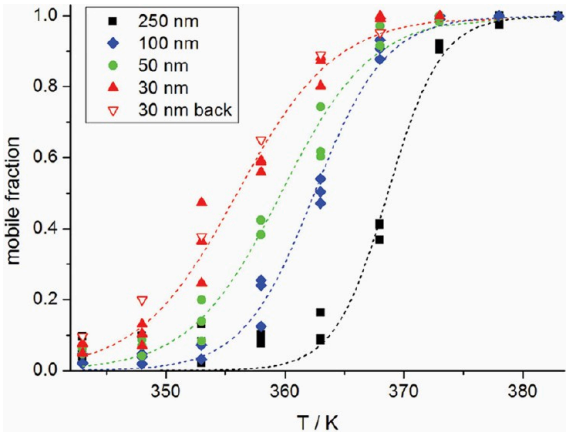

Figure 33. Measured fractions of mobile molecules for different temperatures and film thicknesses (as per the symbols). For all thicknesses, three different movies were analyzed and their mobile fractions were plotted to estimate the scattering of the data. Data were recorded going from low to high T. For 30 nm, data were also recorded during subsequent cooling (open triangles). The lines are to guide the eyes, according to Boltzmann functions. [Reproduced from ref 297. Copyright 2011 ACS.]

Paeng and co-workers used imaging rotational fluorescence correlation microscopy to look into how anchoring or tethering a fluorescent probe molecule to a polymer affected the way segmental dynamics of the polymer were probed.[305] Their probes reported the full range of the host dynamics resulting in similar time scales and β values when the probe size was smaller or comparable to the size of the dynamic heterogeneity of the host polymer. The β value is entirely determined by the width of the time scale distribution averaged alone. When compared to the host dynamics, the larger probe showed a longer ensemble rotation time and a higher β value because it ensemble averaged the neighboring dynamic heterogeneity domains and missed the fast part of the host dynamic heterogeneity. On the other hand, in the case of the restricted probe, motion restriction during tethering—rather than the host matrix's averaging over several dynamic domains—caused the dynamics to slow down. The probe generated a similar β value with the host polymer and was nonetheless smaller or comparable to the extent of the host dynamic heterogeneity, reporting the complete scope of dynamics (see Figure 34). A comparable approach of probing the segmental dynamics of the polymer near the polymer−substrate interface directly using a probe-tethered polymer brush buried in bulk polymer films has been explored.[306] The polymer dynamics near the substrate interface were not perturbed compared with those of the bulk, suggesting it is not sensitive to moderate differences in enthalpic interaction between the polymer and the substrate. Similarly, Lee et al.[307] followed the temperature dependence of the segmental dynamics of the isolated component chain in its blending partner chains of a polymer chain and found it follows the same dynamics as the host component with a horizontal shift corresponding to the T_g modification. Regardless of which polymer was isolated, the local dynamic heterogeneities of the isolated chain were as heterogeneous as the most heterogeneous component or more heterogeneous than either component.

Perhaps the great success of using single-molecule tracking and fluorescence correlation microscopy in PS film and solution is evidence of significant rotational−translational decoupling and Stokes−Einstein (SE)/Debye−Stokes−Einstein (DSE) breakdown near the T_g of the polymer.[97] These data establish that the violation of Debye−Stokes−Einstein prediction is not only the result of ensemble averaging used for dynamic heterogeneity but rather a characteristic of the molecule itself,

https://doi.org/10.1021/acspolymersau.4c00022
ACS Polym. Au 2024, 4, 342−391

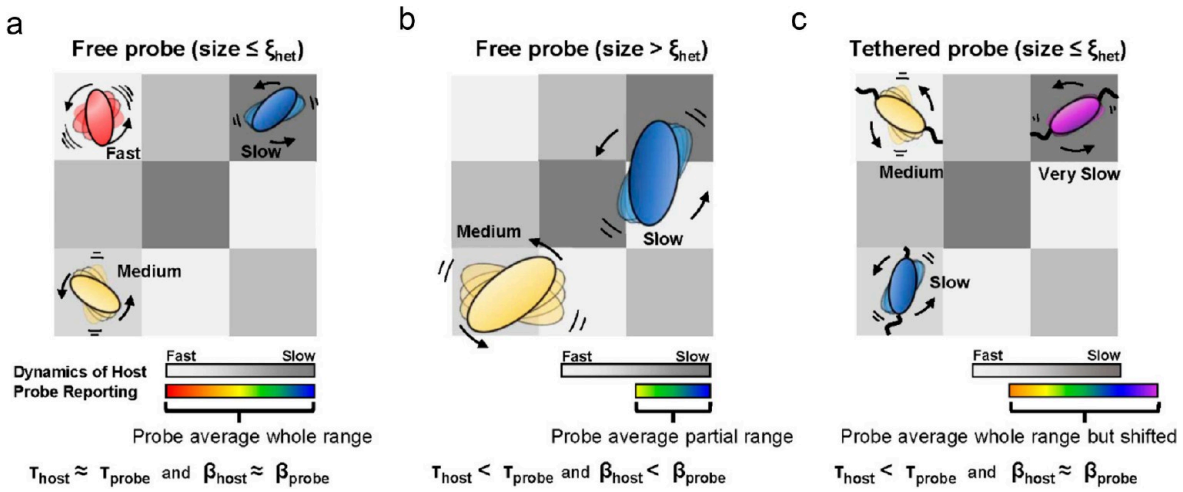

Figure 34. Mechanisms of how probes report dynamics of host polymer according to (a, b) the probe size relative to the length scale of dynamic heterogeneity (ξ_{het}) of the host and (c) tethering. The magnitudes of the averaged τ and β values reported by the probe are determined by the relative position and the width of the time distribution (colored bar) relative to those of the host time distribution (gray bar), respectively. [Reproduced from ref 305. Copyright 2019 ACS.]

as molecules with a greater radius of gyration were found to have a more significant diffusion coefficient and appear to drive the breakdown.[97] The degree of decoupling between rotational and translation motion of a single-molecule close to T_g of PS showed translational diffusion coefficients (D_T) nearly 400 times higher than expected from SE/DSE predictions.[97] SE and DSE relationships predict that the (D_T) and the inverse rotational correlation time ($1/\tau_c$), both depend linearly on (T/η).[97] Deviations from this prediction have been found experimentally in polymers, close to its T_g.[95,121,122] Maldonado-Camargo and Rinaldi[123] reported breakdown of the SE relation for the rotational diffusivity of polymer-grafted spherical nanoparticles in poly(ethylene glycol) melts. A critical molecular weight for the melt polymer was found, below which SE-relation for rotational diffusivity of the polymer-grafted nanoparticles stays accurate and fails above it. Yamamoto and Schweizer[308] developed a statistical dynamical theory to explain deviations from the hydrodynamic Stokes−Einstein (SE) diffusion law in polymer melts, focusing on the nonhydrodynamic friction coefficient linked to microscopic equilibrium structure and polymer melt collective density fluctuations. The study emphasizes the role of entanglement effects in causing significant SE violations, leading to substantial mobility enhancements. Brochard-Wyart and de Gennes[309] proposed the breakdown of the SE relation for the translational diffusivity of nanoparticles when the characteristic length of the particle approximates the characteristic lengths of the polymer melt.

Beyond single dye molecule tracking, Tuteja et al.[310] investigated the diffusion of CdSe quantum dots (QDs) and found them to diffuse approximately 200 times faster in a PS liquid than predicted by the SE relation. The nanoparticles are smaller than the entanglement mesh to create a frictional drag that does not follow continuum expectations. They used a constraint release mechanism to explain the simultaneous 60% viscosity reduction of the mixture to explain their observation. Lin et al.[311] modified the diffusion behavior of the nanoparticles through the slightly entangled PMMA melt medium by changing the effective size of the diffusing nanoparticles by grafting PMMA chains to the nanoparticle thereby decreasing the value of the diffusion coefficient. The polymer-grafted nanoparticles diffuse 100 times slower than predicted by the SE equation. Motion of QD (radius 6.6 nm) was tracked in poly(propylene glycol) (radius of gyration 0.6−2.8 nm) by controlling the functionalization of quantum dots and hence the stickiness with the polymer matrix.[312] It was found that nonsticky QDs follow the Stokes−Einstein (SE) relationship, whereas sticky QDs have slower dynamics. For such sticky nanoparticles, Carroll et al.[313] came up with a crossover mechanism from suppressed to enhanced diffusion, which is observed with increasing polymer molecular weight, supporting the view of Brochard-Wyart and de Gennes.[309] The literature on the motion of nanoparticles in the polymer matrix is rich and well summarized elsewhere.[36,37,309,314]

Photobleaching techniques have successfully determined polymer thin film diffusivity and mobility. Here, we will briefly look into (i) segmental mobility from the rotational anisotropy of fluorescent dyes after photobleaching and (ii) translational diffusion from fluorescence recovery after photobleaching (FRAP). To assess the rotational mobility of a dye, one can observe fluorescence emission after photobleaching using linearly polarized light. This involves selectively exposing a portion of the polymer sample to intense light, permanently preventing the fluorophore from emitting light. In the context of linearly polarized light photobleaching, fluorophores aligned parallel to the incident light are subject to bleaching, resulting in anisotropy in the polarization of fluorescent light immediately after photobleaching. The fluorescent dye molecules undergo reorientation at a consistent temperature or as the temperature rises beyond the glass transition temperature (T_g). If the temperature is below T_g, there may not be sufficient mobility for the dye to reorient within the experiment's time frame. The rotational anisotropy, denoted as $r(T,t)$, can be defined as[69,315,316]

$$r(T,t) = \frac{(\Delta I_{\parallel}(T,t) - \Delta I_{\perp}(T,t))}{(\Delta I_{\parallel}(T,t) + 2\Delta I_{\perp}(T,t))} \quad (36)$$

here, $\Delta I_{\parallel}(T,t)$ and $\Delta I_{\perp}(T,t)$ are the differences in fluorescence intensities between the bleached and unbleached regions for the parallel and perpendicular components of fluorescence measured as a function of time or temperature.[69,315,316]

https://doi.org/10.1021/acspolymersau.4c00022
ACS Polym. Au 2024, 4, 342−391

Paeng et al. determined molecular mobility in confined free-standing PS films by their dye reorientation after photobleaching under polarized light experiments.[69,315] Figure 35 gives an

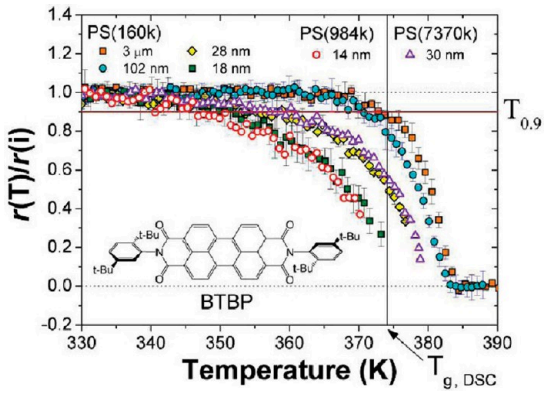

Figure 35. Temperature-ramping anisotropy measurements of the probe molecule *N*,*N*′-bis(2,5-di-*tert*-butylphenyl)3,4,9,10-perylenedicarboximide (BTBP, structure shown as inset) in freestanding PS films of various thicknesses and molecular weights. [Reproduced from ref 69. Copyright 2011 ACS.]

example of fluorescent dye reorientation as a function of temperature in free-standing PS films having a trace amount of dye incorporated into it.[69] Dye molecules did not reorient on the experimental time scale for glassy films, but the rotational anisotropy began to decay as temperature increased.[69] For films thinner than 30 nm, the temperature at which anisotropy began to decay matched T_g reductions, isolating the presence of a bulk-like portion and a more mobile free-surface layer (of thickness ca. 7 nm) in the film. Similar experiments additionally provided information on the presence of a mobile surface layer in free-standing films of other polymers such as in P2VP, PTBS, and PMMA, but interestingly, poly(α-methylstyrene) showed no evidence of a mobile layer at all.[315] All the polymers showing the presence of a mobile layer in free-standing films followed the same observation for supported films on Si/SiO_x substrate.[316]

Chain motion in polymers leading to self-diffusion and viscosity has been studied via fluorescence recovery after the patterned photobleaching (FRAP) technique using fluorescently labeled (covalently bonded) polymers. Bright light exposure was employed to permanently bleach the fluorescent dyes present in the exposed section of the film. Typically, a grating is utilized to generate a pattern consisting of alternating lines that are either bleached or unbleached. As time progresses, the intensity of the bleached area undergoes recovery, facilitated by the diffusion of polymers with unbleached fluorophores into the region and the diffusion of bleached fluorophores out of it. Monitoring the intensity throughout the image over time allows for the extraction of the diffusion coefficient from the decay in amplitude (A) versus time (t), as per the provided relationship

$$A(t) = A(0)\exp\left(-\frac{4\pi^2 Dt}{\lambda^2}\right) = A(0)\exp\left(-\frac{1}{\tau(\lambda)}\right) \quad (37)$$

where D is the in-plane diffusivity, λ is the wavelength of the patterned photobleach, and τ is the characteristic relaxation time measured for several values of λ.[111,317]

Frank et al. conducted measurements on the self-diffusion of PS at a temperature $T_{g,bulk}$ + 40 K.[106] They observed that, for supported films with thicknesses less than 100 nm, the diffusion coefficient decreased by 50% compared to the bulk value, which contradicted expectations based on experimental determinations of T_g and mobility from dye reorientation. Granick and co-workers reported a similar reduction in the self-diffusion coefficient of PDMS films supported on or sandwiched between mica using FRAP.[318] They later extended their studies for PS films adsorbed to quartz substrate and found the absence of a singular Fickian diffusion coefficient. Instead, the diffusion process exhibited a broad and multicomponent spectrum, indicating that surface diffusion's heterogeneity persists and does not average out even over extended periods and length scales which significantly surpass the size of the polymer molecules.[319]

Tsui, Ellison, and co-workers[111] used FRAP to compare the self-diffusion of PS and PiBMA in supported films and compared it to their effective viscosity measured with AFM. While both polymers exhibit a decrease in viscosity when confined, the diffusivity decreased by 50% for PS and remained constant for PiBMA films down to 20 nm thickness. To address differences in viscosity and diffusivity with thickness, they employed a multilayer model.[111] This model assumed that diffusion and viscosity scale differently with local viscosity and could fit both using the same values for the thicknesses and viscosity values of all the layers. Ellison and co-workers further looked into PiBMA nanoconfined films of thickness ranging from 14 to 300 nm in thickness.[320] Multilayered geometries were constructed to systematically investigate the influence of free surfaces (uncapped polymer surfaces directly exposed to air) and surfaces in contact with a secondary polymer (capped). This multilayer approach allowed for the examination of both relatively weak and strong interactions between the polymer and substrate, depending on the presence of hydrogen bonding. The observed T_g–D relationship in nanoconfined thin films deviated from that in the bulk state, as described by relationships such as Williams–Landel–Ferry and Stokes–Einstein.[320] A model was applied that considered the effects of molecular friction and confinement on diffusion in these thin films.

The studies outlined above underscore the significant advancements in polymer characterization at the nanoscale facilitated by fluorescence techniques. These encompass a spectrum of methods, from steady-state temperature-dependent measurements to those tracing fluorescent dyes or particles. Through these techniques, researchers have gained valuable insights into how interfacial interactions and polymer structure profoundly influence polymer properties in thin film confinement. However, challenges such as the lack of standardization regarding dye types (free dye versus dyes covalently bonded to polymer) currently hinder more comprehensive comparisons of mobility and diffusion results. Incorporating a distribution of dye sizes at specific locations in polymer could potentially probe dynamic heterogeneity with more clarity, although this requires further rigorous chemical synthesis to ensure the location-specificity of the dye. In essence, while fluorescence techniques offer extremely powerful tools for studying nanoconfined polymers, refining methodologies will further enhance our understanding of their behavior in such confined environments.

Direct Mechanical Testing

Direct mechanical characterization of polymer thin films is challenging due to the very low thickness of the samples. However, the limitations have been overcome by a few research groups, resulting in the direct mechanical testing of polymer thin films utilizing appropriate modifications. Hence, we can obtain the stress–strain curves for thin films as in bulk samples either

https://doi.org/10.1021/acspolymersau.4c00022
ACS Polym. Au 2024, 4, 342–391

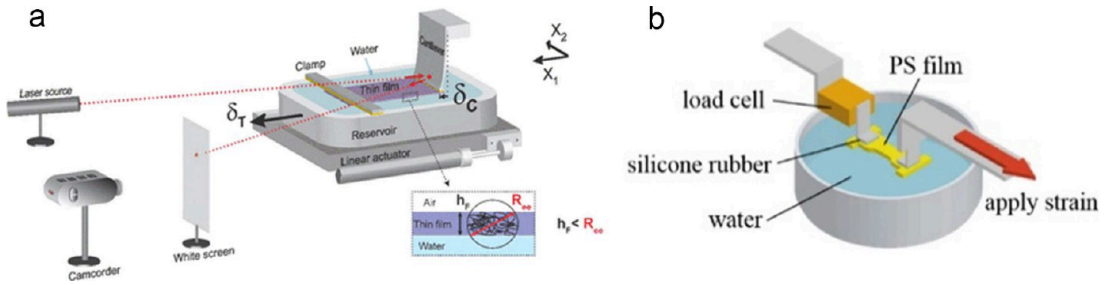

Figure 36. Figure shows the two types of deflection measurement used for the TUTTUT test. (a) Reflective cantilever beam type [Reproduced from ref 102. Copyright 2015 ACS.] (b) Load cell-based measurement. [Reprinted with permission from ref 330. Copyright 2017 Elsevier.]

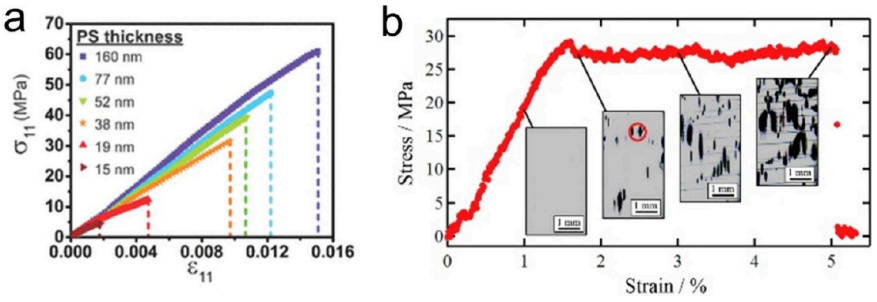

Figure 37. (a) Thickness dependency of the stress−strain curve, showing the reducing slope of the Hooke's law regime which is a result of a reduction in modulus of the films with a reduction in film thickness. [Reproduced from ref 102. Copyright 2015 ACS.] (b) Stress−strain curve of the PS ultrathin film of M_w = 354 kg/mol with a thickness of 105 nm and CCD images of the film during a tensile test at a strain of 1%, 1.7%, 3%, and 5%. The circle in the image shows the appearance of a shear deformation zone. [Reprinted with permission from ref 330. Copyright 2017 Elsevier.]

during applied tension or compression. The direct techniques provide the property of thin polymer films as a whole and not the spatially resolved properties.

The Uniaxial Tensile Tester for Ultrathin Films, TUTTUT. Tensile testing of thin free-standing films on a compliant substrate (often cross-linked PDMS) is a well explored area of research.[321−328] Kim et al.[329] introduced a pseudo-thin film tensile testing technique. The thin film in this technique is supported atop water. Water is ideal due to its high surface tension and low viscosity.[102] This enabled the tensile testing of much thinner films, which was impossible using free-standing or thin films on compliant substrates. The film is allowed to float on the water surface, supporting the thin film. Liu et al.[102] used this technique to find the stress−strain relationship of thin polymer films.

The thin film tester uses a sample grip, which utilizes the van der Waals attraction to hold the thin film in position. TUTTUT is a method that helps us to directly measure the stress−strain relationship of ultrathin polymer films. The technique mainly has two variations: One in which a reflective cantilever grip is used to sense the force acting on the film from the deflection of the cantilever and has a linear actuator for application of strain (Figure 36(a)); the other in which a load cell is attached to the grip, and then strain is applied by moving the other grip (Figure 36(b)). Liu et al.[102] used rectangular strips of thin films, and then a correction was applied for the error that could arise due to the shape of the sample. Later experiments used dog bone-shaped samples, which could provide accurate results.

Thin film after spin-coating was floated on the water surface and held between grips. In the reflective cantilever technique, a laser reflective cantilever will reflect the laser to a camcorder, which helps to determine the cantilever's deflection. Hence, the strain applied on the film can be found out. Alternatively, a load cell can also be used to find out the strain in the film. The technique is unique in being able to extract the mechanical behavior through direct testing, which has been a challenge in the case of thin polymer films. The elastic modulus obtained from TUTTUT is aligned with the values obtained from major nonconventional techniques. The thickness of the PS films is known to influence the elastic modulus, strain at failure, and nominal stress at failure.[203] Figure 37(a) shows the results of TUTTUT on thin PS films of varying thicknesses. The effect of confinement on the modulus of the PS film can be easily realized from the change in slope of the stress−strain curve on varying thickness. The reduction in slope for the Hookean regime is the result of the reducing modulus.[102]

The crazing stress was found to decrease with decreasing thickness for PS films.[102] However, the decrease in crazing stress was much more significant for the higher molecular weight PS, and the decrease was attributed to the reduced interchain entanglements.[330] The dominance of chain mobility over interchain entanglements in strain localization was inferred from a transition from craze formation to shear deformation zones (SDZs) in PS films with a thickness of 20 nm.[331] The yielding and plasticity of the specimens were attributed to the formation of SDZs. Figure 37(b) shows the formation of SDZs during a tensile test. Extensive investigations into the mechanical properties of bisphenol A polycarbonate (BPA PC) revealed distinct shear banding deformations proximate to a clearly defined yield point, irrespective of film thickness. Meanwhile, Young's modulus and maximum stress notably reduced as the film thickness fell below the end-to-end distance radius for the polymer chains. In addition, it was found that the annealing history could be used to control the crystallization of PC thin films, leading to significant changes to the measured tensile properties.[332] Bay et al.[333] found that as the film thickness decreases, a molecular weight-dependent decrease in maximum stress and toughness occurs in both experiments and

https://doi.org/10.1021/acspolymersau.4c00022
ACS Polym. Au 2024, 4, 342−391

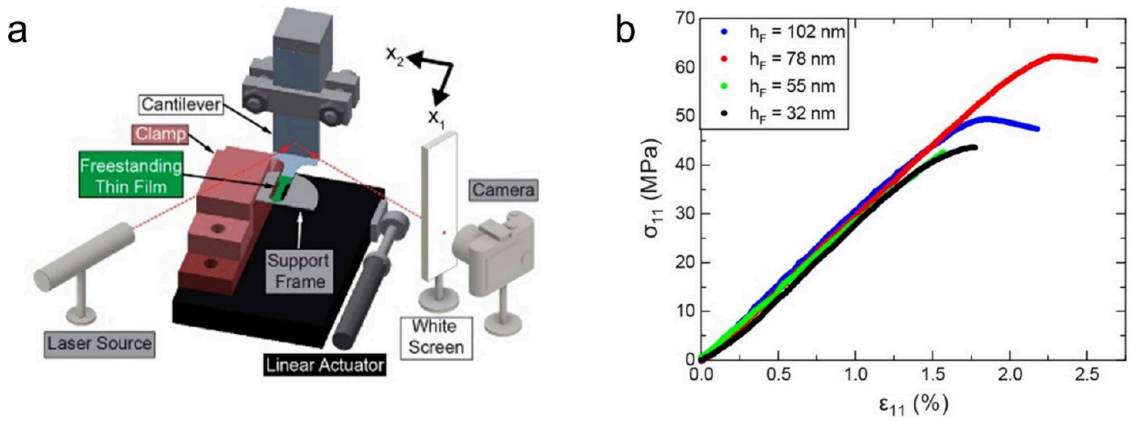

Figure 38. (a) Schematic of TUFF setup. (b) Stress−strain (σ_{11} vs ϵ_{11}) response of four representative 151.5 kDa freestanding PS films with decreasing thickness. σ_{11} is the stress applied in the X_1 direction on the X_1 plane, and ϵ_{11} is the strain applied in the X_1 direction on the X_1 plane. [Reproduced from ref 328. Copyright 2019 ACS.]

simulations, respectively. The study systematically decouples the effect of entanglements and mobility on the failure properties and underscores the importance of considering both factors when designing mechanically robust ultrathin glassy polymer films. Saito et al.[334] used a pseudo-free-standing tensile test (PFSTT) to study the thickness-dependent mechanical properties of polystyrene-*b*-polybutadiene-*b*-polystyrene (SBS) block copolymers. PFSTT is essentially the same as TUTTUT. They found the elastic modulus increased with a decrease in the thickness of the SBS film. Such an increase in Young's modulus and brittle behavior of the SBS films were attributed to the PS-rich subsurface layer having continuous domains of glassy PS.[334] The exploration of the structure−property relationship in polystyrene-*b*-polyisoprene-*b*-polystyrene (SIS) films, where the thickness ranges from 35 to 1000 nm, revealed mechanical properties that are dependent on the strain rate. This strain rate dependency was particularly pronounced in thinner films. It is hypothesized that the stiffening observed in ultrathin SIS films may result from a combination of factors, including PS domain alignment, confinement effects, and surface and interface interactions.[335] Ultrathin cross-linked polybutadiene (PBD) films were found to have an increased Young's moduli with reduced thickness, independent of cross-linker quantity. In-plane swelling decreased, while out-of-plane swelling persisted. Anisotropic deformation was attributed to polymer chain segments at interfaces acting as pseudocross-linking points, suggesting a structure with resistant surface and interface layers alongside an easily deformable inner bulk layer. Models, like a parallel model for in-plane deformation and a series model for out-of-plane deformation, successfully explained the films' anisotropic behaviors.[336]

TUTTUT helped to understand the viscoelastic properties of polymeric thin films and their stress relaxation behavior. These become important considering the miniaturization of semiconducting polymeric materials having subroom temperature T_g.[337] TUTTUT has some unresolved issues. The technique cannot measure the mechanical properties of films below 15 nm in thickness as the vibration of water in the reservoir itself can damage the sample.[337] The exact implication of water as a supporting medium needs to be studied more. Sarkar et al.[268] using the dewetting experiments showed how incubating in water can affect the stability of thin PNBMA films by affecting the viscosity, modulus, and surface tension of the films. in addition, Galuska et al.[338] have shown that there is water uptake in the film on experimenting with Film Over Water (FOW) mode. Measurement using quartz crystal microbalance and neutron reflectivity showed over 9% uptake of water in the films.[338] Hence, the method needs to evolve to overcome these challenges. A free-standing version of the technique without using water as support places a limitation on film thickness that can be tested to ca. 30 nm.[328]

Tensile Tester for Ultrathin Freestanding Films (TUFF). The TUFF method was developed as an alternative to the TUTTUT method to avoid using water as a supporting medium.[328] The concern regarding the effect of contact with water in TUTTUT could be alleviated by using the TUFF method where the film is truly freestanding. The schematic in Figure 38(a) helps us understand the setup being used. The film is held using a steel frame having a slot and an open end at one edge to hold the film against a cantilever. The cantilever stays in contact with the film at the open end of the frame.

The principle of operation remains the same as that of the TUTTUT method. It utilizes a linear actuator to apply strain on the film by moving the steel frame. The deflection in the cantilever is translated to the stress−strain responses of the system. Figure 38(b) shows the typical stress−strain curves obtained from the TUFF measurement. Although the thickness of the film has been varied, the curves almost overlap with each other in the Hookean regime, suggesting the invariable elastic modulus of the polymer film.

On comparing the values obtained via this technique to TUTTUT, we see that the modulus value and the maximum stress attained remain almost the same. This highlights the inert nature of water as a supporting liquid concerning these measurements. On the other hand, the craze stability is found to increase due to the presence of water.[328] Hence, we cannot safely assume that water is not impacting the film. The TUFF seems more reliable considering the absence of any supporting liquid. Even though TUFF has positives, it becomes very challenging to conduct the tests for thinner film samples than 30 nm.[328]

Dynamic Mechanical Analysis for Thin Polymer Films. The dynamic mechanical analyzer allows for studying the mechanical properties over a broad range of temperatures and also for cyclic loading for both bilayer and freestanding films. O'Connor[339] and co-workers used the bilayer configuration to test the films in a DMA analyzer. The film to be tested is mounted on an elastomer substrate having thickness in the

https://doi.org/10.1021/acspolymersau.4c00022
ACS Polym. Au 2024, 4, 342−391

micrometer scale. Although varying the stiffness of the elastomer results in variation in the stress−strain curve of the composites, the values of Young's modulus for the thin polymer films extracted remained the same. The elastomer is in the rubbery plateau region for the testing temperature, and hence the properties of the glassy film on top can be extracted until the failure without being influenced by the properties of the substrate. The greater thickness of the substrate helps in the proper fixing of the sample. Thus, absolute freestanding properties of the material cannot be found out using this technique. Yiu et al.[340] on the other hand conducted the tensile testing of both the bilayer as well as the freestanding films by carefully placing the sample in the holder using a frame and later removing it before conducting the test.

In the bilayer geometry, the elastic modulus of the thin film is obtained from the concept of equivalent strain of both elastomer and polymer thin film layers. The bilayer modulus ($E_{bilayer}$) can be obtained from its stress−strain behavior. The film thickness (h_{PDMS}) and modulus (E_{PDMS}) of PDMS are known values. Thus, for a polymer film of film thickness h, the elastic modulus (E) can be obtained using the rule of mixtures as[340]

$$E = \frac{1}{h}[(h + h_{PDMS})E_{bilayer} - h_{PDMS}E_{PDMS}] \quad (38)$$

Yiu et al.[340] used different strain rates to find out the variation in the values of E. It was observed that variation of E with the film thickness vanishes when the loading rate is above a certain critical value, as seen in Figure 39(b). From Figure 39(a) we can

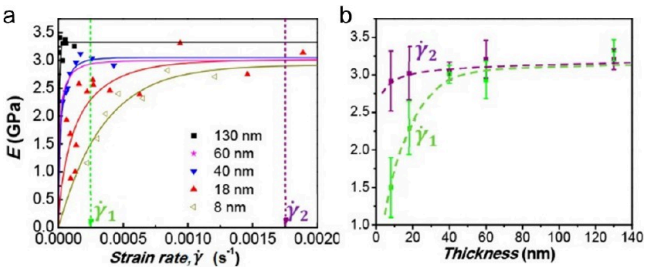

Figure 39. (a) Room-temperature elastic modulus vs strain rate of PS−PDMS bilayers with PS M_w = 1049 kg/mol and various thicknesses h, as indicated in the legend. Solid lines are the best fits to eq 39. (b) Strain rate dependence of the elastic modulus of thin films. Increasing strain rate shows lesser confinement effect. [Reproduced from ref 340. Copyright 2020 ACS.]

observe that the value of the critical loading rate is found to increase with the reduction in thickness. This was attributed to the faster relaxation mechanisms in thin films. When a loading rate twice the critical loading rate was applied, the instantaneous elastic modulus E_0 can be obtained. This instantaneous modulus was found to be independent of the molecular weight of the polymer being used. Further, a relationship was obtained for E as a function of loading rate ($\dot{\gamma}$).[340]

$$E(\dot{\gamma}) = E_0[1 - \exp(-\dot{\gamma}\tau)^{\beta}] \quad (39)$$

Here τ is the relaxation time of the film and β is a constant fit parameter. Tsui and co-workers[341] have done extensive dynamic relaxation studies using the DMA on thin films (5 nm to 185 μm). They found that two mechanisms are present which result in fast relaxations at two different length scales. The surface mobile layer, which has a thickness of 1−10 nm, can be attributed to the fast relaxations observed in films having thicknesses less than 100 nm. However, for films having a thickness greater than 1 μm, the fast relaxation mode extends up to 1 μm. The surface mobile layer in the nanometer scale cannot explain fast relaxations at such a long-range. Thus, the enhanced relaxation can be assumed to show varying origins: locally enhanced segmental motions in the nanoscale outer region (near the air−polymer interface) and an exotic long-range fast mode of relaxation beneath this. These findings explain differing apparent thicknesses of mobile surface layer probes using different techniques.

On comparing the elastic modulus values of the film obtained by the DMA and tensile testing done using TUTTUT, we see that they are pretty comparable. Although the direct mechanical testing of the samples using DMA is a reliable option to find out the exact stress−strain relationship curve of the sample, the effect of the Poisson's ratio is not considered when using the bilayer configuration. The freestanding films with very low thicknesses of less than 40 nm are challenging to measure in this technique. Further investigations are also needed to understand the fundamental origin of the long-range fast mode of relaxation, with the surface shear mode as a potential cause.[341]

Flat-Punch Nanoindentation. Nanoindentation measurements involve indenting a sample using a suitable indenter. Typically, mechanical properties are determined by measuring the indentation on the sample due to an applied force. The applied force results in an impression on the sample being tested and the ratio of the maximum applied load to the residual indentation area gives the hardness of the material. However, the process becomes more challenging when using this technique to thin films supported on a substrate, especially with polymers having time-dependent properties. Here, we will initially discuss the basics of the regular indentation process and will further confine our discussions pertaining to the flat punch indentation technique.

The conventional choice for a nanoindenter is a Berkovich tip. However, to investigate the properties of polymers, Strojny[342] and others opted for either a much sharper tip with smaller included angles or a flat punch. Using a sharper tip offers advantages when dealing with thin film samples, allowing the avoidance of substrate effects due to the shallow depth being probed. Nevertheless, it is essential to acknowledge that no tip is 100% perfect in this context.[342]

In conventional techniques, the hardness (H) is obtained as

$$H = \frac{P_{max}}{A_c} \quad (40)$$

where P_{max} is the maximum load applied and A_c is the area function for the corresponding tip geometry. To calculate the residual area after indentation, the tip geometry plays an important role. According to the Doerner and Nix description (D-N),[343] considering the tip as a spherical shape with a tip radius R, A_c is[342]

$$A_c = \pi\left[R \sin\left(\arccos\left(\frac{R - R_c}{R}\right)\right)\right]^2 \quad (41)$$

and for a pyramidal tip:

$$A_c = \frac{9}{\sqrt{3}}\tan^2\theta(h_c + h_{corr})^2 \quad (42)$$

Here, h_{corr} accounts for the deviation from the perfect three-sided pyramid, h_c is the contact depth, and θ is half of the included angle of the tip.[342] In addition to the D-N method,

https://doi.org/10.1021/acspolymersau.4c00022
ACS Polym. Au 2024, 4, 342−391

other analysis protocols provide the area function. The Oliver–Pharr (O–P) method,[344] which considers the projected contact area and eliminates the need for actually measuring the contact area, is a commonly used one. The projected contact area in the O–P method can be expressed in terms of contact depth (h_c). Contact depth is obtained from the maximum depth of the indentation (h_{max}) and maximum load applied (P_{max}).

$$h_c = h_{max} - \epsilon\left(\frac{P_{max}}{S}\right) \tag{43}$$

where ϵ is the geometric factor depending on the shape of the indenter and S is the unloading stiffness. To calculate the hardness, the projected area (A_p) of contact is required, which can be obtained as follows:[345]

$$A_p = Ch_c^2 \tag{44}$$

$$C = 3\sqrt{3}\tan^2\alpha \tag{45}$$

Here α is the apical angle of the indenter being used. On comparing the values of the hardness of samples obtained by the O–P method to that obtained by measuring the contact area, it can be found that the O–P method overestimates the hardness value.[342,346]

Conventional indentation techniques as mentioned above for polymer films can be used only for very small strains. In addition, the indented area is a function of the indentation depth. The technique relies on models to obtain the actual contact area. Also, the stress–strain response that can be extracted is very limited.[347] A flat punch indenter can resolve most issues of sharp tips. By maintaining a high aspect ratio, the technique can be assumed to produce a purely uniaxial strain with a depth-independent contact area.[347,348]

Cross et al.[348] carried out research using flat punch indenters and established the material flow as a complex function of indentation depth. According to their study, the flat punch indenter, due to the constant area of load distribution, minimizes the effect of surface forces and enables the probe of any depth using any load. Figure 40(a) shows a schematic of the nanoindentation process using a flat punch. The flat punch indentation due to the higher aspect ratio of the indenter, i.e., the ratio of indenter size to the thickness of the polymer film being measured, can help avoid the contribution from the constraining material at the edge of the flat punch. In addition, the ability to apply load throughout the constant area of contact results in higher sensitivity of the instrument.[348] Considering a flat punch of diameter $2a$ and an initial film thickness of the sample as h_0, the aspect ratio is $2a/h_0$. On applying an indentation of depth δ, the residual height of the film will be $h = h_0 - \delta$. The effective compressive strain can be obtained as[348]

$$\epsilon = \frac{h}{h_0} \tag{46}$$

the mean stress $\bar{\sigma}$ is

$$\bar{\sigma} = \frac{P}{\pi a^2} \tag{47}$$

where P is the applied load. To measure the mechanical response using the flat punch indenter, the sample is mounted onto an indenter tilt stage, as shown in Figure 40(a). The tilt stage can be adjusted to maintain the sample parallel to the flat punch face. The alignment of the punch and the sample is tested by scanning the residual impression using AFM. Once the sample is aligned and thermal drift is measured, the experiments can be performed at constant loading rates.[347]

On studying the squeeze flow of thin PS films, Rowland et al.[349] found an inverse relationship of viscosity with molecular weight when compared to bulk behavior. In bulk systems, higher M_w polymers are found to have higher viscosity, which results in higher resistance to flow. However, flat punch indentation studies have shown that when the film thickness was in a confined region, as the M_w of the PS film increased, there was a corresponding increase in compliance. The lower M_w PS films showed a stress–strain plot with a higher slope in the confined regime.[350] On investigating the impact of loading rates and temperature on PS films of 170 nm thickness, Rowland et al.[350] found that at high loading rates, the stress–strain response showed molecular weight-independent behavior, although the stress–strain response showed a loading rate-dependent behavior. However, as the temperature was increased to the viscoelastic region, a molecular weight-dependent stress–strain response was observed for PS films.[350]

Brazil et al.[347] using a flat punch, which is often the thickness of the film, created a state of confined uniaxial strain for the material beneath the punch we can see in Figure 40(b). This allows us to obtain the intrinsic stress vs strain curve directly. Almost all the parameters of stress–strain response curves could be obtained simultaneously.[347] In a truly uniaxial strain, restricting any lateral deformations, the principal stress–strain relationship can be defined as

$$\sigma_{zz} = E\frac{(1-\nu)}{(1+\nu)(1-2\nu)}\epsilon_{zz} = M\epsilon_{zz} \tag{48}$$

$$\sigma_{rr} = \left(\frac{\nu}{1-\nu}\right)\sigma_{zz} \tag{49}$$

$$\epsilon_{rr} = \epsilon_{\theta\theta} = 0 \tag{50}$$

E is Young's elastic modulus, ν is Poisson's ratio, and M is the confined state elastic modulus. According to the von Mises criteria, the plastic deformation takes place at a yield point where the axial stress is Y_0 for unconfined systems. However, in the uniaxial strain case, the yield occurs at a higher stress $Y_c = Y_0(1-\nu)/(1-2\nu)$ due to the lateral constraint. It was found from the stress–strain curve that the linear region in the stress–strain curve changes the slope from M to K, which signifies pure plastic

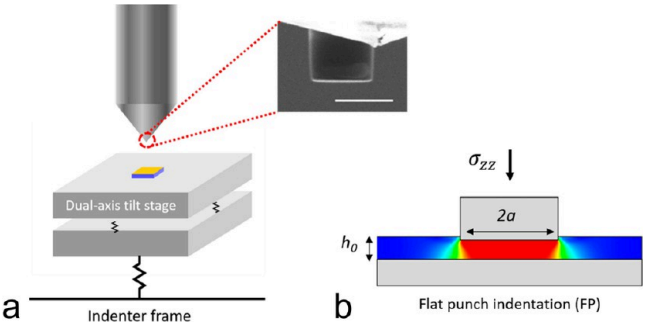

Figure 40. Flat punch indentation of thin films approximates uniaxial strain. (a) Sketch of the flat punch indentation experimental setup. The 2.05 μm diameter diamond flat punch with the schematic of stiff, precision tilt stage system. (b) Two-dimensional representation of the contact geometry, with the film material surrounding the contact acting as a confining jacket and driving the system toward a uniaxial strain state. [Used with permission from ref 347. Copyright 2020 Materials Research Society.]

https://doi.org/10.1021/acspolymersau.4c00022
ACS Polym. Au 2024, 4, 342–391

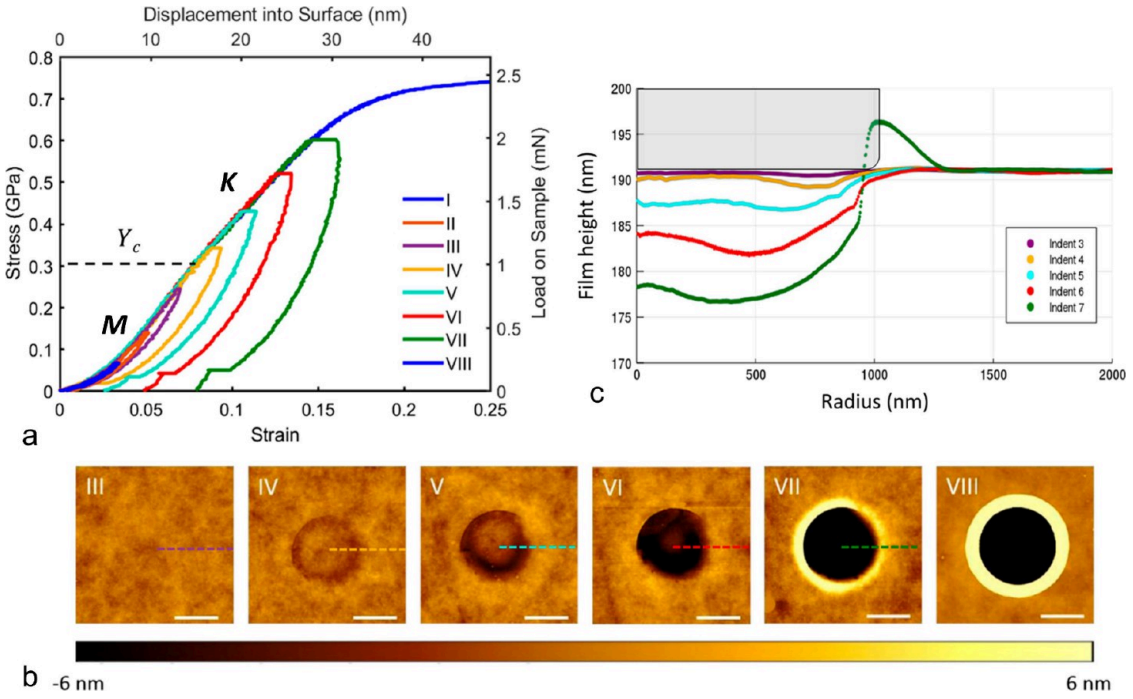

Figure 41. Incremental loading experiments show confined plastic yield. (a) Load−displacement curves for a series of independent intents into 190 nm (aspect ratio (α) = 10.8) PS with incrementing peak load. (b) AFM topography maps of residual strains for indents iii−viii. (c) AFM residual impression profiles for indents iii−vii showing displaced volume. [Used with permission from ref 347. Copyright 2020 Materials Research Society.]

deformation. On applying stress lower than Y_c, there was no change in slope, and no plastic flow was observed as the material regained its shape on removal of the stress. Figure 41(a) shows the stress−strain plots of a series of indents of different zones. Figure 41(b) shows the AFM images of the corresponding indents. It is evident that when the loading is done up to Y_c there is no plastic deformation in the sample. Figure 41(c) shows the residual impression profile of the AFM image. The relationship between stress and strain beyond plastic deformation allows the calculation of Poisson's ratio as

$$\nu = \frac{3K - M}{3K + M} \tag{51}$$

The technique provided modulus values for PS and PMMA close to those reported in the literature. Repeated loading of thin PS film into the plastic regime introduced strain-hardening behavior, which increased the confined yield stress by 66%.[351] This was attributed to residual stresses imparted into the film during the repeated loading.[351] The high aspect ratio (in general 10)[348] has been a prerequisite for extracting the true stress−strain curves using the flat punch indentation experiments. The confinement modulus M is independent of the aspect ratio. However, the value of K depends on the aspect ratio. On investigating the effect of a range of aspect ratio values on the confined modulus, using finite element simulations, it was found that the application of a simple substrate correction factor to the punch-substrate contact stiffness helped obtain the true stress−strain values that stay correct for the range of aspect ratio values investigated (5−100).[352] Brazil et al.[353] noted an increase in densification in high M_w PS films upon applying very large stresses in a confined compression test. Although it was expected that the increase in densification should plateau out once the load crosses over to the extrusion zone, there was a further increase in densification close to 3.4% even in the extrusion zone, which could not be explained by the volume-preserving plastic mechanics.[353] The effect of densification could also be observed when applying the same load repeatedly to PS films and graphene nanosheet network. Sinnott et al.[354] observed an increase in stiffness in the subsequent loading cycles. The densification of the graphene network and, in the case of polymeric glasses, the reduction in the free volume are cited as the reasons for such behavior.[354]

Here, we have discussed majorly the flat punch indentation technique. The flat punch indentation allows the study of the stress−strain curve of the film with minimum error due to the high aspect ratio of the indenter being used, which allows us to assume the strain applied as uniaxial. By utilizing the flat punch, indentation experiments could be conducted for large strains which is not possible in the conventional nanoindentation techniques. However, flat punch indentation requires that the sample be aligned to the punch at all times to obtain error-free values. Aligning the sample is quite challenging as the alignment needs to be checked by scanning the punch impression in AFM. Barring the experimental difficulty, the flat punch indentation is a robust technique to obtain the mechanical properties directly. There is also a possibility of obtaining zero shear viscosity by performing creep experiments using flat-punch nanoindentation.

Creep Test for Thin Polymer Films. The possibility of conducting creep tests on polymer films has been explored using the bubble inflation technique. The experimental setup for TUTTUT and flat-punch nanoindentation also allows creep tests on thin polymer films. Ramezani et al.[355] introduced a new approach by which the creep test could be performed on free-standing thin polymer films. The effect of substrates is eliminated in this technique, and it is a direct method to measure creep in truly free-standing films, unlike the case of TUTTUT.

The technique involves the spin-coated polymer films being crumpled into "filaments", as outlined by Ramezani et al.[355] The

https://doi.org/10.1021/acspolymersau.4c00022
ACS Polym. Au 2024, 4, 342−391

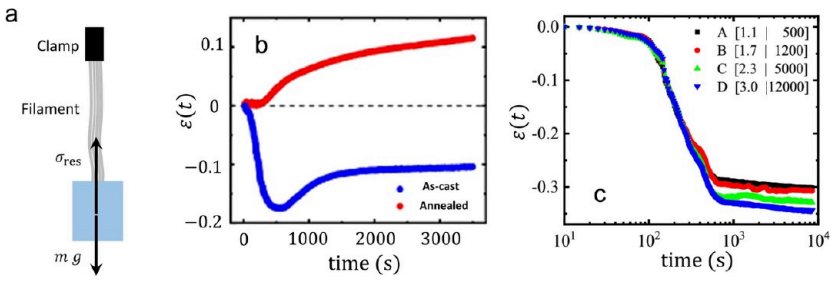

Figure 42. (a) Schematic drawing showing the principle of creep test for thin polymer films, (b) Evolution of Hencky strain in PS filaments (M_w = 524 kg/mol) both annealed and as-cast under stresses of 38 and 45 kPa, respectively at 130 °C. [Reprinted figure with permission from ref 355. Copyright 2020 APS.] (c) Increase in the contraction of the PS (M_w = 524 kg/mol) filaments upon applying a load of 5 kPa with increasing spin-coating speed while preparing the film. The filaments coded as [c|v] in the figure were derived from films obtained by spin-coating of the polymer solution of concentration c (in %w/w) at a rotational speed v (in rpm). [Reproduced from ref 356. available under CC BY license. Copyright 2022 EPJ.]

filament formation happens when lifting the polymer film floating on water using a metal wire. The edges of the filaments are fixed between two clamps made from aluminum foil. After drying the films in a vacuum oven overnight at room temperature, the samples are kept in an oven preset at the testing temperature.[355] Varying loads are hanged to one end of the filament, while the other end is attached to a frame. The variation in the length of the filament is observed using a camera facing the double pyrex glass of the oven. The schematic of the method can be observed in Figure 42(a).

The Hencky strain ($\epsilon(t)$) can be calculated as

$$\epsilon(t) = \ln\left(\frac{L(t)}{L(0)}\right) \tag{52}$$

with $L(t)$ being the length of the filament at time t and $L(0)$ being the initial length at t = 0. The stress applied by hanging mass is calculated as

$$\sigma_{load} = \frac{mg}{WH} \tag{53}$$

g is the acceleration due to gravity, and W and H are the width and height, respectively, of the free-standing film. Considering the Jeffrey model, total strain ($\epsilon(t)$) is the sum of the strain of a recoverable strain (ϵ_r) and the viscous strain (ϵ_v), $\epsilon(t) = \epsilon_r(t) + \epsilon_v(t)$. The Kelvin element, over time, converges to a steady state value ϵ_r^0. Since, at longer times, the creep is dominated by viscous strain, resulting in a linear increase in $\epsilon(t)$, by back extrapolating this linear region the steady state recoverable strain value can be obtained. Considering a biaxial stress state of the prepared thin film, the σ_y will have stress due to the residual stress σ_{res} and the hanging weights σ_{load}. σ_x will have only residual stresses acting on it. Thus, for the Y-axis, the steady state recoverable strain can be expressed as

$$\epsilon_r^0 = (\sigma_y + \nu\sigma_x)/E \tag{54}$$

and for Poisson's ratio ν = 0.5,

$$\epsilon_r^0 = (\sigma_{load} + 0.5{\cdot}\sigma_{res})/E \tag{55}$$

Ramezani et al.[355] observed a contraction in the filament length of PS films initially over time when applying a constant load. The PS filaments lifted the applied loads when the value of the applied stress was lower than the preparation-induced residual stress or molecular recoiling stress in the polymer film. Over time, when the residual stresses relaxed, the filament started elongating. The filaments prepared from annealed films did not show the contraction. They elongated over time as the stresses were applied (Figure 42(b)). The filaments from films of lower thicknesses showed greater contraction initially as compared to the thicker films on applying the same loads. The E was calculated for various external stresses using the creep experiments, and found that the values were similar for films of varying spin-coating speeds. However, the preparation-induced residual stresses were found to increase as the spin-coating speed was increased. The stress values were found to increase by 40% when the spin-coating speed increased from 500 to 12000 rpm.[355] The increase in contraction on the application of the same stress to filaments made from films spin-coated at varying speeds of spin-coating can be seen in Figure 42(c).[356]

Reiter et al.[356] extended the investigation further by studying the isothermal behavior of the PS filaments spin-coated under similar conditions but annealed at different conditions (temperature and time). They also investigated the temperature sweep behavior. While studying the isothermal response of the filaments under constant loads, as the temperature and time of annealing increased, the contraction of the filament was found to decrease. In addition, the temperature dependence of the relaxation shown by thin PS filaments in the creep experiments was similar to the behavior shown by melt-spun PS fibers. They thus noted the generic nature of polymers in "forgetting" the past processing events. The technique, when used in temperature sweep mode, can also help in determining the T_g of the polymer film.[356]

The creep test on filaments from thin films is a simple macroscopic approach that can directly tabulate mechanical properties and stress relaxation in the polymer films. It is very sensitive to the segment-level relaxations expected from polymer films. The ability of the technique to conduct creep tests in temperature sweep mode and isothermal mode helps in observing the glass transition temperature and elastic modulus of the filament using the same setup.

CONCLUSION AND PERSPECTIVE

This review article has discussed various characterization techniques to probe mechanical and rheological properties of thin polymer films. It started with a state-of-the-art background introduction of relevant aspects pertinent to thin confined glassy polymer films. It encompasses recent developments in the field, setting the stage by introducing physical phenomena, such as glass transition, relaxation, and diffusion, along with their roles in deciding thermo-mechano-rheological properties with an emphasis on the physics of polymers far frpm thermodynamic equilibrium. While going through the article, we expect that the reader will be given a basic understanding of the various

https://doi.org/10.1021/acspolymersau.4c00022
ACS Polym. Au 2024, 4, 342−391

Table 1. Summary of Characterization Techniques[a]

Technique	Main principle	Measured quantity	Temperature control	Spatial measurement
PSD	Viscosity-dependent surface morphology evolution on annealing	η	Yes	No
Bubble inflation	Viscoelastic property-dependent curvature formation due to applied pressure	$J_{rubbery}$, J_{glassy}	Yes	No
Wrinkling	Instability due to low-strain localized buckling	G_{glassy}, $G_{rubbery}$, η, ϵ_{frac}, σ_{frac}, σ_{res}	Yes	No
Capillary leveling	Viscosity-dependent evolution of air−polymer interfacial area to minimize Laplace pressure gradient	η	Yes	No
NCNS	Mobility gradient-dependent response to constant shear in supported thin polymer films	$\chi(h)$, η	Yes	Yes
Wetting ridge	Viscosity-dependent growth of ridge on polymer substrate due to unbalanced vertical component at probe liquid interface	η	Yes	No
Dewetting	Mechano-rheological property dependent hole and rim growth due to σ_{cap} and σ_{rec} on annealing	η, σ_{rec} or σ_{res}, $G_{rubbery}$	Yes	No
BLS	Inelastic scattering of incoming photons by thermally activated phonons in the material	$G_{rubbery}$, G_{glassy}, T_g	Yes	No
Fluorescence	Steady-state fluorescence intensity affected by material properties, Tracer tracking	σ_{res}, T_g, η, D_T, D_R, G	Yes	Yes
TUTTUT	Stress−strain response	G_{glassy}, σ_{craze}	No	No
TUFF	Stress−strain response	G_{glassy}, σ_{craze}	No	No
Thin film DMA	Response to dynamic mechanical perturbations	$G_{storage}$, G_{loss}, E_0	No	No
Flat-punch nanoindentation	Stress−strain response	$G_{confined}$, Y	Yes	No
Creep test for thin films	Stress−strain response in filaments from spin-coated polymer films	J_{creep}	Yes	No

[a] J = compliance, G = modulus, η = viscosity, χ = mobility, E_0 = instantaneous elastic modulus, ϵ_{frac} = fracture strain, Y = yield stress, σ_{res} = residual stress, σ_{rec} = molecular recoiling stress, σ_{craze} = crazing stress, σ_{frac} = fracture stress, D_T = translational diffusion coefficient, D_R = rotational diffusion coefficient, σ_{cap}=capillary stress.

experimental techniques available to characterize polymer thin films. Understanding the sensitivity of the technique to certain specific phenomena is an important point to consider. The characterization techniques discussed in this review article have been summarized in Table 1. It discusses the main principle used in each technique, the ability and limitation regarding temperature control and spatial resolution, and information that can be obtained from those. Investigating glassy modulus (elastic modulus below the glass transition) is not possible using the wetting ridge technique or dewetting technique; for that, the investigator requires an indentation, TUTTUT, TUFF, thin film DMA, or wrinkling technique. Similarly, the wetting ridge and capillary leveling might not be that sensitive to the preparation-induced stresses; dewetting and wrinkling techniques might be a better option in such a case. To avoid any substrate effect perturbing the measurement, creep test and DMA for thin polymer films or TUFF techniques can be utilized. To probe the rubbery stiffening observed as a response to large deformations on reducing the thickness of polymer thin films, bubble inflation can be utilized.

The characterization techniques like PSD, wetting ridge, capillary leveling, wrinkling, and dewetting have a relatively simple experimental set and require minimal setup. However, these experimental techniques need careful experimentation taking care of reproducible film surface features being nondestructive. That means noncontact imaging-based tools having simpler assembly and operation can make the whole process of characterization faster and more robust. While there are many ways to analyze a series of large data sets, it needs to be meaningfully intensive for the computational cost. Most such tools need long-duration measurements, often at a temperature high enough to induce artifacts in data acquisition, so ensuring stability is important, spanning a considerable duration. Mathematical models and theoretical considerations, including assumptions being considered (such as defining appropriate boundary conditions in fluid flow), are very important and need to be carefully implemented. The flat punch indentation, BLS, NCNS, bubble inflation, TUTTUT, and DMA are all dependent on specialized equipment and hence could be difficult to set up.

Improving the characterization tools further should proceed toward developing, robust, fast, and easy-to-setup systems, by carefully analyzing each technique's success and limitation at varying experimental variables (such as film thickness, substrate effects, time, temperature, and polymer) to improve the sensitivity of the techniques to a wider range of measurements. Most of the mechano-rheological probes here are well-established from the theoretical, analytical modeling, and experimental output point-of-view. However, future techniques or improvements to current techniques will be more solid by comparing and using generated experimental data sets involving more than one technique, appropriately accounting for each technique's possible limitations. The decoupling of different interdependent properties using different techniques must be thoroughly examined to rule out the possibility of technique-dependent limitations. Experimentation should be well supported not only by theoretical and analytical modeling at the continuum level but should also be established through molecular dynamics simulation.

AUTHOR INFORMATION

Corresponding Author

Mithun Chowdhury − *Metallurgical Engineering and Materials Science, Indian Institute of Technology Bombay, Mumbai 400076, India; Center for Research in Nano Technology and Science, Indian Institute of Technology Bombay, Mumbai 400076, India;* orcid.org/0000-0002-2513-6006; Email: mithunc@iitb.ac.in

https://doi.org/10.1021/acspolymersau.4c00022
ACS Polym. Au 2024, 4, 342−391

Author

Mithun Madhusudanan − *Metallurgical Engineering and Materials Science, Indian Institute of Technology Bombay, Mumbai 400076, India*

Complete contact information is available at: https://pubs.acs.org/10.1021/acspolymersau.4c00022

Author Contributions

CRediT: **Mithun Madhusudanan** formal analysis, investigation, writing-original draft; **Mithun Chowdhury** conceptualization, funding acquisition, project administration, visualization, writing-original draft, writing-review & editing.

Notes

The authors declare no competing financial interest.

■ ACKNOWLEDGMENTS

M.C. acknowledges support by the Anusandhan National Research Foundation (Science and Engineering Research Board), India through the Ramanujan Fellowship (Grant No. SB/S2/RJN-084/2018), the Early Career Research Award (Grant No. ECR/2018/001740), and the Core Research Grant (Grant No. CRG/2023/006329). Additionally, M.C. acknowledges support from IIT Bombay through a SEED (Grant No. RD/0519-IRCCSH0-033). M.C. and M.M. acknowledge the constructive comments from the reviewers. M.M. acknowledges the help of Jotypriya Sarkar in proofreading and preparing graphics.

■ REFERENCES

(1) Lin, Q. Polymeric electronic materials for microelectronics manufacturing: A review. *Polymer* **2023**, *286*, 126395.

(2) Wang, G.; Melkonyan, F. S.; Facchetti, A.; Marks, T. J. All-polymer solar cells: recent progress, challenges, and prospects. *Angew. Chem., Int. Ed.* **2019**, *58*, 4129−4142.

(3) Lipomi, D. J.; Bao, Z. Stretchable and ultraflexible organic electronics. *MRS Bull.* **2017**, *42*, 93−97.

(4) Xu, J.; Wu, H.-C.; Zhu, C.; Ehrlich, A.; Shaw, L.; Nikolka, M.; Wang, S.; Molina-Lopez, F.; Gu, X.; Luo, S.; et al. Multi-scale ordering in highly stretchable polymer semiconducting films. *Nature materials* **2019**, *18*, 594−601.

(5) Zaid, A. N. A comprehensive review on pharmaceutical film coating: past, present, and future. *Drug Design, Development and Therapy* **2020**, *14*, 4613−4623.

(6) Zelikin, A. N. Drug releasing polymer thin films: new era of surface-mediated drug delivery. *ACS Nano* **2010**, *4*, 2494−2509.

(7) Huang, R.; Stafford, C. M.; Vogt, B. D. Effect of surface properties on wrinkling of ultrathin films. *Journal of Aerospace Engineering* **2007**, *20*, 38−44.

(8) Bower, D. I. *An introduction to polymer physics*; Cambridge University Press, 2002.

(9) Vogt, B. D. Mechanical and viscoelastic properties of confined amorphous polymers. *J. Polym. Sci., Part B: Polym. Phys.* **2018**, *56*, 9−30.

(10) Tweedie, C. A.; Constantinides, G.; Lehman, K. E.; Brill, D. J.; Blackman, G. S.; Van Vliet, K. J. Enhanced stiffness of amorphous polymer surfaces under confinement of localized contact loads. *Adv. Mater.* **2007**, *19*, 2540−2546.

(11) Rowland, H. D.; Sun, A. C.; Schunk, P. R.; King, W. P. Impact of polymer film thickness and cavity size on polymer flow during embossing: toward process design rules for nanoimprint lithography. *Journal of Micromechanics and Microengineering* **2005**, *15*, 2414.

(12) Napolitano, S.; Glynos, E.; Tito, N. B. Glass transition of polymers in bulk, confined geometries, and near interfaces. *Rep. Prog. Phys.* **2017**, *80*, 036602.

(13) Hao, Z.; Ghanekarade, A.; Zhu, N.; Randazzo, K.; Kawaguchi, D.; Tanaka, K.; Wang, X.; Simmons, D. S.; Priestley, R. D.; Zuo, B. Mobility gradients yield rubbery surfaces on top of polymer glasses. *Nature* **2021**, *596*, 372−376.

(14) Keddie, J. L.; Jones, R. A.; Cory, R. A. Size-dependent depression of the glass transition temperature in polymer films. *EPL (Europhysics Letters)* **1994**, *27*, 59.

(15) Ellison, C. J.; Torkelson, J. M. The distribution of glass-transition temperatures in nanoscopically confined glass formers. *Nature materials* **2003**, *2*, 695−700.

(16) Ediger, M.; Forrest, J. Dynamics near free surfaces and the glass transition in thin polymer films: A view to the future. *Macromolecules* **2014**, *47*, 471−478.

(17) Chandran, S.; Reiter, G. *Macromolecular Engineering*; John Wiley & Sons, Ltd, 2022; pp 1−30.

(18) Madhusudanan, M.; Chowdhury, M. An entropy generation approach to the molecular recoiling stress relaxation in thin nonequilibrated polymer films. *J. Chem. Phys.* **2024**, *160*, 014904.

(19) Napolitano, S. Irreversible adsorption of polymer melts and nanoconfinement effects. *Soft Matter* **2020**, *16*, 5348−5365.

(20) Reiter, G. The memorizing capacity of polymers. *J. Chem. Phys.* **2020**, *152*, 150901.

(21) Donth, E.-J. *The glass transition: relaxation dynamics in liquids and disordered materials*; Springer Science & Business Media, 2001; Vol. *48*.

(22) Alcoutlabi, M.; McKenna, G. B. Effects of confinement on material behaviour at the nanometre size scale. *J. Phys.: Condens. Matter* **2005**, *17*, R461.

(23) Roth, C. B.; Dutcher, J. R. Glass transition and chain mobility in thin polymer films. *J. Electroanal. Chem.* **2005**, *584*, 13−22.

(24) Cangialosi, D.; Alegria, A.; Colmenero, J. Effect of nanostructure on the thermal glass transition and physical aging in polymer materials. *Prog. Polym. Sci.* **2016**, *54*, 128−147.

(25) Roth, C. B. Polymers under nanoconfinement: where are we now in understanding local property changes? *Chem. Soc. Rev.* **2021**, *50*, 8050−8066.

(26) Cangialosi, D. Physical aging and vitrification in polymers and other glasses: Complex behavior and size effects. *J. Polym. Sci.* **2024**, *62*, 1952−1974.

(27) Cangialosi, D. Glass Transition and Relaxation Phenomena. *Thermal Analysis of Polymeric Materials: Methods and Developments* **2022**, *1*, 227−262.

(28) Reiter, G. Probing properties of polymers in thin films via dewetting. *Glass transition, dynamics and heterogeneity of polymer thin films* **2012**, *252*, 29−63.

(29) McKenna, G. B.; Zhai, M. *Polymer Glasses*; CRC Press, 2016; pp 205−242.

(30) Gunda, M.; Kumar, P.; Katiyar, M. Review of mechanical characterization techniques for thin films used in flexible electronics. *Critical Reviews in Solid State and Materials Sciences* **2017**, *42*, 129−152.

(31) Reiter, G.; Hamieh, M.; Damman, P.; Sclavons, S.; Gabriele, S.; Vilmin, T.; Raphaël, E. Residual stresses in thin polymer films cause rupture and dominate early stages of dewetting. *Nature materials* **2005**, *4*, 754−758.

(32) Chowdhury, M.; Freyberg, P.; Ziebert, F.; Yang, A. C.-M.; Steiner, U.; Reiter, G. Segmental relaxations have macroscopic consequences in glassy polymer films. *Phys. Rev. Lett.* **2012**, *109*, 136102.

(33) Chandran, S.; Baschnagel, J.; Cangialosi, D.; Fukao, K.; Glynos, E.; Janssen, L. M.; Müller, M.; Muthukumar, M.; Steiner, U.; Xu, J.; et al. Processing pathways decide polymer properties at the molecular level. *Macromolecules* **2019**, *52*, 7146−7156.

(34) Bansal, A.; Yang, H.; Li, C.; Cho, K.; Benicewicz, B. C.; Kumar, S. K.; Schadler, L. S. Quantitative equivalence between polymer nanocomposites and thin polymer films. *Nature materials* **2005**, *4*, 693−698.

(35) Sen, S.; Xie, Y.; Bansal, A.; Yang, H.; Cho, K.; Schadler, L.; Kumar, S. Equivalence between polymer nanocomposites and thin polymer films: Effect of processing conditions and molecular origins of observed behavior. *European Physical Journal Special Topics* **2007**, *141*, 161−165.

(36) Kumar, S. K.; Ganesan, V.; Riggleman, R. A. Perspective: Outstanding theoretical questions in polymer-nanoparticle hybrids. *J. Chem. Phys.* **2017**, *147*, 020901.
(37) Bailey, E. J.; Winey, K. I. Dynamics of polymer segments, polymer chains, and nanoparticles in polymer nanocomposite melts: A review. *Prog. Polym. Sci.* **2020**, *105*, 101242.
(38) Shulha, H.; Kovalev, A.; Myshkin, N.; Tsukruk, V. V. Some aspects of AFM nanomechanical probing of surface polymer films. *Eur. Polym. J.* **2004**, *40*, 949−956.
(39) Overney, R.; Buenviaje, C.; Luginbuehl, R.; Dinelli, F. Glass and structural transitions measured at polymer surfaces on the nanoscale. *J. Therm. Anal. Calorim.* **2000**, *59*, 205−225.
(40) Gong, L.; Xiang, L.; Zhang, J.; Chen, J.; Zeng, H. Fundamentals and advances in the adhesion of polymer surfaces and thin films. *Langmuir* **2019**, *35*, 15914−15936.
(41) Passeri, D.; Rossi, M.; Tamburri, E.; Terranova, M. L. Mechanical characterization of polymeric thin films by atomic force microscopy based techniques. *Anal. Bioanal. Chem.* **2013**, *405*, 1463−1478.
(42) Cheng, X.; Putz, K. W.; Wood, C. D.; Brinson, L. C. Characterization of local elastic modulus in confined polymer films via AFM indentation. *Macromol. Rapid Commun.* **2015**, *36*, 391−397.
(43) Cangialosi, D. Dynamics and thermodynamics of polymer glasses. *J. Phys.: Condens. Matter* **2014**, *26*, 153101.
(44) Priestley, R. D.; Cangialosi, D.; Napolitano, S. On the equivalence between the thermodynamic and dynamic measurements of the glass transition in confined polymers. *Journal of non-crystalline solids* **2015**, *407*, 288−295.
(45) Adam, G.; Gibbs, J. H. On the Temperature Dependence of Cooperative Relaxation Properties in Glass-Forming Liquids. *J. Chem. Phys.* **1965**, *43*, 139−146.
(46) Glarum, S. H. Dielectric Relaxation of Isoamyl Bromide. *J. Chem. Phys.* **1960**, *33*, 639−643.
(47) Ngai, K. Universal properties of relaxation and diffusion in complex materials: Originating from fundamental physics with rich applications. *Prog. Mater. Sci.* **2023**, *139*, 101130.
(48) Debenedetti, P. G.; Stillinger, F. H. Supercooled liquids and the glass transition. *Nature* **2001**, *410*, 259−267.
(49) Fukao, K.; Miyamoto, Y. Glass transitions and dynamics in thin polymer films: dielectric relaxation of thin films of polystyrene. *Phys. Rev. E* **2000**, *61*, 1743.
(50) Ellison, C. J.; Ruszkowski, R. L.; Fredin, N. J.; Torkelson, J. M. Dramatic Reduction of the Effect of Nanoconfinement on the Glass Transition of Polymer Films via Addition of Small-Molecule Diluent. *Phys. Rev. Lett.* **2004**, *92*, 095702.
(51) Koh, Y. P.; Simon, S. L. The glass transition and enthalpy recovery of a single polystyrene ultrathin film using Flash DSC. *J. Chem. Phys.* **2017**, *146*, 203329.
(52) Park, C. H.; Kim, J. H.; Ree, M.; Sohn, B.-H.; Jung, J. C.; Zin, W.-C. Thickness and composition dependence of the glass transition temperature in thin random copolymer films. *Polymer* **2004**, *45*, 4507−4513.
(53) Tian, H.; Xu, Q.; Zhang, H.; Priestley, R. D.; Zuo, B. Surface dynamics of glasses. *Applied Physics Reviews* **2022**, *9*, 011316.
(54) Rubinstein, M.; Colby, R. H. *Polymer physics*; Oxford University Press: Oxford, U.K., 2003.
(55) Boucher, V. M.; Cangialosi, D.; Yin, H.; Schönhals, A.; Alegría, A.; Colmenero, J. T g depression and invariant segmental dynamics in polystyrene thin films. *Soft Matter* **2012**, *8*, 5119−5122.
(56) Boucher, V. M.; Cangialosi, D.; Alegría, A.; Colmenero, J. Enthalpy recovery of PMMA/silica nanocomposites. *Macromolecules* **2010**, *43*, 7594−7603.
(57) Forrest, J.; Dalnoki-Veress, K.; Stevens, J.; Dutcher, J. Effect of free surfaces on the glass transition temperature of thin polymer films. *Physical review letters* **1996**, *77*, 2002.
(58) Fakhraai, Z.; Forrest, J. A. Probing Slow Dynamics in Supported Thin Polymer Films. *Phys. Rev. Lett.* **2005**, *95*, 025701.
(59) Efremov, M. Y.; Olson, E. A.; Zhang, M.; Zhang, Z.; Allen, L. H. Glass Transition in Ultrathin Polymer Films: Calorimetric Study. *Phys. Rev. Lett.* **2003**, *91*, 085703.
(60) Hudzinskyy, D.; Lyulin, A. V.; Baljon, A. R. C.; Balabaev, N. K.; Michels, M. A. J. Effects of Strong Confinement on the Glass-Transition Temperature in Simulated Atactic Polystyrene Films. *Macromolecules* **2011**, *44*, 2299−2310.
(61) Baglay, R. R.; Roth, C. B. Communication: Experimentally determined profile of local glass transition temperature across a glassy-rubbery polymer interface with a Tg difference of 80 K. *J. Chem. Phys.* **2015**, *143*, 111101.
(62) Christie, D.; Register, R. A.; Priestley, R. D. Direct measurement of the local glass transition in self-assembled copolymers with nanometer resolution. *ACS central science* **2018**, *4*, 504−511.
(63) Gagnon, Y. J.; Burton, J. C.; Roth, C. B. Development of broad modulus profile upon polymer−polymer interface formation between immiscible glassy−rubbery domains. *Proc. Natl. Acad. Sci. U. S. A.* **2024**, *121*, e2312533120.
(64) Roth, C.; Pound, A.; Kamp, S.; Murray, C.; Dutcher, J. Molecular-weight dependence of the glass transition temperature of freely-standing poly (methyl methacrylate) films. *Eur. Phys. J. E* **2006**, *20*, 441−448.
(65) Mattsson, J.; Forrest, J.; Börjesson, L. Quantifying glass transition behavior in ultrathin free-standing polymer films. *Phys. Rev. E* **2000**, *62*, 5187.
(66) De Gennes, P. Glass transitions in thin polymer films. *Eur. Phys. J. E* **2000**, *2*, 201−205.
(67) White, R. P.; Lipson, J. E. Free volume, cohesive energy density, and internal pressure as predictors of polymer miscibility. *Macromolecules* **2014**, *47*, 3959−3968.
(68) Kawana, S.; Jones, R. A. Character of the glass transition in thin supported polymer films. *Phys. Rev. E* **2001**, *63*, 021501.
(69) Paeng, K.; Swallen, S. F.; Ediger, M. Direct measurement of molecular motion in freestanding polystyrene thin films. *J. Am. Chem. Soc.* **2011**, *133*, 8444−8447.
(70) Yang, Z.; Fujii, Y.; Lee, F. K.; Lam, C.-H.; Tsui, O. K. C. Glass transition dynamics and surface layer mobility in unentangled polystyrene films. *Science* **2010**, *328*, 1676−1679.
(71) Priestley, R. D.; Ellison, C. J.; Broadbelt, L. J.; Torkelson, J. M. Structural relaxation of polymer glasses at surfaces, interfaces, and in between. *Science* **2005**, *309*, 456−459.
(72) Chowdhury, M.; Monnier, X.; Cangialosi, D.; Priestley, R. D. Decoupling of Glassy Dynamics from Viscosity in Thin Supported Poly (n-butyl methacrylate) Films. *ACS Polymers Au* **2022**, *2*, 333−340.
(73) Chowdhury, M.; Guo, Y.; Wang, Y.; Merling, W. L.; Mangalara, J. H.; Simmons, D. S.; Priestley, R. D. Spatially Distributed Rheological Properties in Confined Polymers by Noncontact Shear. *J. Phys. Chem. Lett.* **2017**, *8*, 1229−1234.
(74) Perez-de Eulate, N. G.; Sferrazza, M.; Cangialosi, D.; Napolitano, S. Irreversible adsorption erases the free surface effect on the T_g of supported films of poly (4-tert-butylstyrene). *ACS Macro Lett.* **2017**, *6*, 354−358.
(75) Madhusudanan, M.; Sarkar, J.; Dhar, S.; Chowdhury, M. Tuning the Plasticization to Decouple the Effect of Molecular Recoiling Stress from Modulus and Viscosity in Dewetting Thin Polystyrene Films. *Macromolecules* **2023**, *56*, 1402−1409.
(76) Chen, F.; Peng, D.; Lam, C.-H.; Tsui, O. K. C. Viscosity and surface-promoted slippage of thin polymer films supported by a solid substrate. *Macromolecules* **2015**, *48*, 5034−5039.
(77) Panagopoulou, A.; Napolitano, S. Irreversible adsorption governs the equilibration of thin polymer films. *Physical review letters* **2017**, *119*, 097801.
(78) Housmans, C.; Sferrazza, M.; Napolitano, S. Kinetics of irreversible chain adsorption. *Macromolecules* **2014**, *47*, 3390−3393.
(79) Simavilla, D. N.; Huang, W.; Vandestrick, P.; Ryckaert, J.-P.; Sferrazza, M.; Napolitano, S. Mechanisms of Polymer Adsorption onto Solid Substrates. *ACS Macro Lett.* **2017**, *6*, 975−979.
(80) Nieto Simavilla, D.; Huang, W.; Housmans, C.; Sferrazza, M.; Napolitano, S. Taming the Strength of Interfacial Interactions via Nanoconfinement. *ACS Central Science* **2018**, *4*, 755−759.
(81) Rodríguez-Tinoco, C.; Simavilla, D. N.; Priestley, R. D.; Wübbenhorst, M.; Napolitano, S. Density of Obstacles Affects

Diffusion in Adsorbed Polymer Layers. *ACS Macro Lett.* **2020**, *9*, 318−322.
(82) Koga, T.; Jiang, N.; Gin, P.; Endoh, M. K.; Narayanan, S.; Lurio, L. B.; Sinha, S. K. Impact of an Irreversibly Adsorbed Layer on Local Viscosity of Nanoconfined Polymer Melts. *Phys. Rev. Lett.* **2011**, *107*, 225901.
(83) Koga, T.; Li, C.; Endoh, M. K.; Koo, J.; Rafailovich, M.; Narayanan, S.; Lee, D. R.; Lurio, L. B.; Sinha, S. K. Reduced Viscosity of the Free Surface in Entangled Polymer Melt Films. *Phys. Rev. Lett.* **2010**, *104*, 066101.
(84) Jiang, N.; Sen, M.; Endoh, M. K.; Koga, T.; Langhammer, E.; Bjöörn, P.; Tsige, M. Thermal Properties and Segmental Dynamics of Polymer Melt Chains Adsorbed on Solid Surfaces. *Langmuir* **2018**, *34*, 4199−4209.
(85) Yan, J.; Ma, Z.; Xu, J.; Nie, H.; Yuan, H.; Wang, X.; Wang, T.; Weng, L.-T.; Tsui, O. K. C. Glass Transition of the Surface Monolayer of Polystyrene Films: Effect of Thermal Preannealing. *Macromolecules* **2023**, *56*, 5917−5923.
(86) Yu, X.; Wang, T.; Tsui, O. K. C.; Weng, L.-T. Tuning the Effective Viscosity of Polymer Films by Chemical Modifications. *Macromolecules* **2019**, *52*, 3499−3505.
(87) Braatz, M.-L.; Infantas Meléndez, L.; Sferrazza, M.; Napolitano, S. Unexpected impact of irreversible adsorption on thermal expansion: Adsorbed layers are not that dead. *J. Chem. Phys.* **2017**, *146*, 203304.
(88) Ren, W.; Li, Y.; Tang, Y.; Xu, J.; Zhang, C.; Tsui, O. K. C.; Wang, X. Loosely Adsorbed Chains Expedite the Desorption of Flattened Polystyrene Chains on Flat Silicon Surface. *ACS Macro Lett.* **2023**, *12*, 854−859.
(89) Chowdhury, M.; Priestley, R. D. Discrete mobility on the surface of glasses. *Proc. Natl. Acad. Sci. U. S. A.* **2017**, *114*, 4854−4856.
(90) Matheson, A. J.; Goldstein, M.; Williams, G.; Johari, G. P.; Watts, R. O.; Whalley, E.; Allen, G.; White, J. W. General discussion. *Faraday Symp. Chem. Soc.* **1972**, *6*, 42−47.
(91) Caporaletti, F.; Napolitano, S. The slow Arrhenius process in small organic molecules. *Phys. Chem. Chem. Phys.* **2024**, *26*, 745−748.
(92) Song, Z.; Rodríguez-Tinoco, C.; Mathew, A.; Napolitano, S. Fast equilibration mechanisms in disordered materials mediated by slow liquid dynamics. *Science advances* **2022**, *8*, eabm7154.
(93) Thoms, E.; Napolitano, S. Enthalpy-entropy compensation in the slow Arrhenius process. *J. Chem. Phys.* **2023**, *159*, 161103.
(94) Thoms, E.; Wang, K.; Chandran, S.; Napolitano, S. Fast Processing Affects the Relaxation of Polymers: The Slow Arrhenius Process Can Probe Stress at the Molecular Level. *J. Phys. Chem. Lett.* **2024**, *15*, 4838−4843.
(95) Hall, D. B.; Dhinojwala, A.; Torkelson, J. M. Translation-rotation paradox for diffusion in glass-forming polymers: the role of the temperature dependence of the relaxation time distribution. *Physical review letters* **1997**, *79*, 103.
(96) Ngai, K. Alternative explanation of the difference between translational diffusion and rotational diffusion in supercooled liquids. *J. Phys. Chem. B* **1999**, *103*, 10684−10694.
(97) Mandel, N. L.; Lee, S.; Kim, K.; Paeng, K.; Kaufman, L. J. Single molecule demonstration of Debye−Stokes−Einstein breakdown in polystyrene near the glass transition temperature. *Nat. Commun.* **2022**, *13*, 3580.
(98) Chen, F.; Peng, D.; Ogata, Y.; Tanaka, K.; Yang, Z.; Fujii, Y.; Yamada, N.; Lam, C.-H.; Tsui, O. K. C. Confinement effect on the effective viscosity of plasticized polymer films. *Macromolecules* **2015**, *48*, 7719−7726.
(99) Masson, J.-L.; Green, P. F. Viscosity of entangled polystyrene thin film melts: Film thickness dependence. *Phys. Rev. E* **2002**, *65*, 031806.
(100) Zuo, B.; Tian, H.; Liang, Y.; Xu, H.; Zhang, W.; Zhang, L.; Wang, X. Probing the rheological properties of supported thin polystyrene films by investigating the growth dynamics of wetting ridges. *Soft Matter* **2016**, *12*, 6120−6131.
(101) Torres, J. M.; Stafford, C. M.; Vogt, B. D. Impact of molecular mass on the elastic modulus of thin polystyrene films. *Polymer* **2010**, *51*, 4211−4217.
(102) Liu, Y.; Chen, Y.-C.; Hutchens, S.; Lawrence, J.; Emrick, T.; Crosby, A. J. Directly measuring the complete stress−strain response of ultrathin polymer films. *Macromolecules* **2015**, *48*, 6534−6540.
(103) Xiao, Y.; Bai, P.; Zhang, Z.; Guo, Y. Direct measurement and modeling of viscoelastic−viscoplastic properties of freely standing thin polystyrene films. *J. Chem. Phys.* **2023**, *159*, 214903.
(104) Hall, D. B.; Torkelson, J. M. Small molecule probe diffusion in thin and ultrathin supported polymer films. *Macromolecules* **1998**, *31*, 8817−8825.
(105) Tseng, K.; Turro, N. J.; Durning, C. J. Molecular mobility in polymer thin films. *Phys. Rev. E* **2000**, *61*, 1800.
(106) Frank, B.; Gast, A. P.; Russell, T. P.; Brown, H. R.; Hawker, C. Polymer mobility in thin films. *Macromolecules* **1996**, *29*, 6531−6534.
(107) Pressly, J. F.; Riggleman, R. A.; Winey, K. I. Increased polymer diffusivity in thin-film confinement. *Macromolecules* **2019**, *52*, 6116−6125.
(108) Zuo, B.; Wang, F.; Hao, Z.; He, H.; Zhang, S.; Priestley, R. D.; Wang, X. Influence of the interfacial effect on polymer thin-film dynamics scaled by the distance of chain mobility suppression by the substrate. *Macromolecules* **2019**, *52*, 3753−3762.
(109) Rodríguez-Tinoco, C.; Simavilla, D. N.; Priestley, R. D.; Wübbenhorst, M.; Napolitano, S. Density of obstacles affects diffusion in adsorbed polymer layers. *ACS macro letters* **2020**, *9*, 318−322.
(110) Cangialosi, D.; Boucher, V. M.; Alegria, A.; Colmenero, J. Free volume holes diffusion to describe physical aging in poly (mehtyl methacrylate)/silica nanocomposites. *J. Chem. Phys.* **2011**, *135*, 014901.
(111) Geng, K.; Katsumata, R.; Yu, X.; Ha, H.; Dulaney, A. R.; Ellison, C. J.; Tsui, O. K. Conflicting confinement effects on the T g, diffusivity, and effective viscosity of polymer films: A case study with poly (isobutyl methacrylate) on silica and possible resolution. *Macromolecules* **2017**, *50*, 609−617.
(112) Zhao, J.; McKenna, G. B. Temperature divergence of the dynamics of a poly (vinyl acetate) glass: Dielectric vs. mechanical behaviors. *J. Chem. Phys.* **2012**, *136*, 154901.
(113) Boucher, V. M.; Cangialosi, D.; Alegría, A.; Colmenero, J. Enthalpy recovery in nanometer to micrometer thick polystyrene films. *Macromolecules* **2012**, *45*, 5296−5306.
(114) Boucher, V. M.; Cangialosi, D.; Yin, H.; Schönhals, A.; Alegría, A.; Colmenero, J. T g depression and invariant segmental dynamics in polystyrene thin films. *Soft Matter* **2012**, *8*, 5119−5122.
(115) Boucher, V. M.; Cangialosi, D.; Alegría, A.; Colmenero, J. Accounting for the thickness dependence of the Tg in supported PS films via the volume holes diffusion model. *Thermochim. Acta* **2014**, *575*, 233−237.
(116) Zha, H.; Wang, Q.; Wang, X.; Cangialosi, D.; Zuo, B. Enhanced Free Surface Mobility Facilitates the Release of Free-Volume Holes in Thin-Film Polymer Glasses. *Macromolecules* **2021**, *54*, 2022−2028.
(117) Xu, Q.; Zhu, N.; Fang, H.; Wang, X.; Priestley, R. D.; Zuo, B. Decoupling role of film thickness and interfacial effect on polymer thin film dynamics. *ACS Macro Lett.* **2021**, *10*, 1−8.
(118) Jean, Y.; Cao, H.; Dai, G.; Suzuki, R.; Ohdaira, T.; Kobayashi, Y.; Hirata, K. Free-volume hole properties near the surface of polymers obtained from slow positron annihilation spectroscopy. *Appl. Surf. Sci.* **1997**, *116*, 251−255.
(119) Cicerone, M. T.; Ediger, M. D. Enhanced translation of probe molecules in supercooled o-terphenyl: signature of spatially heterogeneous dynamics? *J. Chem. Phys.* **1996**, *104*, 7210−7218.
(120) Deppe, D. D.; Dhinojwala, A.; Torkelson, J. M. Small molecule probe diffusion in thin polymer films near the glass transition: a novel approach using fluorescence nonradiative energy transfer. *Macromolecules* **1996**, *29*, 3898−3908.
(121) Hall, D. B.; Deppe, D. D.; Hamilton, K. E.; Dhinojwala, A.; Torkelson, J. M. Probe translational and rotational diffusion in polymers near Tg: Roles of probe size, shape, and secondary bonding in deviations from Debye−Stokes−Einstein scaling. *Journal of non-crystalline solids* **1998**, *235*, 48−56.

https://doi.org/10.1021/acspolymersau.4c00022
ACS Polym. Au 2024, 4, 342−391

(122) Cicerone, M. T.; Blackburn, F.; Ediger, M. Anomalous diffusion of probe molecules in polystyrene: evidence for spatially heterogeneous segmental dynamics. *Macromolecules* **1995**, *28*, 8224−8232.
(123) Maldonado-Camargo, L.; Rinaldi, C. Breakdown of the Stokes−Einstein relation for the rotational diffusivity of polymer grafted nanoparticles in polymer melts. *Nano Lett.* **2016**, *16*, 6767−6773.
(124) Bodiguel, H.; Fretigny, C. Reduced viscosity in thin polymer films. *Physical review letters* **2006**, *97*, 266105.
(125) Dalnoki-Veress, K.; Forrest, J.; Murray, C.; Gigault, C.; Dutcher, J. Molecular weight dependence of reductions in the glass transition temperature of thin, freely standing polymer films. *Phys. Rev. E* **2001**, *63*, 031801.
(126) Ellison, C. J.; Mundra, M. K.; Torkelson, J. M. Impacts of polystyrene molecular weight and modification to the repeat unit structure on the glass transition- nanoconfinement effect and the cooperativity length scale. *Macromolecules* **2005**, *38*, 1767−1778.
(127) Li, C.; Koga, T.; Li, C.; Jiang, J.; Sharma, S.; Narayanan, S.; Lurio, L.; Hu, X.; Jiao, X.; Sinha, S.; et al. Viscosity measurements of very thin polymer films. *Macromolecules* **2005**, *38*, 5144−5151.
(128) Suh, K. Y.; Kim, P.; Eui Jeong, H.; Kwan Kim, J. Measurement of viscosity of confined polymer melt using capillary kinetics. *Nanoscale and microscale thermophysical engineering* **2006**, *10*, 263−274.
(129) Khare, R.; de Pablo, J. J.; Yethiraj, A. Rheology of confined polymer melts. *Macromolecules* **1996**, *29*, 7910−7918.
(130) Torres, J. M.; Stafford, C. M.; Vogt, B. D. Elastic modulus of amorphous polymer thin films: relationship to the glass transition temperature. *ACS Nano* **2009**, *3*, 2677−2685.
(131) Chang, J.; Toga, K. B.; Paulsen, J. D.; Menon, N.; Russell, T. P. Thickness dependence of the Young's modulus of polymer thin films. *Macromolecules* **2018**, *51*, 6764−6770.
(132) Askar, S.; Torkelson, J. M. Stiffness of thin, supported polystyrene films: Free-surface, substrate, and confinement effects characterized via self-referencing fluorescence. *Polymer* **2016**, *99*, 417−426.
(133) Kim, H.; Cang, Y.; Kang, E.; Graczykowski, B.; Secchi, M.; Montagna, M.; Priestley, R. D.; Furst, E. M.; Fytas, G. Direct observation of polymer surface mobility via nanoparticle vibrations. *Nat. Commun.* **2018**, *9*, 2918.
(134) Chandran, S.; Handa, R.; Kchaou, M.; Al Akhrass, S.; Semenov, A. N.; Reiter, G. Time allowed for equilibration quantifies the preparation induced nonequilibrium behavior of polymer films. *ACS Macro Lett.* **2017**, *6*, 1296−1300.
(135) Chandran, S.; Reiter, G. Segmental rearrangements relax stresses in nonequilibrated polymer films. *ACS Macro Lett.* **2019**, *8*, 646−650.
(136) Reiter, G.; De Gennes, P. Spin-cast, thin, glassy polymer films: Highly metastable forms of matter. *Eur. Phys. J. E* **2001**, *6*, 25−28.
(137) Yang, Y.; Xu, Q.; Jin, T.; Wang, X.; Napolitano, S.; Zuo, B. Relaxations of entropically stressed polymer glasses. *Macromolecules* **2023**, *56*, 5924−5931.
(138) Kanaya, T.; Miyazaki, T.; Inoue, R.; Nishida, K. Thermal expansion and contraction of polymer thin films. *physica status solidi (b)* **2005**, *242*, 595−606.
(139) Bhattacharya, M.; Sanyal, M.; Geue, T.; Pietsch, U. Glass transition in ultrathin polymer films: A thermal expansion study. *Phys. Rev. E* **2005**, *71*, 041801.
(140) Chung, J. Y.; Chastek, T. Q.; Fasolka, M. J.; Ro, H. W.; Stafford, C. M. Quantifying residual stress in nanoscale thin polymer films via surface wrinkling. *ACS Nano* **2009**, *3*, 844−852.
(141) Askar, S.; Evans, C. M.; Torkelson, J. M. Residual stress relaxation and stiffness in spin-coated polymer films: Characterization by ellipsometry and fluorescence. *Polymer* **2015**, *76*, 113−122.
(142) Chowdhury, M.; Al Akhrass, S.; Ziebert, F.; Reiter, G. Relaxing nonequilibrated polymers in thin films at temperatures slightly above the glass transition. *J. Polym. Sci., Part B: Polym. Phys.* **2017**, *55*, 515−523.
(143) Chowdhury, M.; Sheng, X.; Ziebert, F.; Yang, A. C.-M.; Sepe, A.; Steiner, U.; Reiter, G. Intrinsic stresses in thin glassy polymer films revealed by crack formation. *Macromolecules* **2016**, *49*, 9060−9067.
(144) Tsui, O. K. C.; Wang, Y. J.; Lee, F. K.; Lam, C.-H.; Yang, Z. Equilibrium pathway of spin-coated polymer films. *Macromolecules* **2008**, *41*, 1465−1468.
(145) Yang, Z.; Lam, C.-H.; DiMasi, E.; Bouet, N.; Jordan-Sweet, J.; Tsui, O. K. C. Method to measure the viscosity of nanometer liquid films from the surface fluctuations. *Applied physics letters* **2009**, *94*, 251906.
(146) Welch, P. The use of fast Fourier transform for the estimation of power spectra: A method based on time averaging over short, modified periodograms. *IEEE Transactions on Audio and Electroacoustics* **1967**, *15*, 70−73.
(147) Jwo, D.-J.; Chang, W.-Y.; Wu, I.-H. Windowing techniques, the welch method for improvement of power spectrum estimation. *Comput. Mater. Contin* **2021**, *67*, 3983−4003.
(148) Yu, X.; Yiu, P.; Weng, L.-T.; Chen, F.; Tsui, O. K. C. Effective Viscosity of Lightly UVO-Treated Polystyrene Films on Silicon with Different Molecular Weights. *Macromolecules* **2019**, *52*, 877−885.
(149) Fredrickson, G. H.; Ajdari, A.; Leibler, L.; Carton, J. P. Surface modes and deformation energy of a molten polymer brush. *Macromolecules* **1992**, *25*, 2882−2889.
(150) Chaikin, P. M.; Lubensky, T. C.; Witten, T. A. *Principles of condensed matter physics*; Cambridge University Press: Cambridge, 1995; Vol. *10*.
(151) Cook, H. Brownian motion in spinodal decomposition. *Acta Metall.* **1970**, *18*, 297−306.
(152) Clough, A.; Peng, D.; Yang, Z.; Tsui, O. K. C. Glass transition temperature of polymer films that slip. *Macromolecules* **2011**, *44*, 1649−1653.
(153) Wang, Y. J.; Tsui, O. K. Mean-field description of spinodal growth of surface waves on rupturing films. *Journal of non-crystalline solids* **2006**, *352*, 4977−4982.
(154) Wang, Y. J.; Tsui, O. K. Unconventional spinodal surface fluctuations on polymer films. *Langmuir* **2006**, *22*, 1959−1963.
(155) Lam, C.-H.; Tsui, O. K. C.; Peng, D. Surface dynamics of noisy viscoelastic films by adiabatic approximation. *Langmuir* **2012**, *28*, 10217−10222.
(156) Peng, D.; Yang, Z.; Tsui, O. K. C. Method to measure the viscoelastic properties of nanometer entangled polymer films. *Macromolecules* **2011**, *44*, 7460−7464.
(157) Reiter, G. Dewetting as a probe of polymer mobility in thin films. *Macromolecules* **1994**, *27*, 3046−3052.
(158) Li, R. N.; Chen, F.; Lam, C.-H.; Tsui, O. K. C. Viscosity of PMMA on silica: Epitome of systems with strong polymer−substrate interactions. *Macromolecules* **2013**, *46*, 7889−7893.
(159) Yu, X.; Wang, T.; Tsui, O. K. C.; Weng, L.-T. Tuning the Effective Viscosity of Polymer Films by Chemical Modifications. *Macromolecules* **2019**, *52*, 3499−3505.
(160) Xu, J.; Lv, C.; Du, B.; Wang, X.; Tsui, O. K. C. Effective Viscosity of Unentangled Random Copolymer Films of Styrene and 4-Methoxystyrene with Different Copolymer Compositions. *Macromolecules* **2020**, *53*, 7430−7438.
(161) Joye, D. D.; Poehlein, G. W.; Denson, C. D. A bubble inflation technique for the measurement of viscoelastic properties in equal biaxial extensional flow. *Transactions of the Society of Rheology* **1972**, *16*, 421−445.
(162) O'connell, P.; McKenna, G. Rheological measurements of the thermoviscoelastic response of ultrathin polymer films. *Science* **2005**, *307*, 1760−1763.
(163) O'Connell, P.; McKenna, G. Novel nanobubble inflation method for determining the viscoelastic properties of ultrathin polymer films. *Review of scientific instruments* **2007**, *78*, 013901.
(164) O'Connell, P.; McKenna, G. Dramatic stiffening of ultrathin polymer films in the rubbery regime. *Eur. Phys. J. E* **2006**, *20*, 143−150.
(165) O'Connell, P. A.; Hutcheson, S. A.; McKenna, G. B. Creep behavior of ultra-thin polymer films. *J. Polym. Sci., Part B: Polym. Phys.* **2008**, *46*, 1952−1965.
(166) O'Connell, P. A.; McKenna, G. B. The stiffening of ultrathin polymer films in the rubbery regime: The relative contributions of

membrane stress and surface tension. *J. Polym. Sci., Part B: Polym. Phys.* **2009**, *47*, 2441−2448.
(167) Xu, S.; O'Connell, P. A.; McKenna, G. B. Unusual elastic behavior of ultrathin polymer films: Confinement-induced/molecular stiffening and surface tension effects. *J. Chem. Phys.* **2010**, *132*, 184902.
(168) Xu, S.; O'Connell, P. A.; McKenna, G. B.; Castagnet, S. Nanomechanical properties in ultrathin polymer films: Measurement on rectangular versus circular bubbles. *J. Polym. Sci., Part B: Polym. Phys.* **2012**, *50*, 466−476.
(169) O'Connell, P. A.; Wang, J.; Ishola, T. A.; McKenna, G. B. Exceptional property changes in ultrathin films of polycarbonate: Glass temperature, rubbery stiffening, and flow. *Macromolecules* **2012**, *45*, 2453−2459.
(170) Ngai, K.; Prevosto, D.; Grassia, L. Viscoelasticity of nano-bubble-inflated ultrathin polymer films: Justification by the coupling model. *J. Polym. Sci., Part B: Polym. Phys.* **2013**, *51*, 214−224.
(171) Li, X.; McKenna, G. B. Ultrathin Polymer films: Rubbery stiffening, fragility, and T g reduction. *Macromolecules* **2015**, *48*, 6329−6336.
(172) Yoon, H.; McKenna, G. B. Rubbery stiffening" and rupture behavior of freely standing nanometric thin PIB films. *Macromolecules* **2017**, *50*, 9821−9830.
(173) Chapuis, P.; Montgomery, P. C.; Anstotz, F.; Leong-Hoï, A.; Gauthier, C.; Baschnagel, J.; Reiter, G.; McKenna, G.; Rubin, A. A novel interferometric method for the study of the viscoelastic properties of ultra-thin polymer films determined from nanobubble inflation. *Rev. Sci. Instrum.* **2017**, *88*, 093901.
(174) Schapery, R. A. On the characterization of nonlinear viscoelastic materials. *Polym. Eng. Sci.* **1969**, *9*, 295−310.
(175) Lai, J.; Bakker, A. 3-D Schapery representation for non-linear viscoelasticity and finite element implementation. *Computational mechanics* **1996**, *18*, 182−191.
(176) Park, S.; Schapery, R. Methods of interconversion between linear viscoelastic material functions. Part I—A numerical method based on Prony series. *International journal of solids and structures* **1999**, *36*, 1653−1675.
(177) Perzyna, P. Fundamental problems in viscoplasticity. *Advances in applied mechanics* **1966**, *9*, 243−377.
(178) Stafford, C. M.; Harrison, C.; Beers, K. L.; Karim, A.; Amis, E. J.; VanLandingham, M. R.; Kim, H.-C.; Volksen, W.; Miller, R. D.; Simonyi, E. E. A buckling-based metrology for measuring the elastic moduli of polymeric thin films. *Nature materials* **2004**, *3*, 545−550.
(179) Cerda, E.; Mahadevan, L. Geometry and physics of wrinkling. *Physical review letters* **2003**, *90*, 074302.
(180) Chung, J. Y.; Nolte, A. J.; Stafford, C. M. Surface wrinkling: a versatile platform for measuring thin-film properties. *Adv. Mater.* **2011**, *23*, 349−368.
(181) Biot, M. Bending of an infinite beam on an elastic foundation. *Journal of Applied Mathematics and Mechanics* **1922**, *2*, 165−184.
(182) Bowden, N.; Brittain, S.; Evans, A. G.; Hutchinson, J. W.; Whitesides, G. M. Spontaneous formation of ordered structures in thin films of metals supported on an elastomeric polymer. *Nature* **1998**, *393*, 146−149.
(183) Volynskii, A.; Bazhenov, S.; Lebedeva, O.; Bakeev, N. Mechanical buckling instability of thin coatings deposited on soft polymer substrates. *J. Mater. Sci.* **2000**, *35*, 547−554.
(184) Cai, S.; Breid, D.; Crosby, A. J.; Suo, Z.; Hutchinson, J. W. Periodic patterns and energy states of buckled films on compliant substrates. *Journal of the Mechanics and Physics of Solids* **2011**, *59*, 1094−1114.
(185) Vandeparre, H.; Desbief, S.; Lazzaroni, R.; Gay, C.; Damman, P. Confined wrinkling: impact on pattern morphology and periodicity. *Soft Matter* **2011**, *7*, 6878−6882.
(186) Stafford, C. M.; Guo, S.; Harrison, C.; Chiang, M. Y. Combinatorial and high-throughput measurements of the modulus of thin polymer films. *Rev. Sci. Instrum.* **2005**, *76*, 062207.
(187) Stafford, C. M.; Vogt, B. D.; Harrison, C.; Julthongpiput, D.; Huang, R. Elastic moduli of ultrathin amorphous polymer films. *Macromolecules* **2006**, *39*, 5095−5099.
(188) Chung, J. Y.; Douglas, J. F.; Stafford, C. M. A wrinkling-based method for investigating glassy polymer film relaxation as a function of film thickness and temperature. *J. Chem. Phys.* **2017**, *147*, 154902.
(189) Chan, E. P.; Page, K. A.; Im, S. H.; Patton, D. L.; Huang, R.; Stafford, C. M. Viscoelastic properties of confined polymer films measured via thermal wrinkling. *Soft Matter* **2009**, *5*, 4638−4641.
(190) Agrawal, A.; Luchette, P.; Palffy-Muhoray, P.; Biswal, S. L.; Chapman, W. G.; Verduzco, R. Surface wrinkling in liquid crystal elastomers. *Soft Matter* **2012**, *8*, 7138−7142.
(191) Huang, J.; Juszkiewicz, M.; De Jeu, W. H.; Cerda, E.; Emrick, T.; Menon, N.; Russell, T. P. Capillary wrinkling of floating thin polymer films. *Science* **2007**, *317*, 650−653.
(192) Jiang, H.; Khang, D.-Y.; Song, J.; Sun, Y.; Huang, Y.; Rogers, J. A. Finite deformation mechanics in buckled thin films on compliant supports. *Proc. Natl. Acad. Sci. U. S. A.* **2007**, *104*, 15607−15612.
(193) Song, J.; Jiang, H.; Liu, Z.; Khang, D.-Y.; Huang, Y.; Rogers, J. A.; Lu, C.; Koh, C. Buckling of a stiff thin film on a compliant substrate in large deformation. *International Journal of Solids and Structures* **2008**, *45*, 3107−3121.
(194) Lin, D. C.; Douglas, J. F.; Horkay, F. Development of minimal models of the elastic properties of flexible and stiff polymer networks with permanent and thermoreversible cross-links. *Soft Matter* **2010**, *6*, 3548−3561.
(195) Chan, E. P.; Kundu, S.; Lin, Q.; Stafford, C. M. Quantifying the stress relaxation modulus of polymer thin films via thermal wrinkling. *ACS Appl. Mater. Interfaces* **2011**, *3*, 331−338.
(196) Torres, J. M.; Stafford, C. M.; Vogt, B. D. Manipulation of the elastic modulus of polymers at the nanoscale: Influence of UV- ozone cross-linking and plasticizer. *ACS Nano* **2010**, *4*, 5357−5365.
(197) Torres, J. M.; Stafford, C. M.; Uhrig, D.; Vogt, B. D. Impact of chain architecture (branching) on the thermal and mechanical behavior of polystyrene thin films. *J. Polym. Sci., Part B: Polym. Phys.* **2012**, *50*, 370−377.
(198) Mei, H.; Landis, C. M.; Huang, R. Concomitant wrinkling and buckle-delamination of elastic thin films on compliant substrates. *Mech. Mater.* **2011**, *43*, 627−642.
(199) Nolte, A. J.; Chung, J. Y.; Davis, C. S.; Stafford, C. M. Wrinkling-to-delamination transition in thin polymer films on compliant substrates. *Soft Matter* **2017**, *13*, 7930−7937.
(200) Chung, J. Y.; Lee, J.-H.; Beers, K. L.; Stafford, C. M. Stiffness, strength, and ductility of nanoscale thin films and membranes: a combined wrinkling−cracking methodology. *Nano Lett.* **2011**, *11*, 3361−3365.
(201) Rogers, J. A.; Someya, T.; Huang, Y. Materials and mechanics for stretchable electronics. *science* **2010**, *327*, 1603−1607.
(202) Niu, R.; Liu, G.; Wang, C.; Zhang, G.; Ding, X.; Sun, J. Thickness dependent critical strain in submicron Cu films adherent to polymer substrate. *Appl. Phys. Lett.* **2007**, *90*, 161907.
(203) Lee, J.-H.; Chung, J. Y.; Stafford, C. M. Effect of confinement on stiffness and fracture of thin amorphous polymer films. *ACS Macro Lett.* **2012**, *1*, 122−126.
(204) Cao, Y.-P.; Jia, F.; Zhao, Y.; Feng, X.-Q.; Yu, S.-W. Buckling and post-buckling of a stiff film resting on an elastic graded substrate. *International Journal of Solids and Structures* **2012**, *49*, 1656−1664.
(205) Gurmessa, B. J.; Croll, A. B. Onset of plasticity in thin polystyrene films. *Physical review letters* **2013**, *110*, 074301.
(206) Reese, C. M.; Guo, W.; Thompson, B. J.; Logan, P. K.; Stafford, C. M.; Patton, D. L. Quantifying strain via buckling instabilities in surface-modified polymer brushes. *Macromolecules* **2020**, *53*, 4552−4559.
(207) Huang, H.; Chung, J. Y.; Nolte, A. J.; Stafford, C. M. Characterizing polymer brushes via surface wrinkling. *Chem. Mater.* **2007**, *19*, 6555−6560.
(208) Ilton, M.; Couchman, M. M.; Gerbelot, C.; Benzaquen, M.; Fowler, P. D.; Stone, H. A.; Raphaël, E.; Dalnoki-Veress, K.; Salez, T. Capillary leveling of freestanding liquid nanofilms. *Physical review letters* **2016**, *117*, 167801.

(209) McGraw, J. D.; Jago, N. M.; Dalnoki-Veress, K. Capillary levelling as a probe of thin film polymer rheology. *Soft Matter* **2011**, *7*, 7832−7838.
(210) Bäumchen, O.; Benzaquen, M.; Salez, T.; McGraw, J. D.; Backholm, M.; Fowler, P.; Raphaël, E.; Dalnoki-Veress, K. Relaxation and intermediate asymptotics of a rectangular trench in a viscous film. *Phys. Rev. E* **2013**, *88*, 035001.
(211) Backholm, M.; Benzaquen, M.; Salez, T.; Raphaël, E.; Dalnoki-Veress, K. Capillary levelling of a cylindrical hole in a viscous film. *Soft Matter* **2014**, *10*, 2550−2558.
(212) Benzaquen, M.; Fowler, P.; Jubin, L.; Salez, T.; Dalnoki-Veress, K.; Raphaël, E. Approach to universal self-similar attractor for the levelling of thin liquid films. *Soft Matter* **2014**, *10*, 8608−8614.
(213) Zheng, Z.; Fontelos, M. A.; Shin, S.; Stone, H. A. Universality in the nonlinear leveling of capillary films. *Physical Review Fluids* **2018**, *3*, 032001.
(214) Salez, T.; McGraw, J. D.; Bäumchen, O.; Dalnoki-Veress, K.; Raphaël, E. Capillary-driven flow induced by a stepped perturbation atop a viscous film. *Phys. Fluids* **2012**, *24*, 102111.
(215) Stillwagon, L.; Larson, R. Fundamentals of topographic substrate leveling. *Journal of applied physics* **1988**, *63*, 5251−5258.
(216) Stillwagon, L.; Larson, R. Leveling of thin films over uneven substrates during spin coating. *Physics of Fluids A: Fluid Dynamics* **1990**, *2*, 1937−1944.
(217) Oron, A.; Davis, S. H.; Bankoff, S. G. Long-scale evolution of thin liquid films. *Reviews of modern physics* **1997**, *69*, 931.
(218) Bertozzi, A. L. The mathematics of moving contact lines in thin liquid films. *Notices of the AMS* **1998**, *45*, 689−697.
(219) McGraw, J. D.; Salez, T.; Bäumchen, O.; Raphaël, E.; Dalnoki-Veress, K. Self-similarity and energy dissipation in stepped polymer films. *Phys. Rev. Lett.* **2012**, *109*, 128303.
(220) Salez, T.; McGraw, J. D.; Cormier, S. L.; Bäumchen, O.; Dalnoki-Veress, K.; Raphaël, E. Numerical solutions of thin-film equations for polymer flows. *Eur. Phys. J. E* **2012**, *35*, 1−9.
(221) Benzaquen, M.; Salez, T.; Raphaël, E. Intermediate asymptotics of the capillary-driven thin-film equation. *Eur. Phys. J. E* **2013**, *36*, 1−7.
(222) McGraw, J. D.; Salez, T.; Bäumchen, O.; Raphaël, É.; Dalnoki-Veress, K. Capillary leveling of stepped films with inhomogeneous molecular mobility. *Soft Matter* **2013**, *9*, 8297−8305.
(223) Bertin, V.; Lee, C. L.; Salez, T.; Raphaël, E.; Dalnoki-Veress, K. Capillary levelling of immiscible bilayer films. *J. Fluid Mech.* **2021**, *911*, A13.
(224) Chai, Y.; Salez, T.; McGraw, J. D.; Benzaquen, M.; Dalnoki-Veress, K.; Raphaël, E.; Forrest, J. A. A direct quantitative measure of surface mobility in a glassy polymer. *Science* **2014**, *343*, 994−999.
(225) Rivetti, M.; Salez, T.; Benzaquen, M.; Raphaël, E.; Bäumchen, O. Universal contact-line dynamics at the nanoscale. *Soft Matter* **2015**, *11*, 9247−9253.
(226) Bertin, V.; Niven, J.; Stone, H. A.; Salez, T.; Raphael, E.; Dalnoki-Veress, K. Symmetrization of Thin Freestanding Liquid Films via a Capillary-Driven Flow. *Physical review letters* **2020**, *124*, 184502.
(227) Tanis, I.; Karatasos, K.; Salez, T. Molecular dynamics simulation of the capillary leveling of a glass-forming liquid. *J. Phys. Chem. B* **2019**, *123*, 8543−8549.
(228) Rivetti, M.; Bertin, V.; Salez, T.; Hui, C.-Y.; Linne, C.; Arutkin, M.; Wu, H.; Raphaël, E.; Bäumchen, O. Elastocapillary levelling of thin viscous films on soft substrates. *Physical Review Fluids* **2017**, *2*, 094001.
(229) Pedersen, C.; Niven, J. F.; Salez, T.; Dalnoki-Veress, K.; Carlson, A. Asymptotic regimes in elastohydrodynamic and stochastic leveling on a viscous film. *Physical Review Fluids* **2019**, *4*, 124003.
(230) Benzaquen, M.; Salez, T.; Raphaël, E. Viscoelastic effects and anomalous transient levelling exponents in thin films. *EPL (Europhysics Letters)* **2014**, *106*, 36003.
(231) Derjaguin, B.; Karassev, V. Viscosity studies of liquid boundary layers by the blow-off method. *Prog. Surf. Sci.* **1992**, *40*, 301−308.
(232) Scarpulla, M. A.; Mate, C. M.; Carter, M. D. Air shear driven flow of thin perfluoropolyether polymer films. *J. Chem. Phys.* **2003**, *118*, 3368−3375.
(233) Mate, C. M.; Marchon, B. Shear response of molecularly thin liquid films to an applied air stress. *Physical review letters* **2000**, *85*, 3902.
(234) de Gennes, P.-G.; Brochard-Wyart, F.; Quéré, D.; de Gennes, P.-G.; Brochard-Wyart, F.; Quéré, D. Dewetting. *Capillarity and Wetting Phenomena: Drops, Bubbles, Pearls, Waves* **2004**, 153−190.
(235) Carré, A.; Gastel, J.-C.; Shanahan, M. E. Viscoelastic effects in the spreading of liquids. *Nature* **1996**, *379*, 432−434.
(236) Carre, A.; Shanahan, M. E. Direct evidence for viscosity-independent spreading on a soft solid. *Langmuir* **1995**, *11*, 24−26.
(237) Shanahan, M.; Carre, A. Viscoelastic dissipation in wetting and adhesion phenomena. *Langmuir* **1995**, *11*, 1396−1402.
(238) Wang, F.; Jiang, Z.; Lin, X.; Zhang, C.; Tanaka, K.; Zuo, B.; Zhang, W.; Wang, X. Suppressed Chain Entanglement Induced by Thickness of Ultrathin Polystyrene Films. *Macromolecules* **2021**, *54*, 3735−3743.
(239) Zuo, B.; Zheng, F. F.; Zhao, Y. R.; Chen, T.; Yan, Z. H.; Ni, H.; Wang, X. Stick−slip phenomenon in measurements of dynamic contact angles and surface viscoelasticity of poly (styrene-b-isoprene-b-styrene) triblock copolymers. *Langmuir* **2012**, *28*, 4283−4292.
(240) Jerison, E. R.; Xu, Y.; Wilen, L. A.; Dufresne, E. R. Deformation of an elastic substrate by a three-phase contact line. *Physical review letters* **2011**, *106*, 186103.
(241) Park, S. J.; Weon, B. M.; San Lee, J.; Lee, J.; Kim, J.; Je, J. H. Visualization of asymmetric wetting ridges on soft solids with X-ray microscopy. *Nat. Commun.* **2014**, *5*, 1−7.
(242) Shanahan, M.; Carré, A. Spreading and dynamics of liquid drops involving nanometric deformations on soft substrates. *Colloids Surf., A* **2002**, *206*, 115−123.
(243) Pu, G.; Severtson, S. J. Water evaporation on highly viscoelastic polymer surfaces. *Langmuir* **2012**, *28*, 10007−10014.
(244) Zuo, B.; Qian, C.; Yan, D.; Liu, Y.; Liu, W.; Fan, H.; Tian, H.; Wang, X. Probing glass transitions in thin and ultrathin polystyrene films by stick−slip behavior during dynamic wetting of liquid droplets on their surfaces. *Macromolecules* **2013**, *46*, 1875−1882.
(245) Zuo, B.; He, X.; Wang, Y.; Xu, J.; Yang, J.; Wang, X. Relationship between Segmental Relaxation of Polystyrene Films and Stick−Slip Behavior during Dynamic Wetting of Liquid Droplets on Their Surfaces. *J. Phys. Chem. B* **2015**, *119*, 12325−12335.
(246) Zheng, F.; Zuo, B.; Zhu, Y.; Yang, J.; Wang, X. Probing substrate effects on relaxation dynamics of ultrathin poly (vinyl acetate) films by dynamic wetting of water droplets on their surfaces. *Soft Matter* **2013**, *9*, 11680−11689.
(247) Lu, H.; Chen, W.; Russell, T. P. Relaxation of thin films of polystyrene floating on ionic liquid surface. *Macromolecules* **2009**, *42*, 9111−9117.
(248) Brochard-Wyart, F.; Debregeas, G.; Fondecave, R.; Martin, P. Dewetting of supported viscoelastic polymer films: Birth of rims. *Macromolecules* **1997**, *30*, 1211−1213.
(249) Redon, C.; Brochard-Wyart, F.; Rondelez, F. Dynamics of dewetting. *Physical review letters* **1991**, *66*, 715.
(250) Vilmin, T.; Raphaël, E. Dewetting of thin polymer films. *Eur. Phys. J. E* **2006**, *21*, 161−174.
(251) Saulnier, F.; Raphaël, E.; De Gennes, P.-G. Dewetting of thin-film polymers. *Phys. Rev. E* **2002**, *66*, 061607.
(252) Redon, C.; Brzoska, J.; Brochard-Wyart, F. Dewetting and slippage of microscopic polymer films. *Macromolecules* **1994**, *27*, 468−471.
(253) Martin, P.; Brochard-Wyart, F. Dewetting at soft interfaces. *Physical review letters* **1998**, *80*, 3296.
(254) Wyart, F. B.; Martin, P.; Redon, C. Liquid/liquid dewetting. *Langmuir* **1993**, *9*, 3682−3690.
(255) Vilmin, T.; Raphaël, E. Dewetting of thin viscoelastic polymer films on slippery substrates. *EPL (Europhysics Letters)* **2005**, *72*, 781.
(256) Reiter, G.; Al Akhrass, S.; Hamieh, M.; Damman, P.; Gabriele, S.; Vilmin, T.; Raphaël, E. Dewetting as an investigative tool for studying properties of thin polymer films. *European Physical Journal Special Topics* **2009**, *166*, 165−172.
(257) Damman, P.; Gabriele, S.; Coppée, S.; Desprez, S.; Villers, D.; Vilmin, T.; Raphaël, E.; Hamieh, M.; Al Akhrass, S.; Reiter, G.

Relaxation of residual stress and reentanglement of polymers in spin-coated films. *Physical review letters* **2007**, *99*, 036101.
(258) Chowdhury, M. Thin polymer films out of thermodynamic equilibrium. Ph.D. thesis, Dissertation, Albert-Ludwigs-Universität Freiburg, 2012.
(259) Bodiguel, H.; Fretigny, C. Viscoelastic dewetting of a polymer film on a liquid substrate. *Eur. Phys. J. E* **2006**, *19*, 185−193.
(260) Thoms, E.; Napolitano, S. Enthalpy-entropy compensation in the slow Arrhenius process. *J. Chem. Phys.* **2023**, *159*, 161103.
(261) Nag, P. *Engineering Thermodynamics*; Tata McGraw Hill, 2005.
(262) Kchaou, M.; Alcouffe, P.; Chandran, S.; Cassagnau, P.; Reiter, G.; Al Akhrass, S. Tuning relaxation dynamics and mechanical properties of polymer films of identical thickness. *Phys. Rev. E* **2018**, *97*, 032507.
(263) Mulama, A. A.; Chandran, S.; Roumpos, K.; Oduor, A. O.; Reiter, G. Dewetting Rheology for Determining Viscoelastic Properties of Nonequilibrated Thin Polymer Films. *Macromolecules* **2019**, *52*, 7894−7903.
(264) Lakes, R. *Viscoelastic Materials*; Cambridge University Press, 2009.
(265) Leger, L.; Joanny, J. F. Liquid spreading. *Rep. Prog. Phys.* **1992**, *55*, 431.
(266) Glynos, E.; Chremos, A.; Frieberg, B.; Sakellariou, G.; Green, P. F. Wetting of Macromolecules: From Linear Chain to Soft Colloid-Like Behavior. *Macromolecules* **2014**, *47*, 1137−1143.
(267) Fetzer, R.; Muench, A.; Wagner, B.; Rauscher, M.; Jacobs, K. Quantifying hydrodynamic slip: A comprehensive analysis of dewetting profiles. *Langmuir* **2007**, *23*, 10559−10566.
(268) Sarkar, J.; Madhusudanan, M.; V. C, C.; Choyal, S.; Chowdhury, M. Roles of aqueous nonsolvents influencing the dynamic stability of poly-(n-butyl methacrylate) thin films at biologically relevant temperatures. *Soft Matter* **2023**, *19*, 8193−8202.
(269) Masnik, J. E.; Kieffer, J.; Bass, J. D. Structural relaxations in alkali silicate systems by Brillouin light scattering. *J. Am. Ceram. Soc.* **1993**, *76*, 3073−3080.
(270) Raman, C.; Nagendra Nathe, N. *Proceedings of the Indian Academy of Sciences-Section A*; Springer, 1935; Vol. *2*; pp 406−412.
(271) Hayes, W.; Loudon, R. *Scattering of light by crystals*; Wiley: New York, 1978.
(272) Hartschuh, R.; Ding, Y.; Roh, J.; Kisliuk, A.; Sokolov, A.; Soles, C. L.; Jones, R.; Hu, T.; Wu, W.; Mahorowala, A. Brillouin scattering studies of polymeric nanostructures. *J. Polym. Sci., Part B: Polym. Phys.* **2004**, *42*, 1106−1113.
(273) Johnson, W. L.; Kim, S. A.; Geiss, R.; Flannery, C.; Soles, C.; Wang, C.; Stafford, C.; Wu, W.; Torres, J.; Vogt, B.; et al. Elastic constants and dimensions of imprinted polymeric nanolines determined from Brillouin light scattering. *Nanotechnology* **2010**, *21*, 075703.
(274) Gomopoulos, N.; Cheng, W.; Efremov, M.; Nealey, P.; Fytas, G. Out-of-plane longitudinal elastic modulus of supported polymer thin films. *Macromolecules* **2009**, *42*, 7164−7167.
(275) Carlotti, G. Elastic characterization of transparent and opaque films, multilayers and acoustic resonators by surface Brillouin scattering: a review. *Applied Sciences* **2018**, *8*, 124.
(276) Forrest, J.; Dalnoki-Veress, K.; Dutcher, J. Brillouin light scattering studies of the mechanical properties of thin freely standing polystyrene films. *Phys. Rev. E* **1998**, *58*, 6109.
(277) Forrest, J.; Rowat, A.; Dalnoki-Veress, K.; Stevens, J.; Dutcher, J. Brillouin light scattering studies of the mechanical properties of polystyrene/polyisoprene multilayered thin films. *J. Polym. Sci., Part B: Polym. Phys.* **1996**, *34*, 3009−3016.
(278) Forrest, J.; Dalnoki-Veress, K.; Dutcher, J.; Rowat, A.; Stevens, J. Brillouin light scattering determination of the glass transition in thin, freely-standing poly (styrene) films. *Mater. Res. Soc. Symp. Proc.* **1995**, *407*, 131−136.
(279) Cheng, W.; Sainidou, R.; Burgardt, P.; Stefanou, N.; Kiyanova, A.; Efremov, M.; Fytas, G.; Nealey, P. Elastic properties and glass transition of supported polymer thin films. *Macromolecules* **2007**, *40*, 7283−7290.
(280) Guerette, M.; Huang, L. A simple and convenient set-up for high-temperature Brillouin light scattering. *J. Phys. D: Appl. Phys.* **2012**, *45*, 275302.
(281) Graczykowski, B.; Gueddida, A.; Djafari-Rouhani, B.; Butt, H.-J.; Fytas, G. Brillouin light scattering under one-dimensional confinement: Symmetry and interference self-canceling. *Phys. Rev. B* **2019**, *99*, 165431.
(282) Oh, K. H.; Ko, Y.-H.; Kim, K.-J. Mechanical properties of amorphous PEI, PES, and PVC up to 11 GPa studied by Brillouin light scattering. *Physica B: Condensed Matter* **2020**, *576*, 411722.
(283) Burroughs, M. J.; Christie, D.; Gray, L. A.; Chowdhury, M.; Priestley, R. D. 21st Century Advances in Fluorescence Techniques to Characterize Glass-Forming Polymers at the Nanoscale. *Macromol. Chem. Phys.* **2018**, *219*, 1700368.
(284) Victor, J. G.; Torkelson, J. M. On measuring the distribution of local free volume in glassy polymers by photochromic and fluorescence techniques. *Macromolecules* **1987**, *20*, 2241−2250.
(285) Ellison, C. J.; Torkelson, J. M. Sensing the glass transition in thin and ultrathin polymer films via fluorescence probes and labels. *J. Polym. Sci., Part B: Polym. Phys.* **2002**, *40*, 2745−2758.
(286) Mundra, M. K.; Ellison, C. J.; Behling, R. E.; Torkelson, J. M. Confinement, composition, and spin-coating effects on the glass transition and stress relaxation of thin films of polystyrene and styrene-containing random copolymers: Sensing by intrinsic fluorescence. *Polymer* **2006**, *47*, 7747−7759.
(287) Roth, C. B.; McNerny, K. L.; Jager, W. F.; Torkelson, J. M. Eliminating the enhanced mobility at the free surface of polystyrene: fluorescence studies of the glass transition temperature in thin bilayer films of immiscible polymers. *Macromolecules* **2007**, *40*, 2568−2574.
(288) Mundra, M.; Ellison, C.; Rittigstein, P.; Torkelson, J. Fluorescence studies of confinement in polymer films and nanocomposites: Glass transition temperature, plasticizer effects, and sensitivity to stress relaxation and local polarity. *European Physical Journal Special Topics* **2007**, *141*, 143−151.
(289) Lee, H.-N.; Paeng, K.; Swallen, S. F.; Ediger, M. Dye reorientation as a probe of stress-induced mobility in polymer glasses. *J. Chem. Phys.* **2008**, *128*, 134902.
(290) Askar, S. Effects of Confinement and Interfaces on Stress Relaxation and Stiffness in Polymer Films and Nanocomposites Characterized by Novel Fluorescence Techniques. Ph.D. thesis, Northwestern University, 2017.
(291) Hu, S.; Wang, T.; Wei, T.; Peera, A.; Zhang, S.; Pujari, S.; Torkelson, J. M. Very low levels of n-butyl acrylate comonomer strongly affect residual stress relaxation in styrene/acrylic random copolymer films. *Polymer* **2022**, *260*, 125379.
(292) Rose, K. A.; Molaei, M.; Boyle, M. J.; Lee, D.; Crocker, J. C.; Composto, R. J. Particle tracking of nanoparticles in soft matter. *J. Appl. Phys.* **2020**, *127*, 191101.
(293) Einstein, A. *Investigations on the Theory of the Brownian Movement*; Courier Corporation, 1956.
(294) Mason, T. G.; Weitz, D. A. Optical measurements of frequency-dependent linear viscoelastic moduli of complex fluids. *Physical review letters* **1995**, *74*, 1250.
(295) Mason, T. G.; Ganesan, K.; van Zanten, J. H.; Wirtz, D.; Kuo, S. C. Particle tracking microrheology of complex fluids. *Physical review letters* **1997**, *79*, 3282.
(296) Liu, W.; Wu, C. Rheological study of soft matters: A review of microrheology and microrheometers. *Macromol. Chem. Phys.* **2018**, *219*, 1700307.
(297) Flier, B. M.; Baier, M. C.; Huber, J.; Müllen, K.; Mecking, S.; Zumbusch, A.; Wöll, D. Heterogeneous diffusion in thin polymer films as observed by high-temperature single-molecule fluorescence microscopy. *J. Am. Chem. Soc.* **2012**, *134*, 480−488.
(298) Paeng, K.; Park, H.; Hoang, D. T.; Kaufman, L. J. Ideal probe single-molecule experiments reveal the intrinsic dynamic heterogeneity of a supercooled liquid. *Proc. Natl. Acad. Sci. U. S. A.* **2015**, *112*, 4952−4957.

https://doi.org/10.1021/acspolymersau.4c00022
ACS Polym. Au 2024, 4, 342−391

(299) Paeng, K.; Kaufman, L. J. Single molecule experiments reveal the dynamic heterogeneity and exchange time scales of polystyrene near the glass transition. *Macromolecules* **2016**, *49*, 2876−2885.
(300) Bhattacharya, S.; Sharma, D. K.; De, S.; Mahato, J.; Chowdhury, A. Heterogeneity during plasticization of poly (vinylpyrrolidone): Insights from reorientational mobility of single fluorescent probes. *J. Phys. Chem. B* **2016**, *120*, 12404−12415.
(301) Bhattacharya, S.; Sharma, D. K.; Saurabh, S.; De, S.; Sain, A.; Nandi, A.; Chowdhury, A. Plasticization of poly (vinylpyrrolidone) thin films under ambient humidity: Insight from single-molecule tracer diffusion dynamics. *J. Phys. Chem. B* **2013**, *117*, 7771−7782.
(302) Joung, H.; Kim, C.; Yu, J.; Lee, S.; Paeng, K.; Yang, J. Impact of chain conformation on structural heterogeneity in polymer network. *Nano Lett.* **2022**, *22*, 5487−5494.
(303) Wöll, D.; Braeken, E.; Deres, A.; De Schryver, F. C.; Uji-i, H.; Hofkens, J. Polymers and single molecule fluorescence spectroscopy, what can we learn? *Chem. Soc. Rev.* **2009**, *38*, 313−328.
(304) Tran-Ba, K.-H.; Foreman, K. Single-molecule tracking of dye diffusion in synthetic polymers: A tutorial review. *J. Appl. Phys.* **2023**, *133*, 101101.
(305) Choi, J.; Lee, S.; Choe, J.; Chung, Y.; Lee, Y. E.; Kim, J.; Kim, M.; Paeng, K. How tethered probes report the dynamics of a polymer near the glass transition. *ACS Macro Lett.* **2019**, *8*, 1181−1186.
(306) Chung, Y.; Nam, J.; Son, D.; Lee, H.; Kim, M.; Paeng, K. Direct Observations of Segmental Dynamics at the Polymer−Substrate Interface Enabled by Localizing Fluorescent Probes with Polymer Brushes. *Macromolecules* **2021**, *54*, 4546−4556.
(307) Lee, H.; Kim, T.; Choi, S.; Yang, J.; Kim, M.; Paeng, K. Segmental Dynamics of an Isolated Component Polymer Chain in Polymer Blends Near the Glass Transition. *Macromolecules* **2023**, *56*, 8133−8143.
(308) Yamamoto, U.; Schweizer, K. S. Theory of nanoparticle diffusion in unentangled and entangled polymer melts. *J. Chem. Phys.* **2011**, *135*, 224902.
(309) Brochard Wyart, F.; de Gennes, P.-G. Viscosity at small scales in polymer melts. *Eur. Phys. J. E* **2000**, *1*, 93−97.
(310) Tuteja, A.; Mackay, M. E.; Narayanan, S.; Asokan, S.; Wong, M. S. Breakdown of the continuum Stokes- Einstein relation for nanoparticle diffusion. *Nano Lett.* **2007**, *7*, 1276−1281.
(311) Lin, C.-C.; Griffin, P. J.; Chao, H.; Hore, M. J.; Ohno, K.; Clarke, N.; Riggleman, R. A.; Winey, K. I.; Composto, R. J. Grafted polymer chains suppress nanoparticle diffusion in athermal polymer melts. *J. Chem. Phys.* **2017**, *146*, 203332.
(312) Park, J.; Bailey, E. J.; Composto, R. J.; Winey, K. I. Single-particle tracking of nonsticky and sticky nanoparticles in polymer melts. *Macromolecules* **2020**, *53*, 3933−3939.
(313) Carroll, B.; Bocharova, V.; Carrillo, J.-M. Y.; Kisliuk, A.; Cheng, S.; Yamamoto, U.; Schweizer, K. S.; Sumpter, B. G.; Sokolov, A. P. Diffusion of sticky nanoparticles in a polymer melt: Crossover from suppressed to enhanced transport. *Macromolecules* **2018**, *51*, 2268−2275.
(314) Volgin, I.; Larin, S.; Lyulin, S. Diffusion of nanoparticles in polymer systems. *Polymer Science, Series C* **2018**, *60*, 122−134.
(315) Paeng, K.; Ediger, M. Molecular motion in free-standing thin films of poly (methyl methacrylate), poly (4-tert-butylstyrene), poly (α-methylstyrene), and poly (2-vinylpyridine). *Macromolecules* **2011**, *44*, 7034−7042.
(316) Paeng, K.; Richert, R.; Ediger, M. Molecular mobility in supported thin films of polystyrene, poly (methyl methacrylate), and poly (2-vinyl pyridine) probed by dye reorientation. *Soft Matter* **2012**, *8*, 819−826.
(317) Katzenstein, J. M.; Janes, D. W.; Hocker, H. E.; Chandler, J. K.; Ellison, C. J. Nanoconfined self-diffusion of poly (isobutyl methacrylate) in films with a thickness-independent glass transition. *Macromolecules* **2012**, *45*, 1544−1552.
(318) Wong, J. S.; Hong, L.; Bae, S. C.; Granick, S. Fluorescence recovery after photobleaching measurements of polymers in a surface forces apparatus. *J. Polym. Sci., Part B: Polym. Phys.* **2010**, *48*, 2582−2588.
(319) Yu, C.; Granick, S. Revisiting polymer surface diffusion in the extreme case of strong adsorption. *Langmuir* **2014**, *30*, 14538−14544.
(320) Katsumata, R.; Dulaney, A. R.; Kim, C. B.; Ellison, C. J. Glass transition and self-diffusion of unentangled polymer melts nano-confined by different interfaces. *Macromolecules* **2018**, *51*, 7509−7517.
(321) Macionczyk, F.; Brückner, W. Tensile testing of AlCu thin films on polyimide foils. *J. Appl. Phys.* **1999**, *86*, 4922−4929.
(322) Gianola, D. S.; Eberl, C. Micro-and nanoscale tensile testing of materials. *Jom* **2009**, *61*, 24−35.
(323) Haque, M. A.; Saif, M. T. A. In-situ tensile testing of nano-scale specimens in SEM and TEM. *Experimental mechanics* **2002**, *42*, 123−128.
(324) Chen, X.; Kirsch, B. L.; Senter, R.; Tolbert, S. H.; Gupta, V. Tensile testing of thin films supported on compliant substrates. *Mech. Mater.* **2009**, *41*, 839−848.
(325) Zhu, Y.; Espinosa, H. D. An electromechanical material testing system for in situ electron microscopy and applications. *Proc. Natl. Acad. Sci. U. S. A.* **2005**, *102*, 14503−14508.
(326) Huang, H.; Spaepen, F. Tensile testing of free-standing Cu, Ag and Al thin films and Ag/Cu multilayers. *Acta Mater.* **2000**, *48*, 3261−3269.
(327) Lu, N.; Wang, X.; Suo, Z.; Vlassak, J. Metal films on polymer substrates stretched beyond 50%. *Appl. Phys. Lett.* **2007**, *91*, 221909.
(328) Bay, R. K.; Crosby, A. J. Uniaxial extension of ultrathin freestanding polymer films. *ACS Macro Lett.* **2019**, *8*, 1080−1085.
(329) Kim, J.-H.; Nizami, A.; Hwangbo, Y.; Jang, B.; Lee, H.-J.; Woo, C.-S.; Hyun, S.; Kim, T.-S. Tensile testing of ultra-thin films on water surface. *Nat. Commun.* **2013**, *4*, 1−6.
(330) Hasegawa, H.; Ohta, T.; Ito, K.; Yokoyama, H. Stress-strain measurement of ultra-thin polystyrene films: Film thickness and molecular weight dependence of crazing stress. *Polymer* **2017**, *123*, 179−183.
(331) Bay, R. K.; Shimomura, S.; Liu, Y.; Ilton, M.; Crosby, A. J. Confinement effect on strain localizations in glassy polymer films. *Macromolecules* **2018**, *51*, 3647−3653.
(332) Choi, W. J.; Bay, R. K.; Crosby, A. J. Tensile Properties of Ultrathin Bisphenol-A Polycarbonate Films. *Macromolecules* **2019**, *52*, 7489−7494.
(333) Bay, R. K.; Zhang, T.; Shimomura, S.; Ilton, M.; Tanaka, K.; Riggleman, R. A.; Crosby, A. J. Decoupling the impact of entanglements and mobility on the failure properties of ultrathin polymer films. *Macromolecules* **2022**, *55*, 8505−8513.
(334) Saito, M.; Ito, K.; Yokoyama, H. Mechanical properties of ultrathin polystyrene-b-polybutadiene-b-polystyrene block copolymer films: Film thickness-dependent young's modulus. *Macromolecules* **2021**, *54*, 8538−8547.
(335) Saito, M.; Ito, K.; Yokoyama, H. Film thickness and strain rate dependences of the mechanical properties of polystyrene-b-poly-isoprene-b-polystyrene block copolymer ultrathin films forming a spherical domain. *Polymer* **2022**, *258*, 125302.
(336) Saito, M.; Yamada, N. L.; Ito, K.; Yokoyama, H. Mechanical Properties and Swelling Behaviors of Ultrathin Chemically Cross-Linked Polybutadiene Films. *Macromolecules* **2023**, *56*, 4000−4011.
(337) Zhang, S.; Ocheje, M. U.; Luo, S.; Ehlenberg, D.; Appleby, B.; Weller, D.; Zhou, D.; Rondeau-Gagné, S.; Gu, X. Probing the Viscoelastic Property of Pseudo Free-Standing Conjugated Polymeric Thin Films. *Macromol. Rapid Commun.* **2018**, *39*, 1800092.
(338) Galuska, L. A.; Muckley, E. S.; Cao, Z.; Ehlenberg, D. F.; Qian, Z.; Zhang, S.; Rondeau-Gagné, S.; Phan, M. D.; Ankner, J. F.; Ivanov, I. N.; et al. SMART transfer method to directly compare the mechanical response of water-supported and free-standing ultrathin polymeric films. *Nat. Commun.* **2021**, *12*, 1−11.
(339) Song, R.; Schrickx, H.; Balar, N.; Siddika, S.; Sheikh, N.; O'Connor, B. T. Unveiling the stress−strain behavior of conjugated polymer thin films for stretchable device applications. *Macromolecules* **2020**, *53*, 1988−1997.
(340) Yiu, P. M.; Yuan, H.; Gu, Q.; Gao, P.; Tsui, O. K. Strain Rate and Thickness Dependences of Elastic Modulus of Free-Standing Polymer Nanometer Films. *ACS Macro Lett.* **2020**, *9*, 1521−1526.

https://doi.org/10.1021/acspolymersau.4c00022
ACS Polym. Au 2024, 4, 342−391

(341) Yuan, H.; Yan, J.; Gao, P.; Kumar, S. K.; Tsui, O. K. Microscale mobile surface double layer in a glassy polymer. *Science Advances* **2022**, *8*, eabq5295.
(342) Strojny, A.; Xia, X.; Tsou, A.; Gerberich, W. W. Techniques and considerations for nanoindentation measurements of polymer thin film constitutive properties. *J. Adhes. Sci. Technol.* **1998**, *12*, 1299−1321.
(343) Doerner, M. F.; Nix, W. D. A method for interpreting the data from depth-sensing indentation instruments. *Journal of Materials research* **1986**, *1*, 601−609.
(344) Oliver, W. C.; Pharr, G. M. An improved technique for determining hardness and elastic modulus using load and displacement sensing indentation experiments. *Journal of materials research* **1992**, *7*, 1564−1583.
(345) Miyake, K.; Fujisawa, S.; Korenaga, A.; Ishida, T.; Sasaki, S. The effect of pile-up and contact area on hardness test by nanoindentation. *Japanese journal of applied physics* **2004**, *43*, 4602.
(346) Oliver, W. C.; Pharr, G. M. Measurement of hardness and elastic modulus by instrumented indentation: Advances in understanding and refinements to methodology. *Journal of materials research* **2004**, *19*, 3−20.
(347) Brazil, O.; de Silva, J. P.; Chowdhury, M.; Yoon, H.; McKenna, G. B.; Oliver, W. C.; Kilpatrick, J.; Pethica, J. B.; Cross, G. L. In situ measurement of bulk modulus and yield response of glassy thin films via confined layer compression. *J. Mater. Res.* **2020**, *35*, 644−653.
(348) Cross, G. L.; O'Connell, B. S.; Pethica, J. B.; Rowland, H.; King, W. P. Variable temperature thin film indentation with a flat punch. *Rev. Sci. Instrum.* **2008**, *79*, 013904.
(349) Rowland, H. D.; King, W. P.; Pethica, J. B.; Cross, G. L. Molecular confinement accelerates deformation of entangled polymers during squeeze flow. *Science* **2008**, *322*, 720−724.
(350) Rowland, H. D.; King, W. P.; Cross, G. L.; Pethica, J. B. Measuring glassy and viscoelastic polymer flow in molecular-scale gaps using a flat punch mechanical probe. *ACS Nano* **2008**, *2*, 419−428.
(351) Brazil, O.; de Silva, J. P.; Pethica, J. B.; Cross, G. L. Extrinsic plastic hardening of polymer thin films in flat punch indentation. *Philos. Mag.* **2021**, *101*, 1327−1342.
(352) Sinnott, A. D.; Brazil, O.; Cross, G. L. The effect of contact aspect ratio and film to substrate elastic modulus ratio on stress vs. strain up to the point of yield during flat punch thin film indentation of an elastic-plastic film. *Frontiers in Materials* **2022**, *9*, 906204.
(353) Brazil, O.; Özer, H. Ö.; Watts, B.; Pethica, J. B.; Cross, G. L. Densification of a polymer glass under high-pressure shear flow. *Phys. Rev. B* **2022**, *106*, L060103.
(354) Sinnott, A. D.; Kelly, A.; Gabbett, C.; Moebius, M.; Coleman, J. N.; Cross, G. L. Pressure-dependent mechanical properties of thin films under uniaxial strain via the layer compression test. *J. Mater. Res.* **2024**, *39*, 273.
(355) Ramezani, F.; Baschnagel, J.; Reiter, G. Translating molecular relaxations in non-equilibrated polymer melts into lifting macroscopic loads. *Physical Review Materials* **2020**, *4*, 082601.
(356) Reiter, G.; Ramezani, F.; Baschnagel, J. The memory of thin polymer films generated by spin coating. *Eur. Phys. J. E* **2022**, *45*, 51.

https://doi.org/10.1021/acspolymersau.4c00022
ACS Polym. Au 2024, 4, 342−391